GAP BRIDGING USING CHEMICAL BLOWING AGENTS IN CONTOUR LASER TRANSMISSION WELDING OF THERMOPLASTICS

UTILISATION DES AGENTS D'EXPANSION CHIMIQUE EN SOUDAGE DES THERMOPLASTIQUES PAR LASER TRANSMISSION WELDING

by

Fahmida Mamtaz

A thesis submitted to the Department of Chemistry and Chemical Engineering

In conformity with the requirements for

The degree of Master of Applied Science

Royal Military College of Canada

Kingston, Ontario, Canada

(August, 2016)

Abstract

Laser transmission welding (LTW) is an innovative technique for joining thermoplastics. The laser energy is transmitted through an upper transparent part and is then absorbed by the lower absorbent part. The absorbing pigments such as carbon black convert the laser energy into heat which melts the plastic and creates the weld. Among several laser delivery methods, contour LTW is especially suitable for bigger geometries. However, meltdown, which permits the bridging of small interfacial gaps, does not normally occur with contour LTW. This project explores the novel idea of gap bridging using chemical blowing agents in contour LTW. Chemical blowing agents (CBA) are normally used to make thermoplastic foams. The idea of this project was to incorporate this CBA into the absorbent parts during injection moulding while keeping it undecomposed. During welding, the temperature will rise more where interfacial gaps are present and thus activate the CBA which then releases gas and generates foam. This foam takes part in gap bridging. For this project, Dow LDPE 959S was selected as the base polymer resin. Four different types of CBA were examined. TRACEL® IM 2240 ST was found to be the most suitable among them based on thermal gravimetric analysis (TGA). Injection moulded parts were made with and without CBA while maintaining the same carbon black level in the absorbent part. Welding experiments were carried out on samples with and without CBA. It was found that the presence of CBA lowers the minimum power required to create a weld for a given gap size. The strength of specimens containing CBA was however lower than those without CBA. To model the conversion of CBA, first the chemical kinetics of CBA degradation were measured using TGA. A 2D finite-element method model was then used to find the temperature of different points near the weld seam as a function of time. A Matlab® code was developed to calculate the theoretical percentage of conversion of CBA at different locations along the geometry. The output from the CBA conversion model helped to explain the experimental findings and suggest possible measures to achieve better gap bridging result using the method described in the study.

Résumé

La soudure par transmission laser (LTW, venant du nom anglais « Laser Transmission Welding ») est une technique innovatrice permettant de souder des thermoplastiques. L'énergie du laser est transmise à travers une partie supérieure transparente et est ensuite absorbée par une partie inférieure absorbante. Les pigments absorbants tels que le noir de carbone convertissent l'énergie du laser en chaleur qui fond le plastique et crée ainsi la soudure. Parmi plusieurs méthodes d'émission de laser, Contour LTW est surtout adapté pour de plus grandes géométries. Par contre, la fusion, permettant la pontage de petites lacunes inter-faciales, ne se produit pas d'habitude avec Contour LTW. Ce projet explore l'idée de pontage des lacunes en employant des agents chimiques gonflants dans Contour LTW. Des agents chimiques gonflants (CBA, venant de l'anglais « Chemical Blowing Agents ») sont d'habitude utilisés pour créer des mousses en thermoplastique. L'idée de ce projet est d'incorporer ces CBA dans les parties absorbantes durant le moulage par injection à l'aide d'une injection sans décomposition. Durant le soudage, la température augmentera plus là où les lacunes inter-faciales sont présentes et donc activera les CBA, qui ensuite relâcheront du gaz et produiront de la mousse. Cette mousse participe dans le pontage des lacunes. Pour ce projet, Dow LDPE 959S est sélectionné en tant que la base polymère en résine. Quatre différents types de CBA ont été examinés. TRACEL® IM 2240 ST est celui qui convient le mieux parmi eux en se basant sur l'analyse thermale gravimétrique (TGA, venant de l'anglais « Thermal Gravimetric Analysis »). Les parties moulées par injection ont été créées avec et sans CBA en gardant le même niveau de noir de carbone dans la partie absorbante. Des expériences ont été menées sur les échantillons avec et sans CBA. Il a été découvert que la présence de CBA diminue la puissance minimale requise pour créer la soudure pour une grandeur de lacune donnée. La force des spécimens contenant du CBA est par contre inférieure à ceux sans CBA. Pour montrer la conversion du CBA, les cinétiques chimiques sont tout d'abord mesurées en utilisant la TGA. Un modèle utilisant la méthode d'éléments-clos 2D a ensuite été utilisé pour trouver les températures des différents points près de la soudure en fonction de temps. Un code Matlab® a ensuite été développé pour calculer le pourcentage théorique de la

conversion de CBA en différents lieux de la géométrie. Le résultat du modèle de la conversion du CBA aide à expliquer les conclusions expérimentales et suggère des mesures possibles pour acquérir de meilleurs pontages de lacunes en utilisant la méthode décrite dans l'étude.

Acknowledgements

First of all I would like to express my heartfelt gratitude to my supervisor Dr. Philip Bates, Professor at Royal Military College of Canada. Without his strong guidance, encouragement and support this work would not have been done.

I am thankful to Sina Khosravi for providing his FEM model which I have used in my work. I am also grateful to Tasie Okoro for helping me with the Matlab code. I am thankful to Jennifer Snelgrove, John Perreault and Clarence McEwen from RMC for their assistance to conduct the experimental work. Special thanks to Elizabeth Azhikannickal who trained me to use the laser welding machine and Xinfeng Xu to be there to help me.

I would like to thank my husband Kazi and my son Musaab for their support and motivation. I am also thankful to my parents and my friends. They have always stayed with me with their support and encouragement during this journey.

Table of Contents

List of Tables

List of Figures

List of Symbols

A	Laser absorption coefficient, 1/m
$\boldsymbol{A}$	Pre exponential factor, 1/s
A_1	Apparent laser absorption coefficient, 1/m
A_{1t}	Apparent laser absorption coefficient of transparent part, 1/m
A_{1a}	Apparent laser absorption coefficient of absorbent part, 1/m
A_T	Total absorbance
c	Heat capacity, J/(kg.K)
D	Thickness, mm
D_a	Depth of the absorbent part, m
E	Activation energy, kJ/mol
HDPE	High Density Polyethylene
K	extinction coefficient, 1/m
K	Thermal conductivity, W/(m.K)
LDPE	Low density polyethylene
n	Order of reaction
P	Power, W
$\boldsymbol{P}$	Pressure, Pa
PA6	Polyamide 6
PC	Polycarbonate
POM	Polyoxymethylene
P_{in}	Laser incident power, W
P_{out}	Output laser power after passing the polymer, W
P_0	Threshold power at which first visible melting is observed, W
P''_L	Laser light intensity from the laser head, W/m^2
P_{Lm}	Minimum required power to cause surface softening or melting, W
$P''(y)$	Laser light intensity at depth y, W/m^2
Q	Heat generation term, W/m^3
R	Total reflectance
$\boldsymbol{R}$	Universal gas constant, J/mol.K
R_T	Total reflectance
S	Laser scattering coefficient, 1/m
T	Temperature (℃ or K)
t	Time, s
T_T	Total transmittance
T_m	Melting temperature (℃)
T_i	Initial temperature (℃)
v	Scan speed, mm/s
W	Laser beam width, mm
W_k	Width of the weld line at any corresponding power P_k, mm
η	Surface reflectance
x	Reduced activation energy
α	Extent of conversion
β	Heating rate, K/min
ρ	Density, kg/m^3
ΔH	Latent heat, kJ/kg
$\psi^*(0)$	Normalized power flux distribution at the center of the scattered beam,W/m^2
σ	Scattering standard deviation, m
δ	The scattered fraction of each micro beam after passing through the transparent part.

Chapter 1

Introduction

This chapter introduces the idea of laser transmission welding as a plastic joining method, laser beam delivery techniques and their pros and cons. Later it discusses the problems associated with gaps at the weld interface and various methods of gap bridging which is the objective of this thesis.

1.1 Laser Transmission Welding

1.1.1 Concept of Laser Transmission Welding

Laser transmission welding (LTW) is a technique used to join thermoplastics. Most natural thermoplastics are generally transparent to laser light. Adding absorbing pigments (like carbon black) to a thermoplastic material can make it laser absorbent. In LTW, the laser beam passes through the transparent part and is absorbed by the absorbent part as shown in Figure 1.1. The absorbing pigments convert the laser energy into heat which is then conducted into the transparent part. This heat causes melting in both parts. The molten thermoplastic on both sides of the interface then mix together which after cooling provides a weld. Clamping pressure is required to ensure intimate contact between the two parts to be welded. (Moskvitin et al, 2013)

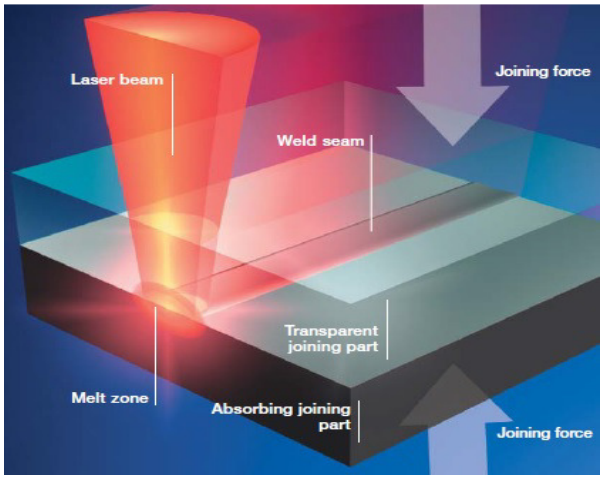

Figure 1. 1: Laser transmission welding (Leister, 2010)

1.1.2 Advantages/Disadvantages of Laser Transmission Welding

LTW is a well-recognized joining method today. Some of the main advantages of this technique are given below. (Leister, 2010)

- Laser transmission welding is a non-contact, flexible method of joining. It gives high weld strength with aesthetically good weld seam. It does not show any wear.
- LTW offers faster processing time. It can be easily automated. (Grewell, 1999)
- It is a vibration free processing. There is no development of particulates. This is a huge advantage particularly for fluid reservoirs and medical components.
- Welding can be done without relative part movement in LTW. It offers a great advantage for sophisticated electrical components which can be damaged by vibration or other types of movement.
- Energy delivery can be controlled precisely in LTW. (Bryden, 2000) The heat affected zone (HAZ) is small depending on the laser beam dimensions. Generates very little level of flash.

- No consumables (adhesive, fastener) are needed in laser welding.
- It is applicable for a wide range of thermoplastics, nearly all. Even plastics with glass fiber reinforcement can be welded by laser.

Like all other welding methods, laser welding also comes with some disadvantages. Some are identified below.

- Laser welding is a relatively expensive joining technique. It involves huge capital cost as laser welder machines are usually very expensive. (Steen and Mazumder, 2010)
- The interaction between the laser beam and the material is very complicated and poorly understood yet. (Chen, 2009) There are issues regarding degradation which affects strength of the material. (Okoro, 2013) The width of the weld is not directly controllable although it is related to the dimensions of the laser beam and scattering of the laser beam in the transparent part.

1.1.3 Industrial applications

Automotive industries have been using LTW for several decades for metals. Fiat used a CO_2 laser to weld metal power train components back in 1975 (Blais, 2006). Today, laser welding is used to manufacture a variety of automotive components such as engine and transmission parts, alternators, solenoids, fuel injectors, fuel filters, air conditioning equipment and air bags (TWI, 2013). Regarding the automotive body assembly, two main types of laser welding are being employed currently. The first one is the replacement of resistance welding or adhesive bonding, where lap joints are utilized on pressed components for body-in-white assembly. The second one is the laser butt welding of flat metal sheets which are subsequently formed into pressings.

These pressings are called tailored blanks (TWI, 2013). Figure 1.2 shows some of the examples of laser welded parts produced in industry. LTW of plastics is gaining popularity for biomedical applications as well. LTW can provide a clean hygienic surface free from material residue which is very much desirable in medical fields. Cardiac pacemakers, defibrillators, guide wires, catheters, hearing aids, orthodontic appliances, prosthetics and surgical tools are some of the examples of laser welded medical accessories. (Laserstar, 2014)

Figure 1. 2: Some of the industrially produced laser welded parts (Leister, 2010)

1.1.4 Types of LTW

There are several different ways to supply laser energy to the welding interface. Based on the laser delivery technique, LTW can be divided into three general categories: simultaneous, quasi-simultaneous and contour welding. Figure 1.3 shows the three categories of LTW.

In simultaneous welding, the entire weld interface is continuously irradiated by laser energy for the duration of welding cycle. Clamping pressure allows the molten material to flow out of the interface. With the proper weld geometry, this allows the transparent and absorbing components to move inwards towards the weld seam which allows the bridging of any small gaps present in the interface. This phenomenon is known as meltdown. This process often needs a large number of fiber optic cables coupled with the laser and placed around the periphery of the weld. To weld larger items such as air intake manifolds and headlamps, the cost becomes significantly high for the combined laser and fiber optic system which makes the simultaneous welding process cost-prohibitive. (Chen, 2009)

In quasi-simultaneous welding, the laser beam is moved quickly and repeatedly along the weld interface using mirrors. This process offers a lot of flexibility in welding process. Similar to simultaneous welding, with the proper geometry, it also facilitates meltdown. A problem associated with this technique is the significant increase in beam spot area as the incident angle decreases over a long weld path. Power per unit area thus varies at different positions which can cause inconsistent weld strength. This limits the applicability of quasi-simultaneous welding to small and less complicated geometries.

In contour LTW, the laser beam moves along the weld line just once. This technique has a high flexibility and it is much more suited to medium to large scale geometries. The problem associated with contour welding is that at any given instant, only a short segment along the weld line is molten. This unfortunately restricts material collapse and meltdown (Chen, 2009).

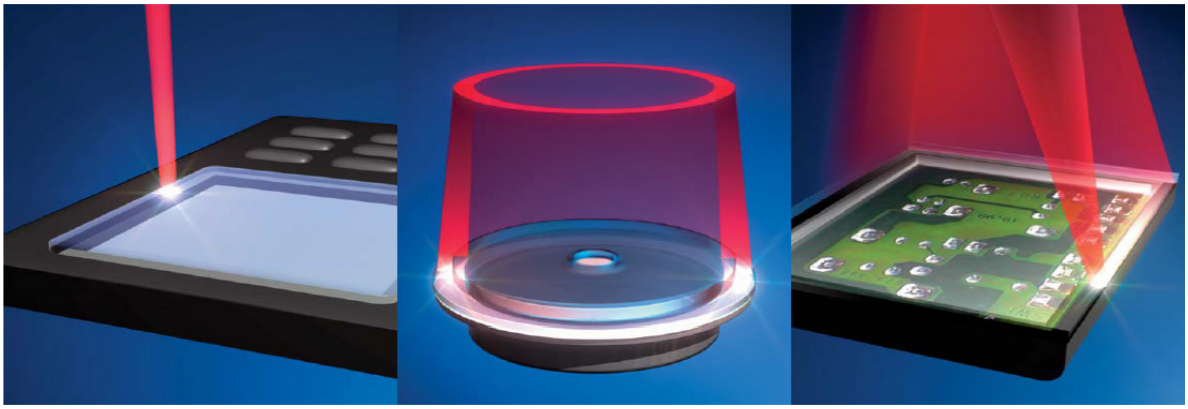

(a) (b) (c)

Figure 1. 3: Types of LTW (a) contour LTW (b) simultaneous LTW (c) quasi-simultaneous LTW (Leister, 2010)

1.2 Gap issues

1.2.1 Problems caused by gap

For industrial applications, it is often necessary to weld parts that have large and complicated geometries. Contour LTW is often the most suitable among all the laser welding processes for these types of applications. However, the major obstacle associated with contour LTW is the presence of small gaps in the interface. Gaps can exist naturally in the mating parts due to various reasons. Among them are: poor dimensional control of mating part features, inadequate clamping force, poor clamping location, warping, and a poor joint design. Contour LTW can bridge very small gaps (on the order of ten micrometers) by thermal expansion of the molten

material (Wippo et al, 2012). Gaps that exceed this dimension can cause leakage, weak or no joint locally in the weld line. The presence of these gaps interrupts thermal conduction between the two mating parts. This causes the temperature of the absorbent part to rise abruptly. If the thermal expansion does not create contact between the two parts and bridge the existing gap, thermal degradation of the absorbent part can occur (Ven and Erdman, 2007).

1.2.2 Possible solutions

Bridging gaps in the interface is a crucial issue in contour LTW. Injection moulded plastic parts can often have dimensional irregularities due to thermal residual stresses which are normally compressive at the surface and tensile at the core. These stresses can cause sink marks (Cao, 2010). Adjustment in settings for injection moulding or modifications in the part design can reduce warping or sink marks. However, in cases where gaps are unavoidable, bridging of gaps at the time of welding is required.

A possible solution of gap problems can be a specialized weld fixture design. Another method is to maximize the thermal expansion of the molten thermoplastic material which facilitates gap bridging. This method can be achieved by adjusting the process and material parameters during contour LTW. The penetration depth of the laser can be increased by using low concentrations of absorbing pigments (Chen, 2009). Larger optical penetration depth, when combined with high laser powers and low scan speeds (resulting in high temperatures) means greater thermal expansion of the material.

A relatively newer approach of gap bridging in contour LTW is the use of foaming thermoplastics (Klein and Wissemborski, 2012). Additives are mixed with the base plastic resin

during their production through injection moulding or other methods. When the laser beam heats the absorbent part, these additives undergo conversion reactions and release gases. This facilitates formation of foam which expands and bridges the interfacial gap.

1.3 Objectives

1.3.1 Experimental gap bridging

The idea of this project is to use chemical blowing agent (CBA) to improve gap bridging in contour LTW of thermoplastics. CBAs are normally used in thermoplastic foam industries to make plastic foams. Figure 1.4 (a) shows a fire resistant thermoplastic foam panel as an example of plastic foam. Foams help decrease the density of a product which in turn saves material and reduces cost. These CBAs are stable chemical compounds at room temperature. However, when heated above a certain temperature for a certain time, they undergo a chemical reaction and release gas. This released gas generates bubbles in the molten plastic material creating thermoplastic foam.

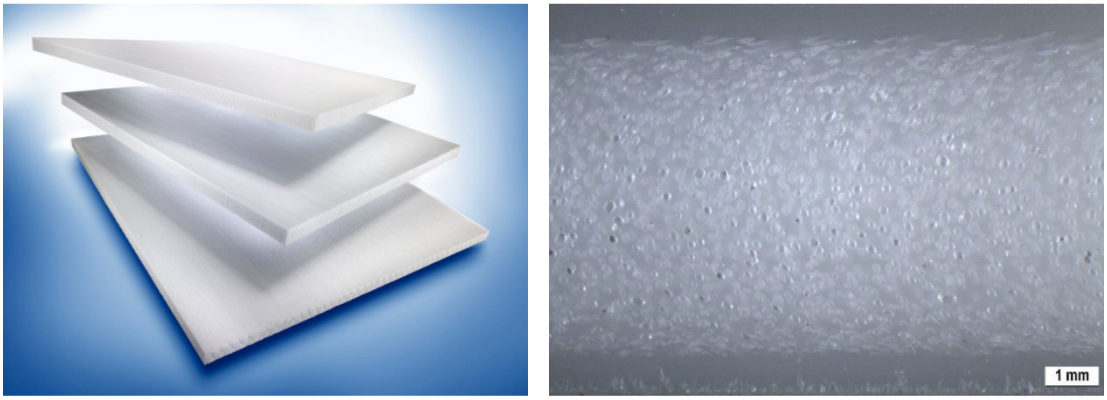

(a) (b)

Figure 1. 4: (a) Fire resistant thermoplastic foam panel (b) Injection moulding of thermoplastic foam (Thermoplastic foam, 2015)

In this project CBA was incorporated along with the absorbing pigments (Carbon black) with thermoplastic resin at the time of injection moulding of the absorbent part. The moulding conditions were kept in such a way that ensures minimal degradation of the CBA during the production. The injection moulded absorbent parts so produced thus contained unreacted CBA. At the time of contour LTW, when laser beam passed through the transparent part and hit the absorbent part, its temperature increased. Conduction between the two mating parts allowed some of the heat to be transferred to the transparent part. However the places where the gaps were present, the temperature went up even higher because there was no conduction. The combination of this high temperature along with the irradiation time caused the CBA to degrade and form foam which allows the bridging of gap. The experimental gap bridging work involved the key steps stated below.

- A number of commercial chemical foaming agent samples were obtained from suppliers. The decomposition temperature and percentage of gas release were determined through thermal degradation analysis by TGA instruments. This work is described in Chapter 3.
- A low melting point polymer needed to be selected to keep the chemical blowing agent unreacted at the time of injection moulding. The temperature of the injection moulding was kept as low as possible. The low temperatures require certain fluidity in order to fill the part. Material selection is described in Chapter 4.
- Experiments were performed to assess the level of gap bridging possible and the resultant weld strength and weld microstructure of the CBA-containing systems. The experimental procedure and results are described in Chapter 5.

1.3.2 Modelling of gap bridging

This modelling-component of this project provides a numerical technique to predict the decomposition of the CBA as a function of welding conditions (power and speed), material parameters (CB level, thermal properties) and position inside the absorbent part. The key features of the modelling work are mentioned below.

- The kinetic modelling of the CBA was performed by thermogravimetric analysis (TGA). The kinetic parameters were determined to describe the degradation reaction of the CBA as a function of temperature and time. This work is described in Chapter 3.
- A 2D thermal finite element method (FEM) model was constructed using COMSOL® MULTIPHYSICS software. This model determined temperature distribution at different locations as a function of time given known other process and material parameters. This is described in Chapter 6.
- The kinetic model for CBA degradation was combined with the temperature time profiles from FEM model and used to predict the theoretical percentage of degradation of the CBA at different locations during LTW. These results are described in Chapter 6.

Chapter 2

Literature review

This chapter focuses on reviewing the previous works related to this project. It starts with basics of LTW, related theories and process parameters. Later it introduces gap issues and possible solutions to this problem. Following this, gap bridging experiments and modelling work are discussed in detail.

2.1 Fundamentals of LTW

2.1.1 Overview of lasers

The word "Laser" is an abbreviation for light amplification by stimulated emission of radiation. The phenomenon of stimulated emission was first predicted by Einstein in 1916 through his analysis of radiation from hot objects. He postulated that there must be a radiant term based on a photon of radiation striking an excited species and causing it to release excitation energy. It was found that the stimulated photons are in phase and travelling in the same direction as the stimulating photons. A photon originated from the energy change between an excited state and a lower state is usually spectrally pure if the change is between electronic or vibrational quantum states. (Steen and Mazumder, 2010)

According to Einstein, there are three major ways of interaction between the atom and the electromagnetic field. They are: spontaneous emission, absorption and stimulated emission. Among them stimulated emission is the most significant for lasers. Stimulated emission is the

reverse process of absorption. In this process, the atom gives up its excess energy to the field in the form of photon. This added photon has the same frequency, phase and sense of polarisation. It propagates in the same direction as the wave that induced the atom to undergo this transition. This makes amplification of light which produces coherent laser light. (Steen and Mazumdar, 2010)

2.1.2 Laser beam characterization

Hundreds of lasing systems have been developed since 1960, but only a few of them are commercially significant for material processing. The most commonly used lasers in modern industry are: CO_2 lasers, solid state lasers (with lamp or diode pumping) and fiber lasers. CO_2 lasers are used at a wavelength of 10.6μm. Their significant shortcoming is the low efficiency and high absorption by plastics during transmission. Both solid state and fiber lasers operate at 1.0-2.1μm. There has been a lot of research work done recently with diode lasers and they are now available at a wide range of wavelengths, high efficiency and convenient compact form. Because of their relatively low absorption during transmission through plastics, they are the laser of choice for LTW.

There are several laser-related parameters that are critical for laser transmission welding (LTW). They are the wavelength (discussed in section 2.1.3.3), the power and the distribution of power within the beam itself. The total output power from a laser can be easily found by using a power meter. The determination of the spatial distribution of the power flux over the laser beam cross section is known as beam power-profiling. There are various techniques for laser beam power-profiling. Non-electric tools such as fluorescing plates, acrylic mode burners, burning wood/paper or observing laser beam reflection have been used for power-profiling. They are

rapid and inexpensive but limited in terms of consistency and intensity resolution. Electrical devices like camera based beam analyzers are also popular but they have severe limitations on tolerance of maximum beam intensity without damage. (Mayboudi et al, 2006)

Mechanical scanning techniques for beam profiling have been used for a long time. The main idea here is to move a small opening (a pinhole, a thin slit or a knife edge) under the beam while measuring the total beam power passing through the opening using an optical power meter. These techniques are simple, relatively inexpensive and tolerant to high laser powers. Their disadvantages are that they are time consuming and their resolution is limited by the number of samples taken. Figure 2.1 shows a typical 1 D power flux distribution profile for a high power diode laser, measured by both pin hole and knife edge method. (Mayboudi et al, 2006)

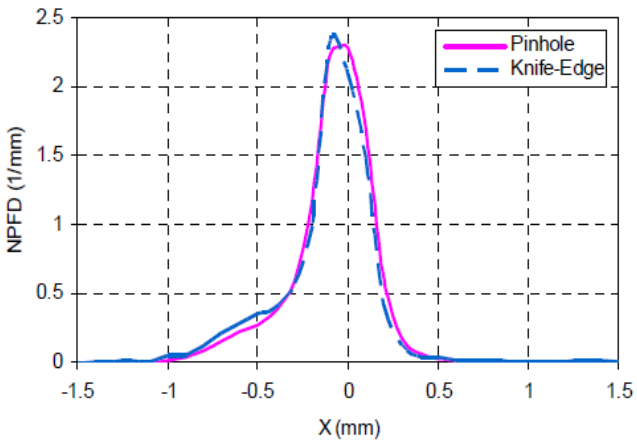

Figure 2. 1: A typical 1D power flux distribution profile for a diode laser. (Mayboudi et al, 2006)

However, a method called TEDD-LS (Transverse energy density distribution-Line Scan) has been developed which does not require any expensive equipment. Details can be found in section 2.1.3.4.

2.1.3 Optical parameters

When laser light travels through a thermoplastic part, a number of interactions happen. Some of the energy is reflected away from the part either at the incident surface or within the bulk volume of the plastic. Some portion of the light is absorbed by the material. The remainder of the energy is transmitted through the thermoplastic part. Therefore, to describe laser transmission welding, these three important parameters should be understood first. Total reflectance (R_T) is defined as the ratio of the reflected laser energy to the total input energy reaching to the incident surface of the thermoplastic part. Total absorbance (A_T) is the ratio of the laser energy absorbed by the thermoplastic to the total input energy. Total transmittance (T_T) is the ratio of the energy that passes through the plastic part to the total input energy. The mathematical relation between the three of them is as follows**:**

$$R_T + A_T + T_T = 1 \qquad \textbf{(2.1.)}$$

2.1.3.1 Reflection

When light travels from one medium to another, it can be reflected or refracted at the interface. This causes a change in the travelling direction and speed of the light. This occurs at boundaries between the polymer and air, the polymer and any reinforcements, fillers, or additives, and, in the case of semi-crystalline polymers, between amorphous and crystalline phases. Due to their different refractive indices, laser light passing through these different phases can be reflected and refracted.

During LTW, as the laser beam passes through the transparent part, reflective losses can occur in two forms. Laser light can be reflected from the top or the bottom surface which is known as

surface reflectance. It can also be reflected by the bulk volume of the thermoplastic which is termed bulk reflection.

A number of works have examined laser light reflectance during LTW. Rhew et al (2003) measured the reflectance and transmittance of PC and HDPE with a power meter attached to a circular rotating rail. For both PC and HDPE, thickness was found to have no effect on reflectance. Increasing the angle of incidence was found to increase reflectance for both. Wang et al (2009) determined the transmittance and reflectance of PP, PC and PA6 by using a spectrophotometer equipped with an integrating sphere. It was found that there is almost no influence of wavelength (for a range of 200-2500 nm) on reflectance for PC and PP. Reflectance of PA6 however exhibited a more complex dependence on wavelength. Glass fiber reinforced PA samples showed increased reflectance with increasing sample thickness related to the back scattering triggered by glass fibers. Azhikannickal et al (2012) used thermal imaging technique for measuring laser light reflection from unreinforced nylon 6. It was observed that reflectance slightly decreases with increasing thickness. At larger thickness, scattering and absorption prevent further reflection originating from the bulk and the bottom.

2.1.3.2 Absorption

When a laser beam passes through the top transparent part during LTW, some of the energy is absorbed by the part, some is reflected, and the remaining energy reaches the absorbent part. The absorbent part has carbon black pigments which makes the absorbance much higher and converts the energy into heat which causes melting of the polymer and thus enables welding.

For a single scattering polymer, the well-known Bouguer-Lambert law can be used to describe the absorbance. According to Bouguer-Lambert law (Chen, 2009), at any depth y along the beam direction, the laser light intensity $P''(y)$ will be related to other parameters as follows:

$$P''(y) = (1-\eta)\, P''_L\, e^{-Ky} \qquad \textbf{(2.3)}$$

Where P''_L is the normally incident laser light intensity from the laser head, η is the surface reflectance of the polymer and K is the extinction coefficient which is a summation of two basic parameters.

$$K=A+S \qquad \textbf{(2.4)}$$

A is the laser absorption coefficient and S is the scattering coefficient. For a non-scattering polymer, S=0. For a non-absorbing, single scattering polymer, A=0. If absorption is much larger than scattering, then the scattering portion can be ignored and it can be assumed that $K \approx A$.

Chen (2009) developed a modified version of this Bouguer Lambert law which can be applied to non-scattering, single-scattering or even multi-scattering polymers. According to this modified Bouguer Lambert Law, the output laser power (P_{out}) after passing a polymer of thickness D can be calculated as:

$$P_{out} = T_T P_{in} = P_{in}\,(1-R_T)\, e^{-A_1 D} \qquad \textbf{(2.5)}$$

Where P_{in} is the incident power, R_T is the total reflectance, T_T is the total transmittance and A_1 is termed as apparent laser absorption coefficient.

The apparent absorption coefficient (A_1) gives a measurement of absorption of light energy across the whole section perpendicular to the light's original laser beam entry direction. It takes into account the absorbed light energy travelling both along the original beam incident direction and along the increased path length resulting from scattering.

The work of Chen has shown that the relationship between the apparent absorption coefficient and CB level is linear. For natural polycarbonate (PC), which is an amorphous thermoplastic, the A_1-CB line passes through the origin which shows that absorption coefficient of unpigmented PC is almost 0. On the other hand, for polyamide (PA6) and PA6GF, there is a positive nonzero intercept. This shows that these unpigmented semi-crystalline thermoplastics have some absorption even without any CB because of their internal scattering and absorption.

Chen (2009) also developed a novel method called the direct scan method for measuring the laser absorption coefficient of absorbent parts. In this method, the speed of the laser beam along with the dimension of the beam is adjusted in such a way that the irradiation time becomes very small. For that short irradiation time, convective and conductive heat losses can be assumed negligible. A series of scans are made with a range of low to high laser powers. The minimum power required to just cause the melting of the surface can be used to deduce the absorption coefficient if one knows the material's heat capacity and melting/softening temperature.

2.1.3.3 Transmission

When a thermoplastic part is irradiated by a laser beam, after reflection, and absorption, the rest of the energy passes through the part which is termed transmission. Amorphous polymers, like PC usually have a relatively high transmission. On the other hand, semi-crystalline polymers involve much more absorbance and scattering which in turn decreases the transmission. (Kagan et al, 2002)

There are a number of researchers who investigated the transmittance of polymers during LTW. Rhew et al (2003) measured the transmittance of PC and high density polyethylene (HDPE) at varying thickness and incident angles of the laser beam. The effect of thickness on the transmittance of PC was found negligible. At an incident angle of 0º, PC showed a transmittance of 90% which decreases with increasing incident angle. On the other hand for HDPE, it was observed that the transmittance decreases with increasing thickness which is due to its semi-crystalline nature. At a thickness of 1.52 mm, the transmittance of HDPE was found to decrease with increasing incident angle. At higher thicknesses, the transmittance was so low that it was not possible to identify the effect of changing incident angle.

Wang et al (2009) investigated the effect of thickness, surface roughness and filler content on the transmittance of polypropylene (PP), PC and PA6. It was observed that the transmittance monotonically decreases with increasing glass fibre content (from 0 to 60%) for polyarylamide (PAmXD6). The surface roughness was found to have very little impact on the transmittance of PC.

2.1.3.4 Scattering

When laser light passes through the polymer matrix, scattering occurs due to reflection and refraction inside the bulk. As described earlier, this can be caused by the existence of crystalline/amorphous phases, or reinforcements/ fillers/additives inside the polymer matrix.

Vegte et al (2007) performed a laser light scattering experiment on PA6, PA46 and PBT. Sample plates were placed on the laser beam and the resulting scattered profiles were recorded using a thermal camera. The diameter of the scattered light was observed to be material dependent.

Bates et al (2007) examined the effect of different thickness and glass fibre content on LTW of polyamide mXD6. It was found that the glass fibers increase scattering and absorption, which causes the transmission to decrease rapidly with part thickness. Similar types of experiments were conducted by Grewell et al (2004) with nylon 6. The minimum power required to weld was found to be proportional with glass fiber content (0-45%).

To model the LTW process, it is necessary to know the distribution of power intensity of the beam that reaches to the welding surface after scattering inside the top transparent part. Thermographic methods have been reported to use by a number of researchers (Haberstroh et al, 2002) to characterize the scattering. These methods involve discrepancies because the conduction often widens the apparent beam area. Zak et al (2010) developed a technique to measure the transverse energy density distribution (TEDD) of a laser beam after having passed through the laser-transparent part. This technique assumes no conductive heat loss if the beam is moved quickly enough. Series of scans are taken with gradually increasing laser power, measuring weld line width each time. The power used to first melt the surface of the absorbing part as well as the line widths at higher powers are used to calculate the distribution of the laser energy after scattering inside the transparent part. Validation was done by comparing the results with the values measured by pinhole method for the same laser.

2.1.4 Process parameters

There are different categories of LTW (contour, simultaneous and quasi-simultaneous) based on laser delivery technique. Each of them has distinctive features. However, in this study, only contour LTW is relevant to this research so it will be the main focus of the discussion.

In contour LTW, the main process parameters are: laser power and laser scan speed. Two other parameters, holding time and clamping pressure also have some impact on LTW. The temperature at the weld depends on energy density at the weld interface. Energy density at the interface is determined by the laser power (W), the spatial distribution of the power from the laser, power losses due to reflection and absorption during transmission, scattering of the transmitted power, and the irradiation time which is related to the scan speed. The energy density is therefore proportional to the power and inversely proportional to the scan speed. If the temperature in the welding zone is not sufficiently high, melting and molecular diffusion will not occur and a strong joint will not be formed. On the other hand, excessive heating might cause degradation in the welding zone resulting in porosity, charring or burning. Regardless, there is generally a wide range of conditions in which acceptable quality joints can form for a specific material. The majority of the polymers are welded at the range of 0.1-2.0 J/mm^2 (Moskvitin et al, 2013). Application of the same energy density will result in the same quality joint provided the beam is moving fast enough. (Bates et al, 2013)

2.1.4.1 Laser Power and Scan Speed

It has been shown by a number of LTW studies (Grewell and Benatar, 2003; Coelho et al, 2000; Huang et al, 2013; Chen, 2009) that increases in laser power with a constant scan speed will

initially increase weld strength. At higher heat inputs, weld strength decreased which is a result of polymer degradation. Weld width was also observed to increase with laser power at a constant scan speed.

Russek et al (2003) performed contour LTW experiments on PA with a constant power and decreasing scan speeds. By examining microtomed slices, different kinds of weld zones were observed: Just adhesion, good weld and decomposition. Furthermore, from the burst pressure test of the welded samples, it was clear that for a good weld an optimum selection of laser power and scan speed is required.

For LTW, a parameter called line energy is used very often to discuss the combined effect of laser power and scan speed. Line energy (LE) is the ratio of laser power (W) and scan speed (mm/s).

$$LE = \frac{P}{v} \qquad \textbf{(2.6)}$$

However, one cannot perform a contour LTW with a very slow moving classroom laser pointer even if the desired *LE* is reached. Most of the energy will be lost to surroundings due to conduction. Bates et al (2013) developed a model to determine the critical scan speed above which the effect of conduction during the heating phase can be neglected. This critical speed depends on material and laser characteristics.

Bates et al (2007) examined the effect of line energy on contour welded semi-aromatic polyamide parts. A wide range of power (2-160W) combined with 2 scan speeds (50 and 100 mm/s and two thicknesses (1 mm and 2 mm) were employed. The shear strength values found were 50-60% of the tensile strength of the material which suggested reasonably good welds. It

was observed that the results of the two different scan speeds, plotted as a function of *LE* are superimposable which suggested that *LE* can be used to correlate contour LTW data for that speed range. Similar types of experiments were performed by Russek et al (2003) for PA which revealed similar results.

Similar experiments were conducted by Baylis et al (2003) which involved pyrometer measurements during contour LTW of thermoplastic elastomers to PP and nylon to itself. Increasing line energy was found to increase temperature in general. The effect of doubling both power and speed and maintaining the same *LE* was found to increase temperature as well as weld width. However, the effect of doubling the power and speed on weld strength was not so consistent. The high temperature at the interface might have caused degradation. These observations suggest that their initial speeds may have been below the critical scan speed discussed earlier. Haberstroh and Hoffmann (2008) performed a contour welding study with PC and POM (Polyoxymethylene). For PC, weld strength increased with increasing *LE* up to a certain extent and then started decreasing. This was because of decomposition. This phenomenon suggests that, *LE* is a suitable parameter only to a certain extent. Power intensity distribution profile and laser material interaction have an influence on welding process.

Chen (2009) developed a "non-contact method" for determining approximate start-up conditions for contour LTW. In this non-contact method, the laser transparent part and absorbent parts are kept separated using shims. Then a series of scans are made increasing the power for each scan while keeping the scan speed set at the desired value. The surface of the absorbent part is then examined for visual melting or damage. The *LE* at which the absorbent part starts to degrade,

which is very strongly related to carbon black level, often indicates the conditions required for the formation of a good weld when the two parts are in contact.

2.1.4.2 Clamping Pressure

Acherjee et al (2012) studied the effect of clamp pressure for contour LTW of PMMA and ABS. Weld strengths tend to increase with a combination of high laser power (18-21 W) and low clamp pressure (1.5 MPa), or low laser power (9-12W) and high clamp pressure (2.7 MPa). Clamp pressure ensures good conduction between the two materials. Too high clamp pressure can cause molten material to flow out and cause undesirable residual stress. An optimum value should be chosen for maximum weld quality. Huang et al (2013) experimented with PC and PA66GF and found similar results.

Ven and Erdman (2007) performed contour LTW with PVC and showed that weld strength does not vary significantly for a clamp pressure range of 0.5-4 MPa.

2.1.4.3 Part thickness

The thickness of the transparent part is a very important parameter for LTW as it affects the transmittance, absorbance and scattering which have been discussed earlier. The amount of laser energy that reaches the welding interface thus depends on the thickness of the transparent part. Semi-crystalline materials cause much more scattering compared to amorphous materials. Filler and reinforcements such as glass fibers also increases scattering. (Kagan et al, 2002; Bachmann and Russek, 2003; Vegte et al, 2007). For amorphous materials like PC, thickness does not have a significant effect on transmission. (Rhew et al, 2003)

Bates et al (2007) investigated the effect of part thickness on contour LTW for polyamide. Power required to initiate weld was found to be strongly dependent on part thickness. At higher thickness, more power is required to compensate the losses due to scattering and absorption. The effect on weld width as a function of power at different thicknesses was also observed in this work. At thicknesses such as 0.5 or 1 mm, no significant variation in beam width was found while at 2 mm the beam width increased significantly with increasing power. Lee and Ballou (2007) presented a linear relationship between laser energy transmission and thickness for 30% GF reinforced PA. Similarly, Coelho et al (2000) measured the energy density required to achieve maximum weld strength for samples of PP and PE with varying thicknesses. Increasing the energy density was needed for increasing thickness.

2.1.4.4 Carbon black level

Carbon black (CB) is the most commonly used additive to increase the absorbance of the laser absorbent part during LTW. It absorbs laser light and converts it to thermal energy. However, there are certain applications where optically transparent joints are needed, so CB cannot be applied. For such cases, a process called Clearweld^{TM} (Woosman and Sallavanti, 2003) was invented by TWI. They use materials that strongly absorb in the near infra-red spectrum while remaining virtually colorless. A thin layer of these materials are applied at the interface of the two pieces of plastic to be joined and an optically clear weld is formed.

According to Potente et al (1998), if the absorbent part contains a high level (in this case 0.5%) of CB, it can be assumed that the radiation energy is completely absorbed in a very thin layer which is called surface absorption. If the absorbent part contains a small quantity of CB, then absorption will occur over a higher thickness. Other studies by Russek et al (2003) and Chen

(2009) showed that lower CB concentration means larger optical penetration depth, and larger molten volume which facilitates better gap bridging provided a higher *LE* is applied.

2.1.4.5 Test specimen design

To assess the strength of laser welded joints, different test specimens have been used by researchers. Butt joints are commonly used to evaluate the tensile strength of hot plate or vibration welding, but it is almost impossible to join by LTW. To solve this problem, several T shaped geometries have been developed. The simplest T-weld consists of a horizontal transparent plate welded to a vertical absorbent plate. Flexing of the horizontal plate during testing might cause non uniform stress field at the weld zone. (Potente et al, 2002)

Lap joint geometries have been used for many weld strength studies. (Wu et al, 2003; Xu et al, 2003) Lap joints do not involve any meltdown therefore it is suitable for contour LTW. (Chen et al, 2007)

A number of studies have been done using a lap joint with a perpendicular weld to pull direction. (Wu et al, 2003; Xu et al, 2003) To study the effect of weld orientation, Chen et al (2007) performed a study with PC. Without any interfacial gap, no difference in strength was observed. With 102 μm gap, a weld direction perpendicular to the pull direction was found to give 25% lower weld strength than a weld direction parallel to the pull direction. The difference is the result of increased bending and peel stress in case of perpendicular weld.

2.2 Bridging gap in contour LTW

2.2.1 Issues with gap

Gaps can occur between mating parts for a variety of reasons. Large injection-moulded parts are often warped or contain sink marks. Weld or mould fixture tolerances can cause dimensional irregularities in mating parts. Inadequate clamping force or poor clamping location can also create gaps at the interface. Gaps prevent conduction of heat locally across the interface from the hotter absorbent part to the cooler transparent material. Thus leakage or weak joints can form. It also causes the temperature of the absorbent part to rise significantly higher which can lead to thermal decomposition. (Ven and Erdman, 2007)

2.2.2 Solution of gap issues

Techniques like simultaneous and quasi-simultaneous LTW can bridge small gaps through meltdown. On the other hand in contour LTW, meltdown does not normally occur. This makes gap bridging a big issue for contour LTW. (Russek et al, 2003; Kirkland, 2004; Klein and Wissemborski, 2012) A number of different solutions have been proposed which are discussed below.

2.2.2.1 Gap friendly design and processes

Clever weld fixture design can reduce or eliminate gap problems. Kirkland (2004) proposed a wedge-type tongue and groove joint which ensures intimate contact between the mating surfaces. Globo® welding, which is a modification of contour welding, involves a rotating glass sphere to create pressure locally while delivering laser energy can also help to close gaps.

(Leister, 2010) Grewel et al (2002) proposed a transparent pressure bladder which is made of two laser-transparent sheets making a closed volume within which fluid can be selectively introduced to create pressure to build intimate contact between mating parts.

2.2.2.2 Improvement through process parameter/material selection

Ven and Erdman (2007) developed a 2D model to simulate bridging of very small gaps (12.7μm and 25.4μm) in contour LTW. Operating parameters were selected by the model to create sufficient thermal strain to bridge those gaps. The agreement between the model predicted and the experiment determined weld width was adequate but not excellent. This is likely due to the assumption of all the nodes in the modeled plane being at ambient temperature initially which is not true.

In a separate study Russek et al (2003) showed that lower CB levels leads to larger molten volume and better gap bridging capability. Chen (2009) performed a detailed study on this concept. It was observed that a lower CB content with a higher laser energy facilitates gap bridging by thermal expansion. For any given scan speed, surface damage of the transparent part limits maximum power that can be delivered into the welding interface. Damage in the welding interface also sets a limit to the power that can be applied to further improve gap bridging. The maximum bridgeable gaps at a scan speed of 25mm/s were found to be 0.2, 0.4 and 0.25 for PC with 0.05 wt% CB, PA6 with 0.025 wt% CB and PA6GF with 0.05 wt% CB respectively.

2.2.2.3 Foaming

Klein and Wissemborski (2012) proposed laser induced foaming (LIS) as a method of gap bridging. The LIS process was originally developed for laser marking to generate raised structures (e.g. braille) on plastic surfaces. There are some laser sensitive LIS active substances which are added to the plastic before processing by either injection moulding or extrusion. When they come in contact with the laser beam, they undergo chemical reaction which creates localized foam in the polymer matrix. Up to 500 μm raised areas were reported to be formed by this LIS process. The authors experimented with HDPE and successfully bridged gaps up to 350 μm with a drop in weld strength of about 40%. However, the work by Klein and Wissemborski (2012) was not published in a peer-reviewed journal and many technical details are unfortunately missing.

2.2.3 Chemical blowing agents review

2.2.3.1 Introduction

A blowing agent is defined as a substance which can produce a cellular structure in a polymer mass. Blowing agents might include gases that expand when pressure is released, liquids that develop cells when they change to gases or chemical agents that either decompose or react under the influence of heat/catalyst to form a gas. Blowing agents play a very important role in manufacturing and performance of polymer foams. They affect both density and cellular microstructure and morphology of the foam. The choice of foaming agent during manufacturing of foam is often inter-linked with processing conditions. There are a wide variety of physical blowing agents that are commonly used in industry, (Eaves, 2004) however this study will focus only on chemical blowing agents which will be discussed in the following sections.

2.2.3.2 Types of chemical blowing agents

Chemical blowing agents (CBA) are defined as compounds which liberate gas(es) because of chemical reactions such as thermal decomposition. CBAs are generally divided into two major categories: exothermic and endothermic. However there are certain cases in which the required properties are such that one single type of CBA cannot satisfy all requirements. In these cases blends of endo and exothermic CBAs have been used.

During their decomposition, endothermic CBAs absorb heat which leads to broader decomposition temperature and time range. Most of the endothermic CBAs release CO_2 as the main blowing gas. These compounds are generally of white color with a white residue. The level of use of these products is normally twice than that of exothermic CBA. Regarding toxicity considerations, these compounds are known as safe because their ingredients are essentially food additives.

Exothermic compounds generate heat during their decomposition. This does not manifest significant change in temperature of molten polymer matrix though. Once the decomposition starts, it is difficult to stop it before it reaches completion. This causes rapid decomposition within a narrow temperature range. The usual level of usage of exothermic CBA is 0.3-0.5 wt% for foam applications. (Eaves, 2004)

Table 2.1 provides a short list of CBAs that are commonly used with their main features. Decomposition temperature is defined as the temperature range at which these compounds undergo chemical reaction and release gases.

Table 2. 1: Commonly used CBAs (Eaves, 2004; Zweifel et al, 2008)

CBA	Type	Decomposition Temperature (˚C)	Gas yield @ STP (ml/g)	Applications	Blowing gas
Azodi carbonamide (ADC)	Exo	205-215	220	PVC,PE,PP, ABS,PS,PA, PPO,TPE	N_2,CO, NH_3, CO_2
p-Toluene sulfonyl hydrazide (TSH)	Exo	105-110	115	EVA,EPDM, SBR,CR, NBR,NR	N_2,H_2O
4,4-Oxybis (benzene Sulphonyl -Hydrazide) (OBSH)	Exo	155-165	120-125	PE-LD,EVA, NBR/PVC, EPDM/CR, SBR,CR,NBR NR,PUR	N_2,H_2O
p-Toluene sulfonyl semicarbazide (TSSC)	Exo	226-235	120-140	PP,ABS, PE-HD, PVC-U,PPO, PS-HI,PA	N_2,CO_2, NH_3
Dinitroso pentamethylene tetraamine (DNPT)	Exo	195	190-200	NR,SBR,HI-PS, CR,BR, PVC-P	N_2,NH_3, HCHO
Polyphenylene Sulfoxide (PPSO)	Exo	300-340	80-100		SO_2,CO, CO_2
5 Phenyl Tetrazole (5PT)	Endo	240-250	190-210	ABS,PPE,PC PA,PBT,LCP	N_2
$NaHCO_3$ /Citric acid	Endo	150-230	240-185	PS,ABS,PA, PE,PP,PVC-U	CO_2,H_2O

2.2.3.3 Processing and Application

Commercial CBAs are available in different forms. Masterbatches of different particle sizes in polymeric carrier are common. Powder concentrates, or even surface coated powders are also available. On the other hand, blowing agent pastes, or dispersions in liquid carriers are also found for convenience. Among all CBAs, azodicarbonamide and its modifications account for about 85%, followed by sulfonylhydrazides. Derivatives of sodium carbonate and bicarbonates with citric acid are ranked third in commercial significance. TSSC and 5PT are specially used for high temperature applications. (Zweifel et al, 2008)

Foam extrusion processes generally start with introducing the granular thermoplastics. Then blowing agents are added in masterbatch form. Similar methods are applied for foam injection moulding. For the processing of unplasticized PVC, powdered CBA is directly added as one of the component of the dry blend. CBA containing PVC pastes are made in mixers with high speed stirrers. (Zweifel et al, 2008)

PVC is possibly the most common polymer used to make foam which can be found as floor and wall coverings, embossed tapestry, bath and gymnastic mats and so on. Expanded polystyrene foams are used for packaging and insulation applications. (Eaves, 2004) Foamed PP films are widely used in food packaging. Foams made of cross-linked LDPE or NBR/PVC blends are used as insulating materials. (Zweifel et al, 2008)

2.3 TGA for kinetic analysis

2.3.1 Overview of TGA

Thermogravimetric analysis (TGA) is a method in which a change in physical and chemical properties of a material is measured as a function of temperature or time. It is a widely used method for studying the thermal degradation behaviour of a material. (Jimenez et al, 2009; Jimenez et al, 2010; Vyazovkin et al, 2011) It is discussed here as it will be used to characterize CBAs.

Thermal analysis is applicable only for thermally stimulated processes. The rate of a thermally stimulated single step reaction generally has three major variables: temperature *(T)*, extent of conversion *(α)* and pressure ***(P)***.

$$\frac{d\alpha}{dt} = k(T)f(\alpha)h(\boldsymbol{P}) \qquad \textbf{(2.7)}$$

Generally, the effect of pressure is neglected in most of the kinetic computations. (Vyazovkin et al, 2011) However it should be realized that pressure might have a considerable effect in cases where the reactants or products are gases. The temperature dependence of the process rate is usually expressed through the Arrhenius equation given below. (Jimenez et al, 2009; Jimenez et al, 2010; Vyazovkin et al, 2011)

$$k(T) = \boldsymbol{A}\, exp\left(\frac{-E}{\boldsymbol{R}T}\right) \qquad \textbf{(2.8)}$$

Where $\boldsymbol{R}$ is the universal gas constant. E and $\boldsymbol{A}$ are known as activation energy and pre exponential factor respectively. Using the definition of $k(T)$, the following equation can be developed.

$$\frac{d\alpha}{dt} = \boldsymbol{A}\, exp\left(-\frac{E}{\boldsymbol{R}T}\right) f(\alpha) \qquad \textbf{(2.9)}$$

Thermal analysis instruments can run both isothermally (T=const.) or at constant heating rate, which is described most often as:

$$\beta = \frac{dT}{dt} \qquad \textbf{(2.10)}$$

Integration of equation 2.9 leads to an expression which does not have any analytical solution. A number of approximate solutions have been proposed by researchers. These approximations lead to a variety of approximate integrals. Though it is possible to determine the kinetic parameter using only 2 heating rates, it is recommended to use 3-5 to obtain accurate results. There are processes where the temperature variation might not follow Arrhenius equation, so the experimentally determined parameters are often referred to as apparent or effective. (Vyazovkin et al, 2011)

One important thing to keep in mind is that the thermal analysis instruments control the reference/furnace temperature precisely, and it is assumed that the sample temperature is exactly the same as the reference. It might not be true if there is poor heat conduction especially if the sample mass is big. Some researchers suggest this is one of the causes of shifting of the TGA curve towards higher temperature at higher heating rates. (Park et al, 2000). Wu et al (1993) performed TGA on PVC at 3 different heating rates (1, 2 and 5.5 K/min). These three different heating rates are indicated by the numbers 1, 2 and 3 respectively in Figure 2.2. They suggested that there might be slight differences in reaction mechanism at higher heating rates. This phenomenon was more evident from observing the residual weight fraction. More char was found to be produced at lower heating rates as shown in Figure 2.2.

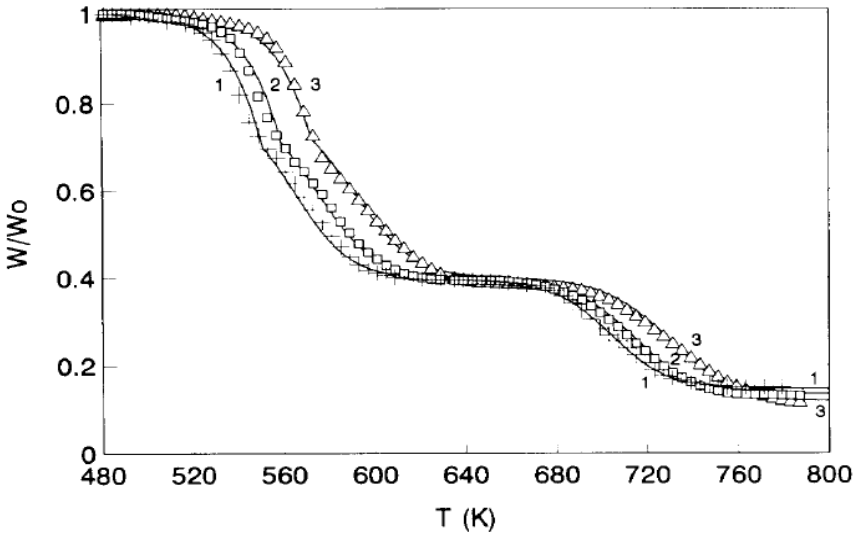

Figure 2. 2: Pyrolysis of PVC at 1, 2 and 5.5 K/min heating rates (Wu et al, 1993)

The extent of conversion α is known as the fraction of the overall change in a physical property. Thus α range from 0 to 1 as the process progresses towards completion. $f(\alpha)$ is referred to as the reaction model and represents the dependence of process rate on α. Reaction models have different forms, some of them are presented in Table 2.2. (Chrissafis, 2009)

Placing the value of β in equation 2.9, the following expression is found which is the basis for kinetic analysis.

$$\frac{d\alpha}{dT} = \frac{\boldsymbol{A}}{\beta}\exp\left(-\frac{E}{\boldsymbol{RT}}\right)f(\alpha) \qquad \textbf{(2.11)}$$

The three parameters which describe the kinetics of the reaction: $\boldsymbol{A}$, E and $f(\alpha)$ are commonly known as kinetic triplet. The purpose of kinetic analysis is to determine the kinetic triplet of a thermally stimulated process such as CBA degradation.

Table 2. 2: Different kinetic models with conversion function *f(α)* (Chrissafis, 2009)

Class	Kinetic model	Symbol	*f(α)*
n-th order reactions	First order	F_1	$1-\alpha$
	Second order	F_2	$(1-\alpha)^2$
	n^{th} order	F_n	$(1-\alpha)^n$
Diffusion	1-D diffusion	D_1	$1/2\alpha$
	2-D diffusion	D_2	$[-\ln(1-\alpha)]^{-1}$
	3-D diffusion-Jander	D_3	$3/2(1-\alpha)^{2/3}[1-(1-\alpha)^{1/3}]$
	3-D diffusion-Ginstling-Brounshtein	D_4	$3/2[(1-\alpha)^{-1/3}-1]^{-1}$
Phase boundary reactions	Contracting area	R_2	$2(1-\alpha)^{1/2}$
	Contracting volume	R_3	$3(1-\alpha)^{2/3}$
	Prout-Tompkins	B_1	$\alpha(1-\alpha)$
	Prout-Tompkins expanded	B_n	$(1-\alpha)^n\alpha^m$
	Prout-Tompkins first order with autocatalysis	C_1	$(1-\alpha)^{(1+KcatX)}$
	n^{th} order with autocatalysis	C_n	$(1-\alpha)^{n(1+KcatX)}$
Nucleation and nuclei growth	Avrami Erofeev	A_2	$2(1-\alpha)[-\ln(1-\alpha)]^{1/2}$
	Avrami Erofeev	A_3	$3(1-\alpha)[-\ln(1-\alpha)]^{2/3}$
	Avrami Erofeev	A_n	$n(1-\alpha)[-\ln(1-\alpha)]^{(n-1)/n}$

The procedure described above is only applicable for a single step reaction. It should always be kept in mind that degradation processes might involve multiple step kinetics. In that case, multiple sets of parameters should be chosen to describe the kinetics. However, in some cases with multiple steps, only one step determines the overall kinetics. In such cases assuming a single step reaction kinetics works. (Vyazovkin et al, 2011)

2.3.2 Kinetic triplet determination

2.3.2.1 Iso-conversional method

Iso-conversional methods rely on the principle that the reaction rate at constant extent of conversion only varies with temperature. These methods can be used to calculate activation energy (as a function of α) without any previous assumption on reaction model $f(\alpha)$. For this reason these methods are also known as "model free" methods. (Vyazovkin et al, 2011; Chrissafis, 2009; Jimenez et al, 2009) Commonly used iso-conversional methods include both the differential and integral categories. The most common differential iso-conversional method is the Friedman method. Integral iso-conversional methods include Kissinger-Akahira-Sunose (KAS) method, Ozawa-Flynn-Wall method (OFW) among others.

The Friedman method is the most common differential iso-conversional method used to calculate the activation energy. If we take logarithm of both sides of equation 2.9, the following expression can be found.

$$ln\left(\beta \frac{d\alpha}{dT}\right) = \ln\{\boldsymbol{A}\, f(\alpha)\} - \left(\frac{E}{\boldsymbol{RT}}\right) \qquad \textbf{(2.12)}$$

For a constant α, $f(\alpha)$ is also a constant and the term $ln\{\boldsymbol{A}f(\alpha)\}$ becomes a constant. Thus the activation energy E_α can be calculated from the slope of the plot of $ln[\beta(d\alpha/dt)_\alpha]$ versus $1/T_\alpha$. Theoretically the Friedman method is more accurate than other methods as it does not involve any approximations. However, practically applying this differential method to integral data such as TGA data requires numerical differentiation which often introduces noise and results in inaccuracy. (Vyazovkin et al, 2011)

The Ozawa-Flynn-Wall (OFW) method is based on measuring the temperature at a constant value of α and plotting it against the heating rate. It is represented by the following equation. (Chrissafis, 2009)

$$ln\beta_i = \text{Const} - 1.052\left(\frac{E}{RT}\right) \quad \textbf{(2.13)}$$

E_α can be found from the slope of the straight line plotted using the equation above.

The Kissinger-Akahira-Sunose (KAS) method is more accurate compared to OFW method. It is based on the following equation. (Vyazovkin et al, 2011)

$$ln\left(\frac{\beta}{T^2}\right) = const. - \left(\frac{E}{RT}\right) \quad \textbf{(2.14)}$$

E_α can be found from the slope of the plot of $\ln(\beta/T^2)$ versus 1/T.

It is recommended to perform a series of runs with different heating rates and measure the value of E_α for a wide range of α (0.05-0.95). A significant variation in E_α with α indicates a kinetically complex process. Integral methods are based on an assumption that E_α remains constant over the whole integration interval, which is often not true. Violation of this assumption introduces error in E_α value. However, if the difference between the maximum and minimum E_α is more than 20-30% of the average E_α, then one should consider using a differential method or computationally more complex integral methods which involve integration over small segments. (Vyazovkin et al, 2011)

2.3.2.2 Selecting reaction model

Picking the appropriate kinetic model is a critical step for model fitting. The kinetic parameters will be all meaningless if the reaction model is incorrect. One must consider: the type of the reaction, morphology of the reactants, possibility of multiple reactions etc. In case of multiple

overlapping reactions, non-linear regression analysis is required. For single step reactions, there are a variety of numerical and graphical methods available depending on the type of data. (Vyazovkin et al, 2011) For constant heating rate experiments, observing the shapes of so-called $y(\alpha)$ and $z(\alpha)$ plot are very useful. (Malek, 1992; Vyazovkin et al, 2011) If E_α (calculated from model free method) do not vary significantly with α, then the $y(\alpha)$ and $z(\alpha)$ functions are:

$$y(\alpha) = \left(\frac{d\alpha}{dt}\right) \exp(x) \quad \textbf{(2.15)}$$

$$z(\alpha) = \pi(x)\left(\frac{d\alpha}{dt}\right)\left(\frac{T}{\beta}\right) \quad \textbf{(2.16)}$$

The term x is known as reduced activation energy which is equal to (E/RT) and is used for simplicity. $\pi(x)$ is an approximation of the temperature integral of equation 2.9. There are several approximate expressions available, and the following one was chosen by Malek (1992).

$$\pi(x) = \frac{x^3 + 18x^2 + 88x + 96}{x^4 + 20x^3 + 120x^2 + 240x + 120} \quad \textbf{(2.17)}$$

Using the equations above, one can plot $y(\alpha)$ and $z(\alpha)$ curves from experimental data. Figure 2.3 shows some of the theoretical $y(\alpha)$ and $z(\alpha)$ master plots. Each one of these curves represents one reaction model from Table 2.2. Reaction model should be chosen from the best match of these theoretical and experimental $y(\alpha)$ and $z(\alpha)$ curves.

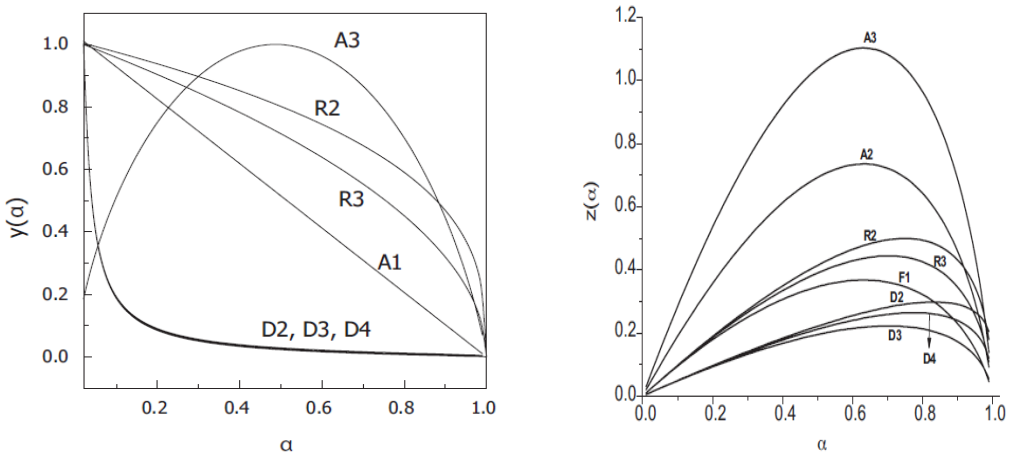

Figure 2. 3: Theoretical *y(α)* and *z(α)* master plots for different types of reaction models presented by different letters (Vyazovkin et al, 2011)

Another important parameter to observe from these plots is the corresponding value of α at which the curves reach their maximum. For *y(α)* plots, this parameter is referred to as α_M, and for *z(α)* it is α_p^{∞}. Vyazovkin et al (2011) reported values of these parameters for different reaction models. Malek (1992) has developed a procedure which summarizes all these information and allows one to pick the most suitable model. Observing the shape of the y(α) plots and using the α_M and α_p^{∞} values, the appropriate reaction model can be chosen using this flow chart proposed by Malek. Figure 2.4 shows the procedure schematically. RO stands for reaction order model, SB stands for the Sestak-Berggren's equation and JMA represents Johnson-Mehl-Avrami equation which is used for crystallization kinetics.

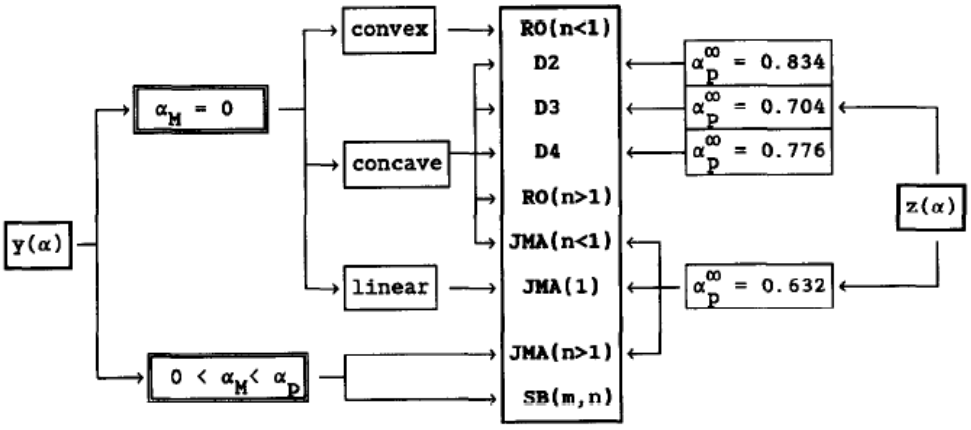

Figure 2. 4: Schematic diagram for determination of kinetic model from experimental data (Malek, 1992)

2.3.2.3 Model fitting

Derivation of the kinetic parameters to represent the conversion and temperature dependence of the reaction rate is known as model fitting. Basically it involves minimizing the difference between experimental and theoretical data on the reaction rate. This minimization can be done by either linear or non-linear regression methods. Non-linear regression methods are computationally complex and time consuming but they offer better accuracy than linear methods.

Linear model fitting methods are applicable once the rate equation is converted to a linear form. For a single step reaction, it is very simple to do so. Rearranging and taking the logarithm on both sides gives a linear plot. However, for multi-step reactions, it might not be possible to linearize the equation and in those cases non-linear regression methods should be employed.

Once a linear plot is obtained, the rest of the procedure can be done by several ways. (Vyazovkin et al, 2011) A very useful method is the combined kinetic analysis suggested by Jimenez et al (2009). It proposes the following expression of *f(α)*

$$f(\alpha) = c(1-\alpha)^n\alpha^m \quad \textbf{(2.18)}$$

This equation is known as the modified form of the Sestak-Berggren empirical equation. By adjusting the parameters *c, n* and *m,* it can fit any reaction model presented in Table 2.2. Thus it works as an umbrella function which covers any common reaction model. Putting the value of *f(α)* in equation 2.9 and taking logarithm, the following expression is found which is the basis of this combined kinetic analysis method.

$$ln\left(\frac{\frac{d\alpha}{dt}}{(1-\alpha)^n\alpha^m}\right) = lncA - \left(\frac{E}{RT}\right) \quad \textbf{(2.19)}$$

Parameters that give the best linearity of the above equation are chosen as best fit values and then the corresponding *E* and ***A*** can be calculated easily.

Non-linear model fitting methods are applicable for any kind of reaction mechanism (single or multiple step). Non-linear regression is based on minimizing the difference between calculated and measured data. Least square method calculates this difference in the form of residual sum of squares (RSS).

$$\text{RSS} = \sum(y_{exp} - y_{calc})^2 = min \quad \textbf{(2.20)}$$

y_{exp} might be the rate *(dα/dt)* of the process measured from thermal instrument. y_{calc} would then represent the calculated value of rate by substituting the variables *(T, α)* and parameters *(E, A).* RSS is thus measured and compared with the previous value. This method continues to take new sets of parameters and calculate the RSS unless the minimum is obtained. (Vyazovkin et al, 2011)

2.4 Modelling of gap bridging

2.4.1 Modelling of LTW

Modelling of the LTW process enables one to optimize process variables to obtain the desired quality weld. There have been many modelling studies proposed to describe LTW process. These can be categorized into three types described below.

2.4.1.1 Analytical Modelling approach

Potente et al (1998) proposed a physico-mathematical model to describe the heating phase of contour LTW performed by a Nd:YAG laser. They made a number of assumption's (constant heat flow, negligible conduction along weld seam and seam width, negligible convection etc.) to make it analogous with single sided heat impulse welding. Although their work was based on assuming surface absorption which requires a high CB level, introducing a correction factor would make it applicable for low CB level as well.

Grewell and Benatar (2003) modelled heat flow during contour LW using (1) a simple moving point heat source (2) a Gaussian distributed heat source. For both of the cases, semi-infinite body and constant material properties were assumed. A coherent single diode laser with 828 nm wavelength and two focal spots (25 and 50 μm) were used. Both of the models predicted weld width accurately for 25 μm lens, but distributed model was found more accurate for 50 μm lens.

Chen (2009) proposed a simple analytical 1D model to estimate the effect of parameters on temperature and thermal expansion at the interface for a non-contact method. It is applicable only for non-scattering polymers. This model allows one to calculate maximum bridgeable gap for given weld conditions. Bulow et al (2009) presented an analytical model to determine the

minimum line energy for welding (MLEW). Their expression of MLEW was directly related to upper melt zone thickness and heat diffusion parameter along with other material and laser parameters. In their work they introduced scattering particles (TiO2) to increase the optical path length which facilitates decrease in cycle time.

2.4.1.2 Finite difference method (FDM)

Kurosaki (2005) proposed a 1D finite difference method to obtain temperature profiles during CO_2 laser welding. They carried out the simulation for welding of LDPE films, with and without the use of a heat sink (which is a laser transmissive part kept in contact with the laser irradiated surface to stop overheating and burning). The temperature profiles obtained from the model shows that the use of heat sink moves the maximum temperature region towards the center of the thermoplastic part. The weld interface should be set on such depth. This method allows one to carry out welding without pigmentation of the bottom part.

Hadriche et al (2010) presented a 2D finite difference model to study the effect of laser power and scan speed on the weld microstructure. A diode laser was employed to contour weld PP. This model included convection, conduction through the pieces and heat generation from absorption. Coupling the heat equation and the kinetic crystallization, it was possible to measure the evolution of crystallinity throughout the process. Bulow et al (2009) used Monte-Carlo simulation to describe the optics to FDM model contour LTW of polyethylene octane elastomer (POE). The output from their model was in good agreement with experimental data.

2.4.1.3 Finite element method (FEM)

Ven and Erdman (2007) constructed a 2D model for contour LTW of PVC to predict internal temperature and pressure. The mathematical programming was done using MATLAB. Heat transfer components include: convection and radiation from top and bottom surfaces, conduction within each material and between the two materials, reflections at both surfaces and heat generation from absorption. Temperature dependent properties were stored in lookup tables. Comparison of the experimental and model predicted weld width gave a difference of 4.3% which suggests a good agreement. Maram (2010) used a 2D transient thermal model to obtain the temperature-time profile for welding of blended polybutylene terephthalates (PBT) and polyethylene terephthalate (PET). To describe the scattered profile reaching in the interface, the TEDD-LS method developed by Zak et al (2010) was employed. The laser beam moves through the 2D plane perpendicularly, giving a time dependent heating profile. The beam power distribution profile was obtained by pin-hole method. His model was used in this study for modelling purpose.

A 3D model was developed by Mayboudi et al (2007) using an ANSYS FEM code. In her work, the beam was assumed to have uniform distribution along the shorter dimension. The processing time for this model was 36 hours. Chen (2009) also developed a 3D thermal FE model to simulate heat transfer during contour LTW of PC, PA6 and PA6GF. To reduce the computing time, a mass flow was introduced in the model which made the model time independent. Comsol® multiphysics software was employed and both contact and non-contact methods were modelled. This model predicted weld width and HAZ (heat affected zone) reasonably. However the temperature in the transparent part near the incident surface was found

to be overestimated. The reason is probably the larger volume of material than considered in the model which absorbs the energy. Geiger et al (2009) carried out FEM analysis to simulate contour LTW of PP. The molten pool geometries determined experimentally was found in good accordance with model predicted ones.

Speka et al (2008) proposed a 3D model using COMSOL for welding of PMMA-ABS/PC. The laser spot was assumed circular to reduce computing time. Infrared thermography was used to calibrate the model. Ilie et al (2009) FEM modelled contour LTW of ABS using COMSOL. To describe the scattering, they applied an inverse algorithm which allows obtaining an equivalent material than causes the same attenuation and broadening. In the next step applying Mie theory and Monte Carlo method, the profile shape is obtained.

2.4.2 Modelling of degradation

FEM models described above can predict temperatures as a function of time during LTW, but they do not give any measure of thermal degradation. Maram (2010) developed a technique for measuring degradation during LTW. He used the Freeman-Carroll method to determine kinetic parameters to describe the thermal degradation behaviour of PBT/PET blend. He then used these parameters in combination with the temperature time profiles obtained from FEM model to describe amount of degradation. It was found that above 80W the percentage of degradation becomes significant. At this power range, weld strength also started to decline which confirms the validity of this approach. Okoro (2013) carried out similar experiments for simulating thermal degradation with PC and PA6. He developed a MATLAB code to perform integration of the kinetic rate equation and calculate the amount of degradation.

Chapter 3

Analysis of Chemical Blowing Agent

This chapter provides a short review of the chemical blowing agent (CBA) samples used in this research. It describes the thermogravimetric analysis (TGA) of the CBA samples to determine the kinetic triplet for the degradation reaction. It also discusses the kinetic modelling which is required to assess the degradation of CBA during foaming.

3.1 CBA Samples used

This project started with a brief survey of the CBA samples commonly available in market. The most important criterion of selecting CBA was the decomposition temperature. For this work the CBA needs to be incorporated with the base resin (LDPE) without being decomposed during injection moulding. To fulfil this requirement the decomposition temperature of the CBA must be higher than the melting point of the base resin LDPE (110ºC). Four different CBA samples were obtained for this project. The first 3 are from Tramaco GmbH and last one from Bergen International. The name of the samples and the properties are given in Table 3.1.

Table 3. 1: Basic properties of the CBA samples

Sample Name	Appearance	BA content (%)	Decomposition temperature (ºC)	Exo/ Endo thermic	Gas yield (ml/g)	Compatibility
TRACEL® IM 2240 ST (5-Phenyl tetrazole)	Grey granule	20	240	Exo thermic	130	PC, PETP, PBTP
TRACEL® NE 7200 (NaHCO3 + Citric acid)	White pellet	65	145-200	Endo thermic	83	PE, PP
TRACEL® NE 2555 (NaHCO3 +Citric acid)	White pellet	25	135-155	Endo thermic	24	EVA, LDPE, TPO, TPE, TPU & PS
BERGEN XO-331 (Modified Azo Dicarbon amide)	White pellet	N/A	245-250	Exo thermic	N/A	N/A

3.2 TGA of CBA samples

TGA experiments were carried out using TGA Q50 V.20.13 Build 39 instrument located at Royal Military College of Canada. Experiments were performed on all of the CBA samples. Figure 3.1 shows the sample weight as a function of temperature for TRACEL® IM 2240 ST, TRACEL® NE 7200 and BERGEN XO-331 for a heating rate of 5℃/min. Weight loss curves for other heating rates can be found in Appendix B.

Initial results showed that TRACEL® NE 7200 started to release gas at relatively low temperature (about 150˚C) which is not acceptable for this project as the aim is to keep the CBA undecomposed during injection moulding. For this reason, TRACEL® NE 7200 was not considered for this project in spite of having the largest gas yield. BERGEN XO-331 was found to have a higher decomposition temperature (about 200˚C) but its gas yield was lower compared to that of TRACEL® IM 2240 ST. For this reasons TRACEL® IM 2240 ST was chosen finally and the kinetic analysis was performed on it. It will be referred to as 5PT.

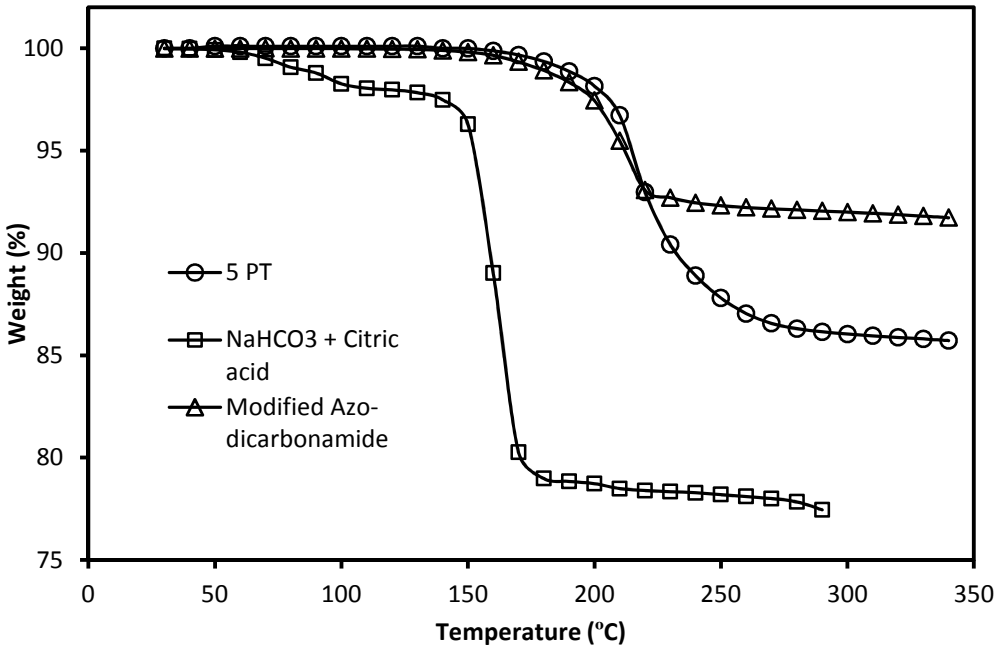

Figure 3. 1: Thermal decomposition curve for TRACEL® IM 2240 ST (5 PT), TRACEL® NE 7200 (NaHCO3+ Citric acid) & BERGEN XO-331 (Modified Azodicarbonamide) at 5℃/min heating rate

Figure 3.2 describes the thermal degradation behaviour of 5PT. Four different heating rates were applied (5, 10, 15 and 20˚C/min) for this case. Weight loss starts at about 200ºC and continues up until 300ºC where it levels off. This indicates that the majority of the decomposition of CBA and gas release occurs within this temperature range (200 ºC -300 ºC).

To make sure that there is no significant weight loss after this temperature, the sample was further heated up to 340ºC. It can be found that the weight of the residue after decomposition is slightly different for different heating rates. There might be a slightly different decomposition mechanisms taking place at higher heating rates. Same type of observation in TGA curves was reported by Wu et al (1993).

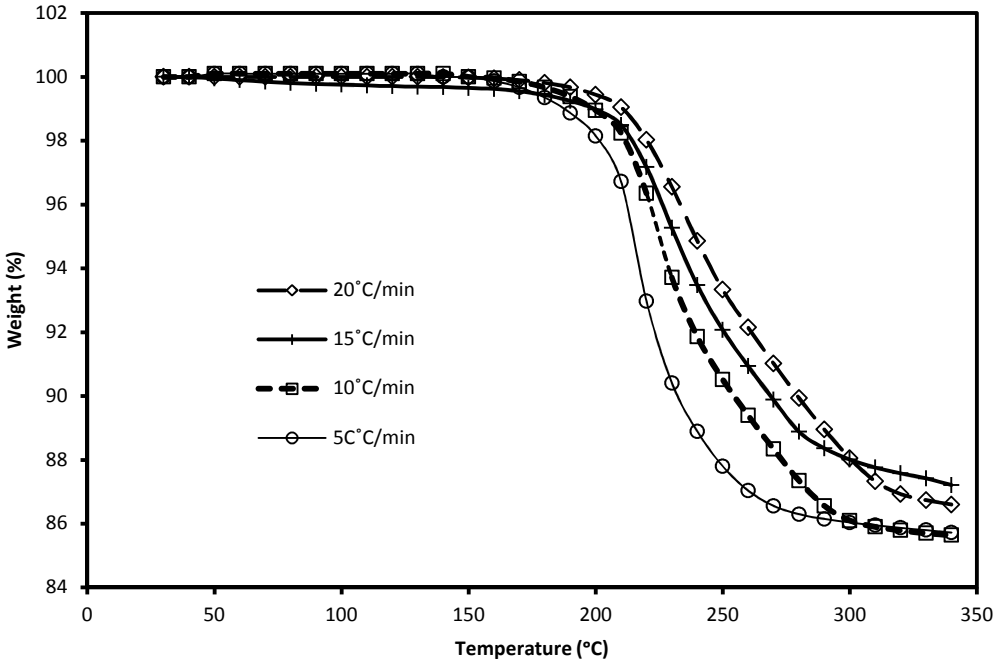

Figure 3. 2: Thermal decomposition curves for 5PT

For all of the TGA curves, one thing is commonly observed: that the curves shift to higher temperatures with higher heating rates which is expected and normal. The reason for this behaviour is explained in section 2.3.1.

3.3 Kinetic analysis of 5PT

3.3.1 Calculation of activation energy (model free method)

As discussed in the literature review chapter, the first step of kinetic analysis is to determine activation energy. Three different methods (Friedman, KAS and OFW) were employed for this purpose.

Figure 3.3 shows the values of activation energy calculated by three different methods. The KAS and OFW methods (presented by equations 2.13 and 2.14) give almost same values while Friedman method gives 19% larger values of activation energy. However, Friedman method is more sensitive to experimental noises as discussed in literature review section 2.3.2.1.(Vyazovkin et al, 2011). The average value of activation energy (125 kJ/mol) by two other methods are taken for kinetic triplet determination.

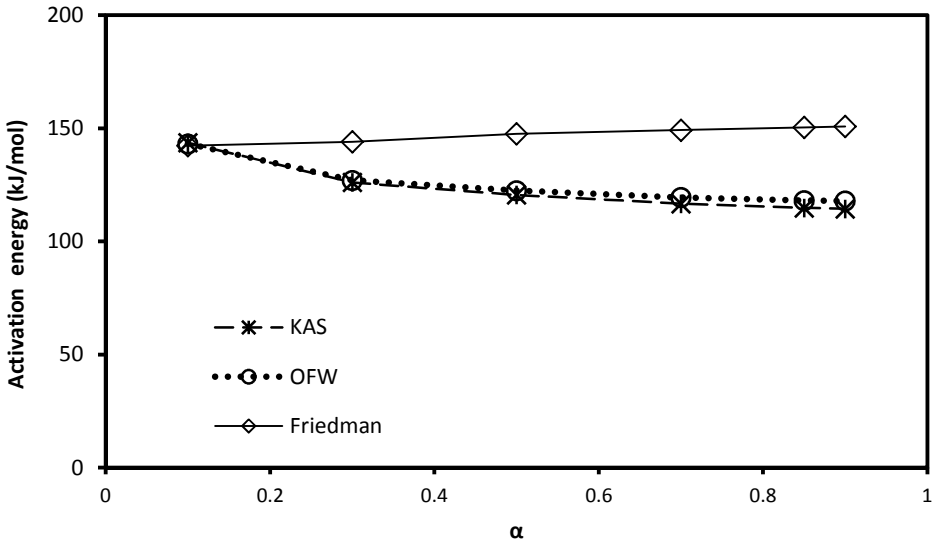

Figure 3. 3: Activation energy *(E)* versus *α* for 5PT by three different methods

3.3.2 Model selection for reaction

Once the activation energy is determined, the next step is to observe the shapes of y(α) and z(α) plots and to determine the maximums using the method described in section 2.3.2.2 .

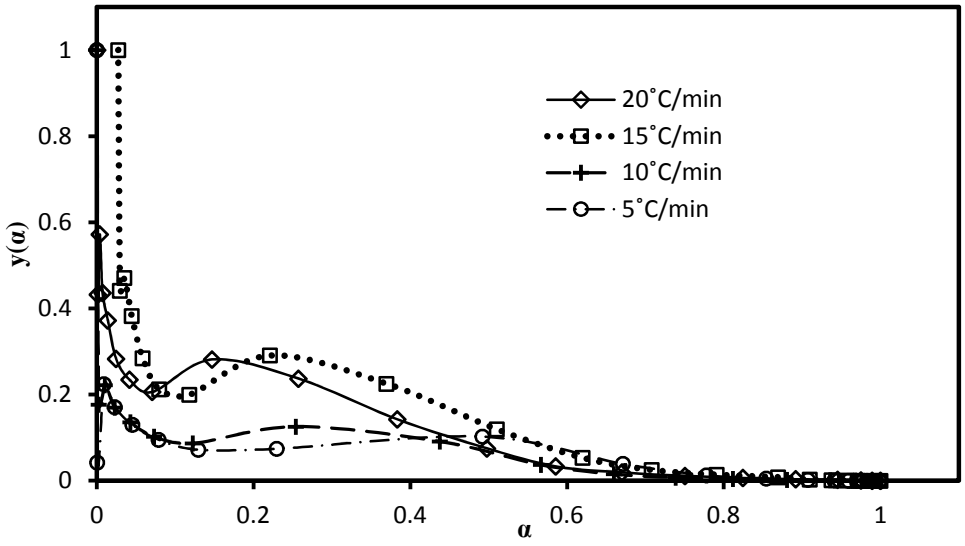

Figure 3. 4: Experimental *y(α)* versus *α* plot for 5PT at different heating rates

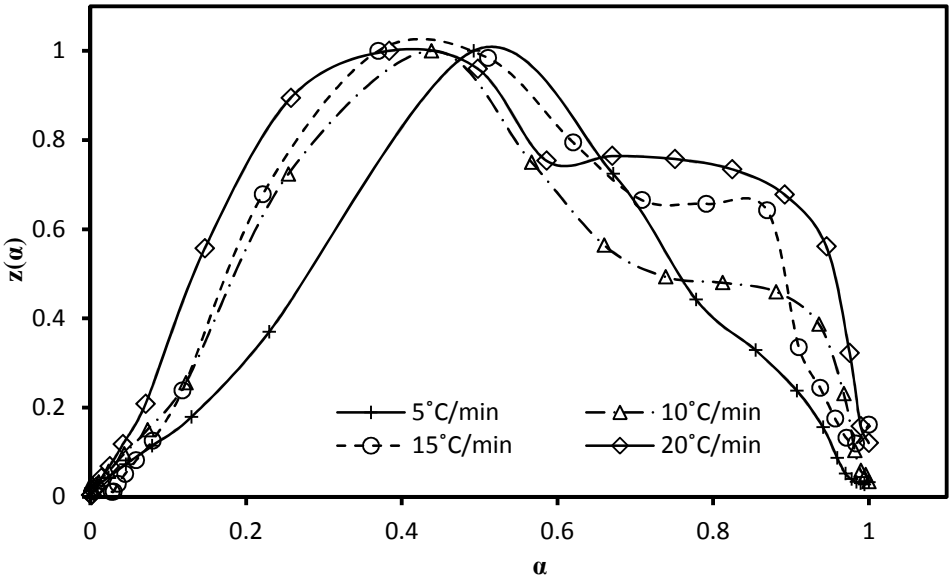

Figure 3. 5: Experimental *z(α)* versus *α* plot for 5PT at different heating rates

It can be seen from Figure 3.4 that $y(\alpha)$ plots have concave shape, with a α_M at 0. It can also be seen from Figure 3.5 that α_P^{∞} value ranges from 0.36-0.49. Using the above three findings and following the flowchart given in the literature section 2.3.2.2., a RO model [$f(\alpha) = (1-\alpha)^n$] with $n>1$ was found to be suitable to describe this reaction.

3.3.3 Determining kinetic triplet

Once the RO model is chosen, the determination of n and $\boldsymbol{A}$ parameters are relatively straight forward. According to literature review section 2.3.2.3., with the temperature kept constant, $ln\ (d\alpha/dt)$ versus $(1-\alpha)$ plot gave the value of n as its slope. The value of $\boldsymbol{A}$ was calculated from the intercept. 9 different temperature values were taken for this purpose which gave 9 different values of n and $\boldsymbol{A}$. Average value of n (1.6) and $\boldsymbol{A}$ (2.4×10^{12} 1/s) were used for model fitting. Figure 3.6 shows one typical $ln\ (d\alpha/dt)$ versus $(1-\alpha)$ plot at 513K temperature.

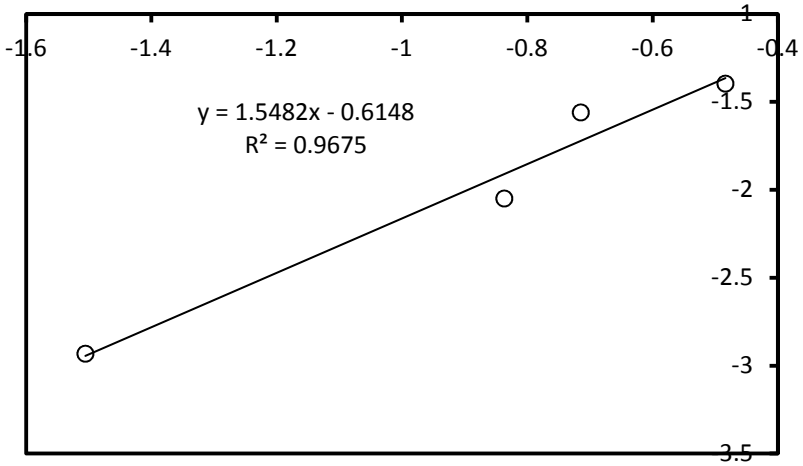

Figure 3. 6: ln (dα/dt) versus (1-α) at constant temperature (513K)

3.3.4 Model fitting`

Using the kinetic parameters obtained above, the TGA weight as a function of temperature predicted by the kinetic model was calculated and compared with the experimental TGA data points to assess the validity of the model. The equation to describe the kinetic model is given below.

$$\frac{d\alpha}{dt} = 2.4 \times 10^{12} e^{\left(\frac{-E}{RT}\right)} (1-\alpha)^{1.6} \quad \textbf{(3.1)}$$

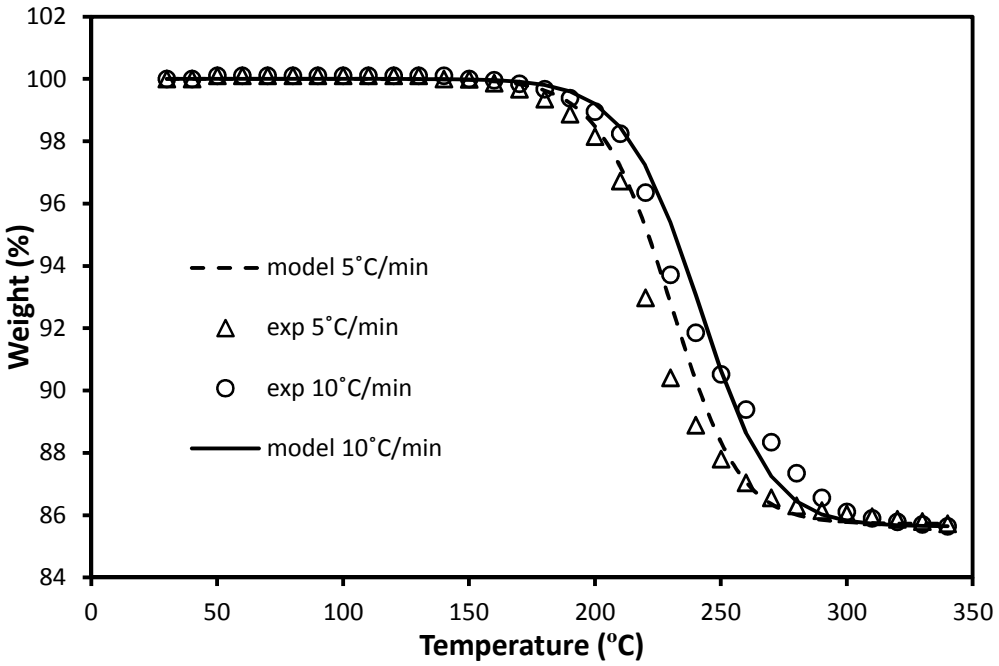

Figure 3. 7: Experimental and model predicted thermal degradation at two different heating rates (5 and 10˚C/min)

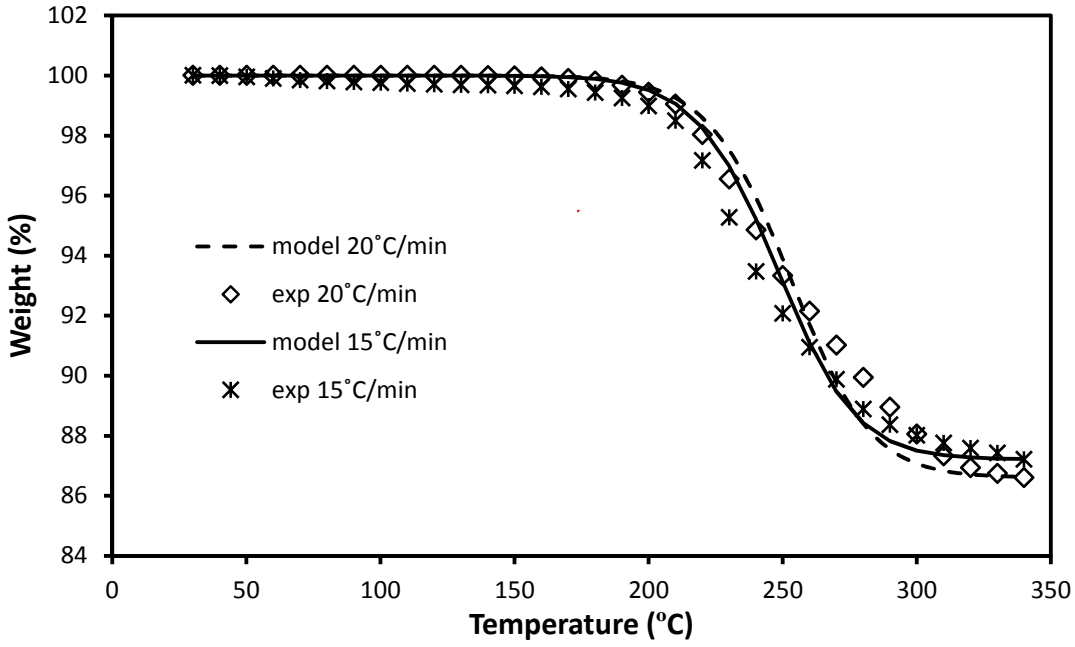

Figure 3. 8: Experimental and model predicted thermal degradation at two different heating rates (15 and 20˚C/min)

It can be seen from figures 3.7 and 3.8 that, the prescribed kinetic model gives a match that is within 2.66% to experimental TGA curves.

Chapter 4

Material

4.1 Base resin

For this project, LDPE material was sourced from DuPont Canada. LDPE was chosen as base resin because of its low melting point. One of the challenges of this project was to incorporate the CBA with the base resin during injection moulding without allowing the CBA to decompose. A low melting point and high flow-rate were therefore necessary to keep the temperature of injection moulding lower than typical decomposition temperatures of 5PT while allowing the thin walled part to be filled. Table 4.1 represents some general properties of the resin. High melt flow index allows proper mixing of the CBA with the base resin during injection moulding and allows the thin walled parts to be moulded without using high injection pressures or temperatures.

Table 4. 1: Properties of the resin

Property	Unit	For Dow LDPE 959S
Density	g/cm^3	0.923
Melt Index	g/10 min	55
Tensile Strength	MPa	11
Melting Temperature	ºC	110

DSC tests were performed using the DSC Q100v9.6 Build 290 TA instrument located at Royal Military College of Canada to ensure the melting point of the sample is the same as mentioned. The weight of the sample was 6.34 mg and 10℃/min heating rate was applied. Figure 4.1 shows DSC results for the resin.

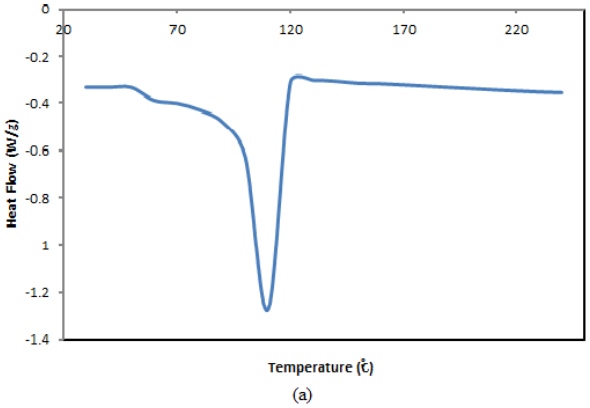

Figure 4. 1: DSC data for Dow LDPE 959S

4.2 Carbon Black

A Carbon black masterbatch with 2.6 wt% CB concentration, supplied by the Color Master Inc. was used in this study. This masterbatch is made of carbon black named Monarch 880, compounded with a linear low density polyethylene (LLDPE) carrier.

4.3 Chemical Blowing Agent

The procedure of CBA selection is described in section 3.1 & 3.2 in details. The CBA, TRACEL®IM 2240 ST was supplied by Tramaco GmbH. This chemical is a polymer bound 5-phenyl-tetrazole with 20% blowing agent content. The decomposition temperature is about 200℃ according to the manufacturer. The recommended use level for structural foam production is 1.5%-2%.

4.4 Manufacturing the test samples

4.4.1 Formulation

Two sets of test samples were made, with and without CBA. The top transparent parts were made only with natural LDPE. Black parts were made by mixing the CB masterbatch with LDPE to obtain 0.05% CB concentration. This CB concentration is generally considered low and favourable for a deeper penetration of laser energy. As discussed in section 2.2.2.2., for a better gap bridging, deeper laser penetration is necessary (Chen, 2009).

To make parts with foaming agent, the CBA masterbatch was added to LDPE along with CB, to obtain a CBA concentration of 5% and CB concentration of 0.05%. In this case, the CBA level was generally higher than normal recommended level for foaming applications. Table 4.2 represents the details of formulation of both sets of sample for a batch of 1 Kg material.

Table 4. 2: Formulation of the absorbent samples with and without CBA

Sample	Without CBA (g)	With CBA (g)
LDPE	980.77	730.77
CB masterbatch	19.23	19.23
CBA masterbatch	0	250

4.4.2 Injection moulding

To make rectangular plastic plaques from the base resin and masterbatches, an Engel 55 ton injection moulding machine from Royal Military College of Canada was used. Mixing of the components was done manually before charging into the injection moulding machine. The plaques made by the moulding machine had a dimension of 100mm×100mm×3.2mm. The conditions shown in Table 4.3 were used in order to minimize CBA decomposition in the injection moulding machine.

Table 4. 3: Operating conditions of Injection moulding

Plastification Phase	
Barrel Temperature	130℃
Nozzle Temperature	130℃
Screw speed	240 rpm
Back pressure	40 bar
Injection Phase	
Boost cut off	10 mm
Boost Pressure	50 bar
Stroke	56 mm
Injection time	1.6s
Holding Phase	
Pressure at first 4s	30 bar
Pressure at next 4s	40 bar
Cooling Phase	
Cooling time	22s
Mold Temperature	18℃

4.4.3 Cutting to make test strips

After injection moulding, each rectangular part was cut using a band saw to obtain test samples of dimension 90mm×25mm×3.2mm which were used to perform pull tests after welding. Each of the rectangular part thus gave 3 test samples. The dimensions of the sample plaques and test strips are shown in Figure 4.2.

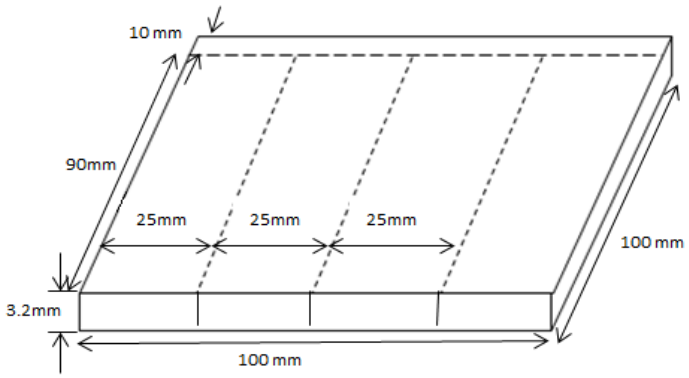

Figure 4. 2: Dimensions of the plaque and test strips

Chapter 5

Experimental Work

5.1 Equipment and Procedure

5.1.1 Laser workstation

All the welding experiments have been done using a continuous-wave diode laser Rofin-Sinar DLx16 (940 nm wavelength) and UW200 workstation as shown in Figure 5.1. The laser head can be moved up and down along z axis, and the welding fixture along x and y axis. It thus provides a three axis linear motion system. The maximum travel speed is 150 mm/s. The laser beam is made up of 100 separate laser diodes which in combination make a single focused spot. A maximum of 160W power can be delivered by this machine. The focal point of the laser is 82.5 mm distant from the laser head.

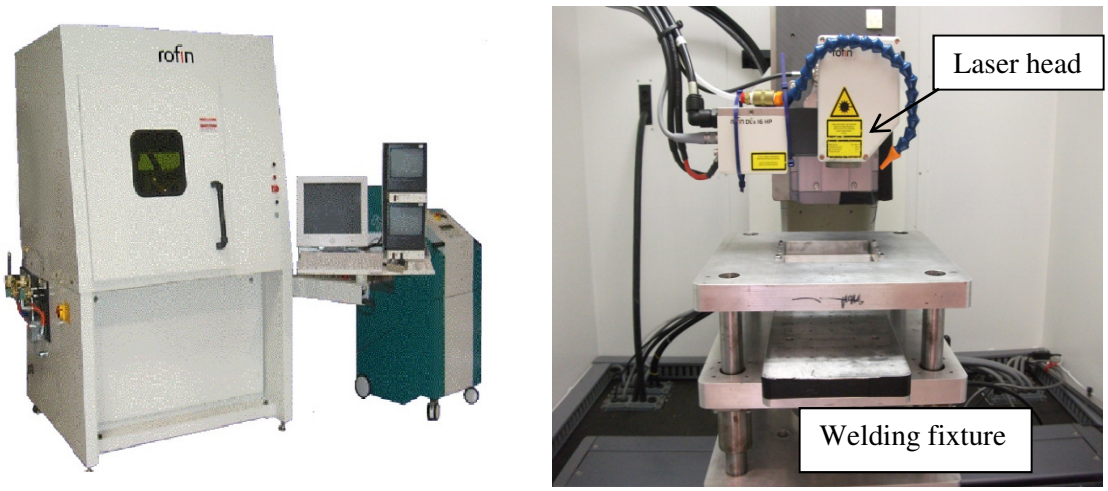

Figure 5. 1: Rofin-Sinar DLx16 HP diode laser in UW200 workstation with a close-up view of the laser head.

5.1.2 Determination of the process window

In order to determine the laser welding conditions for LDPE, the non-contact method developed by Chen (2009) was used. A laser transparent and a laser absorbent part were separated by 0.5mm shims and clamped together. The working distance, which is the distance between the bottom of the laser head and the absorbent part, was kept at 82.5 mm. This working distance is chosen because this is the focal point and thus gives the most uniform power distribution (Chen, 2009). A series of 15 mm long scans were made. For a scan speed 25 mm/s, the laser power was increased in 1 W increments for every scan while for 50 mm/s the increment was 2W. After scanning, the surface of the absorbent part was investigated carefully for visible signs of melting and degradation. According to Chen, the power which causes degradation at this non-contact test would create a good weld when both the parts are in contact because thermal conduction will decrease the temperature of the interface.

The test was performed on samples with and without CBA. Two scan speeds (25 and 50 mm/s) were used for this test. Figure 5.2 shows the results of this non-contact test. It can be seen that regardless of having or not having CBA, the operating window for welding is similar. In general it can be said that melting starts at 0.4-0.5 J/mm *LE*, while degradation starts at 0.7-0.8 J/mm. The graphs are extrapolated backward to obtain operating conditions for scan speed 5 and 15 mm/s. It can be found that for 25 mm/s scan speed, degradation starts at 18W and 20W for samples with and without CBA respectively. When these parts are in contact, powers in this range should therefore create a weld. The similarity between the two graphs is due to the same CB concentration of 0.05 % being used in each case. The CB concentration affects the power required to cause either melting or degradation for a given material and laser system.

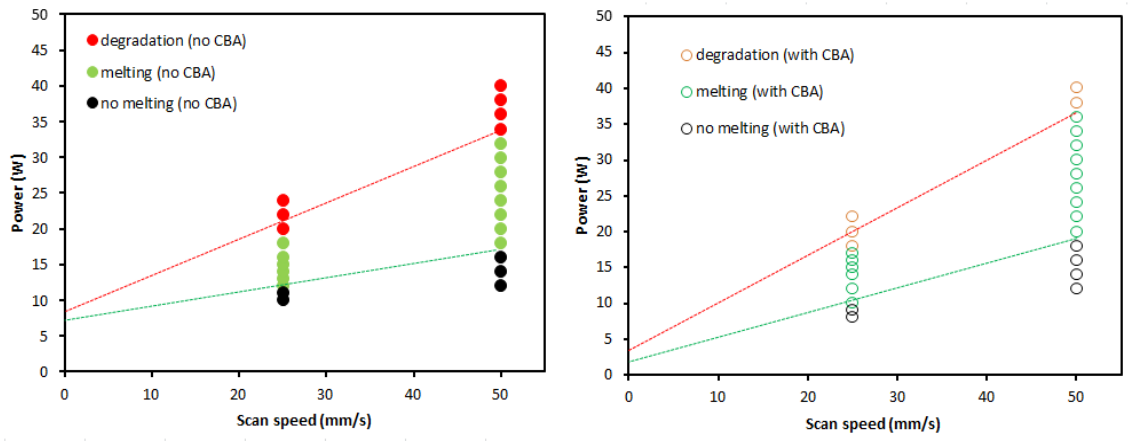

Figure 5. 2: Results of non-contact method for samples (a) without CBA (b) with CBA. The green line stands for the start of melting while the red line stands for degradation

5.1.3 Laser fixture

To perform the pull-test for the weld strength study, the geometry described in Figure 5.3 was employed. The mating sample strips were 90 mm in length. An overlap length of 20 mm was used during welding, and by moving and adjusting the position of the clamping fixture, the weld line (15 mm) was made in the middle of the overlap region. Thus the weld line started and ended 2.5 mm away from both the edges. Figure 5.4 shows a real welded sample. The orientation of the weld line parallel to the pull direction was suggested by Chen. (Chen et al, 2007)

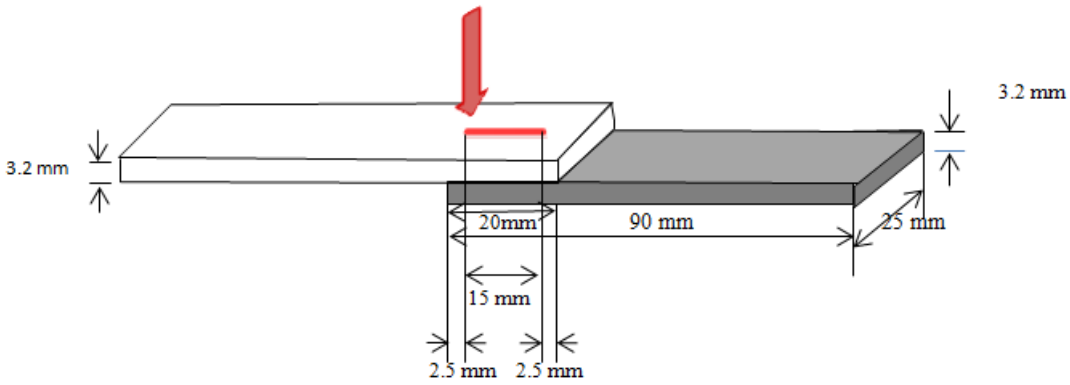

Figure 5. 3: Dimensions of the lap shear weld specimen

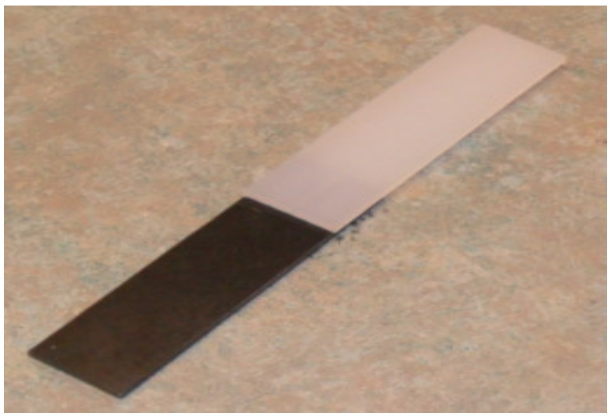

Figure 5. 4: Image of the welded sample after taking out from the laser fixture

A purpose-built laser fixture was made in order to hold the samples with the shims together while applying clamp force. A metal mask was used to ensure the length of weld is 15mm every single time. This mask was attached to the lower surface of the upper clamping fixture using an adhesive tape.

Pins were used on the fixture to position the samples in the same location for every weld. On one side, spring loaded pins were used to allow for a little dimensional irregularity. To hold the shim between the samples better, two pins were employed. This combination kept the samples

from moving in the fixture during loading while allowing the welded assembly to be easily removed after welding. Figure 5.5 shows some of the images of the laser fixture.

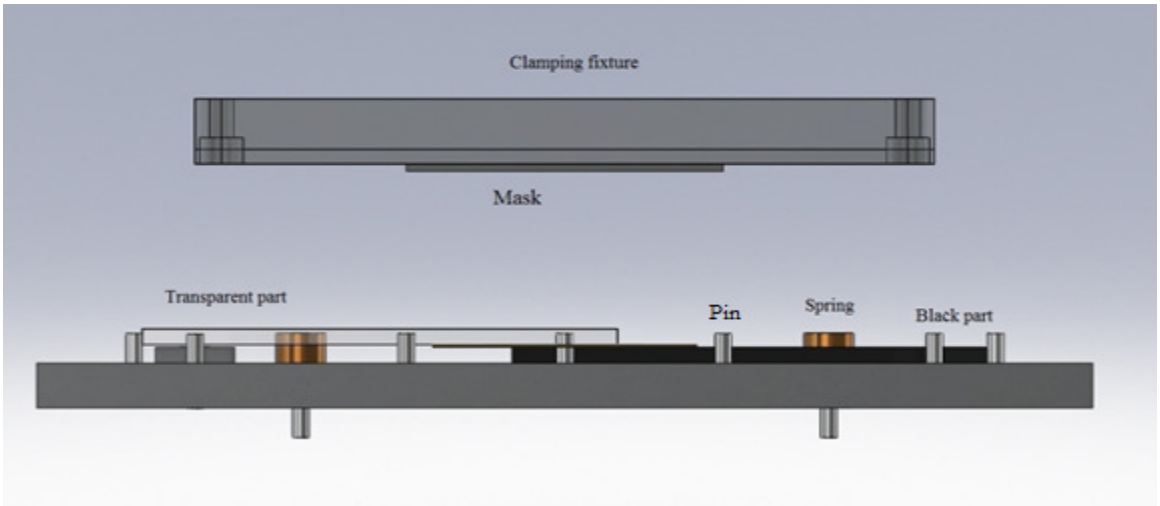

(a)

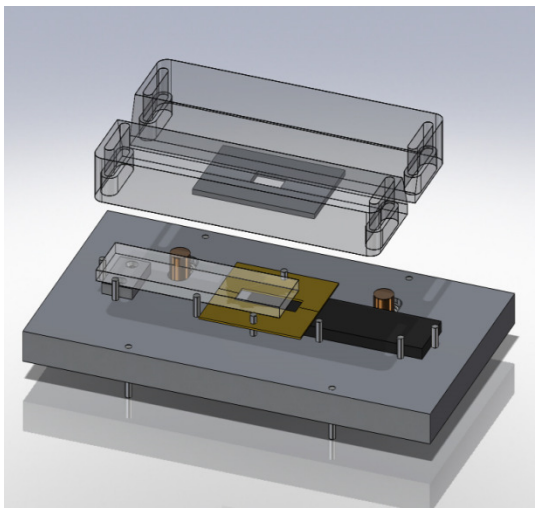

(b)

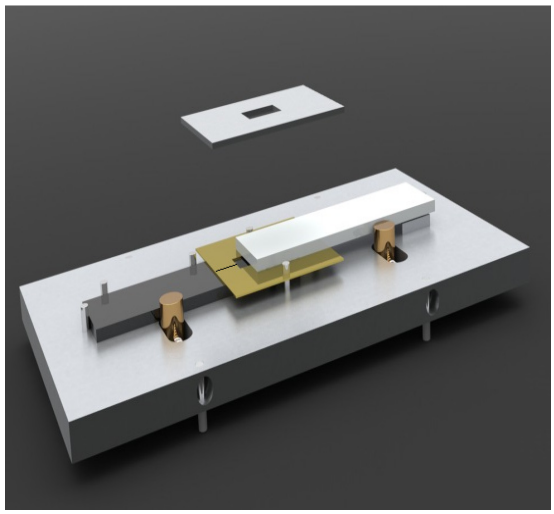

(c)

Figure 5. 5: (a) Side view of the laser fixture with mating parts, shim and mask. View from top with (b) and without (c) the upper clamping fixture

5.2 Welding study

Welding experiments were performed at three different scan speeds (5, 15 and 25 mm/s) with both formulations (with and without CBA). Details of the formulation can be found on Table 4.2. At first, samples were welded without any gaps. Then gaps were introduced using shims and the power was increased gradually starting from the point at which a weld would be created without the gap. The minimum power required for welding a specific gap was obtained for each formulation. To determine minimum power required, the samples were put in the laser fixture. The laser was run increasing the power 1 W each time. Then the samples were taken out to find if they are welded or just come out as separate pieces. A weld was detected by the joining of the top and bottom part. Once a weld was found, the power was decreased by 1/2W and more tests were conducted to make sure below that "specific" power which created the weld, the samples did not join. Then the welding test was repeated with that minimum power, 2 more times to make replicates, which were later used in the weld strength test. Six different gap sizes were bridged successfully (0.127-0.762 mm). In a second series of experiments, a fixed gap (0.508 mm) was used to assess the effect of laser power on weld strength. Three replicates have been taken for all the experimental data points to check the repeatability of the tests.

The tensile shear strength of the welded samples was determined by pull-testing. These pull-tests were performed by INSTRON 4206 Universal testing machine located at RMC. The cross head speed was set at 5 mm/min. Once the assembly is positioned in the grips, the universal testing machine gives the load as a function of extension, and the load at yield can be found where the slope of the curve is 0. Figure 5.6 shows one sample output plot for pull-test. The three different colors of the plot represent 3 replicates.

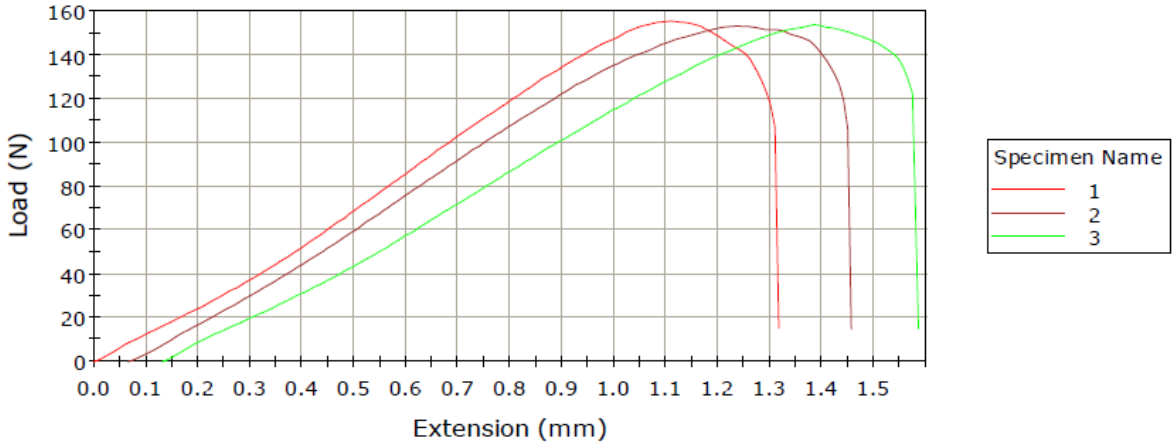

Figure 5. 6: Load versus extension to break a sample with CBA welded at 15W, 5 mm/s and 0 gap.

Once load at yield is found, the apparent weld strength can be calculated by dividing it by the cross sectional area of the weld. Image J software was used to calculate the length and width of the weld. To determine the width, 10 different readings were taken along the weld line and then the average value was used to calculate the cross sectional area.

5.2.1 Welding at 0 gap and different power/speed

Figures 5.7-5.9 show the weld strength as a function of laser powers for three different scan speeds (5, 15 and 25 mm/s). The starting point with 0 weld strength is taken when a weld line is just formed at the interface but the samples are still separable without applying any force. The highest strengths for samples with and without CBA were found to be approximately 7-8 and 8-9 MPa respectively. The tensile strength value of LDPE is 11 MPa according to the manufacturer. The shear strength value is thus 70-80% of the tensile strength which is comparable to other studies (Chen, 2009; Maram, 2010). Summary of the weld strength results are presented in table 5.1.

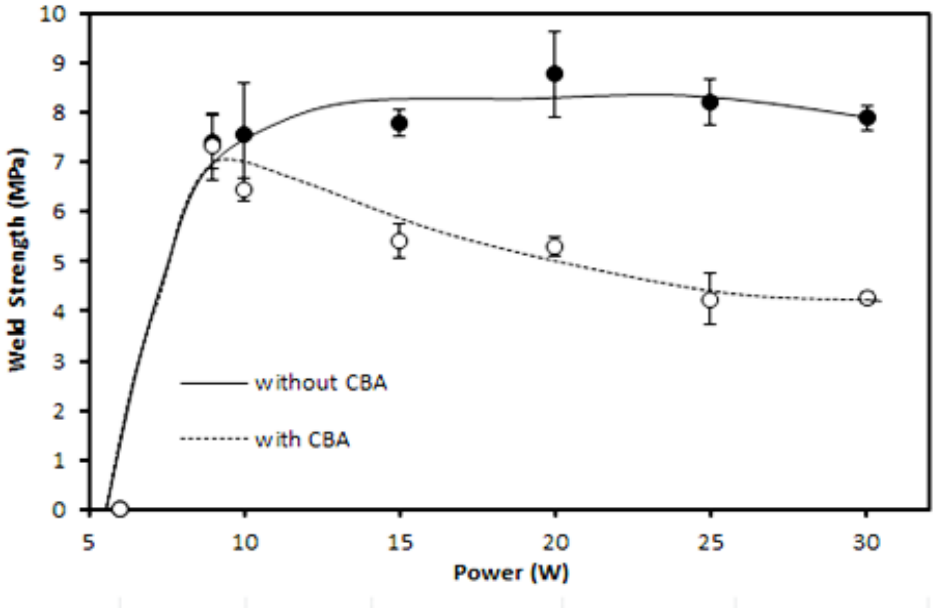

Figure 5. 7: Apparent weld strength at different powers at scan speed 5 mm/s. (Error bars represent maximum/minimum values)

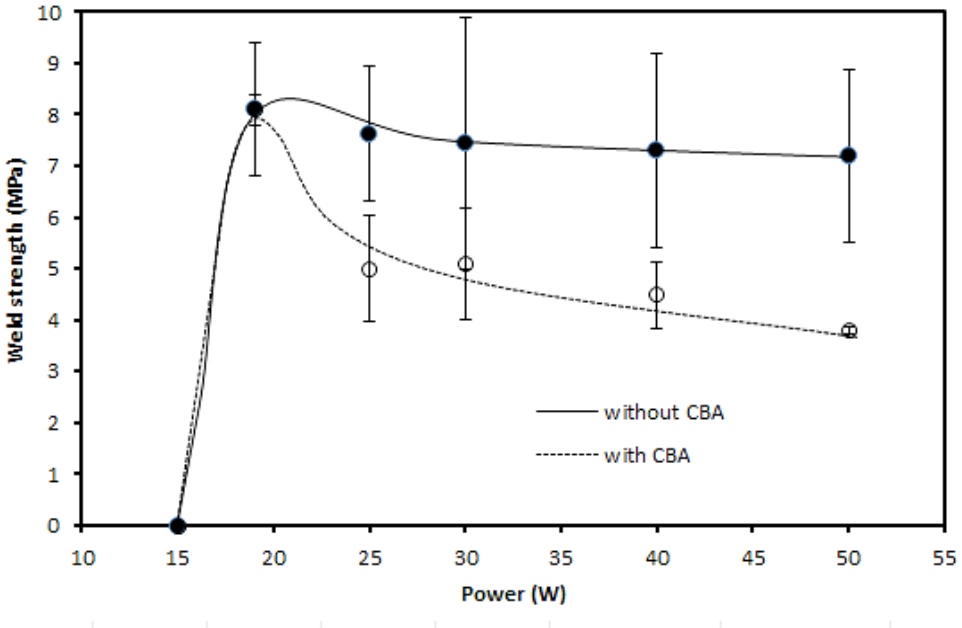

Figure 5. 8: Apparent weld strength at different powers at scan speed 15 mm/s. (Error bars represent maximum/minimum values)

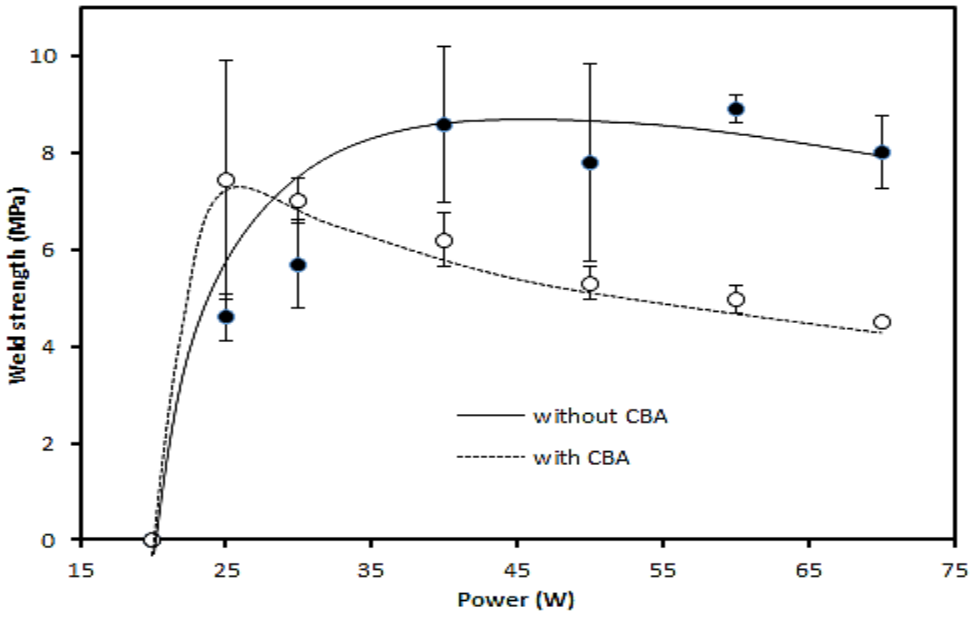

Figure 5. 9: Apparent weld strength at different powers at scan speed 25 mm/s (Error bars represent maximum/minimum values)

Table 5. 1: Maximum apparent weld shear strengths achieved at 0 gap with different scan speeds

Scan speed (mm/s)	Without CBA		With CBA	
	Highest weld strength (MPa)	Percentage of Original material strength	Highest weld strength (MPa)	Percentage of Original material strength
5	8.8	80%	7.3	66%
15	8.1	74%	8.1	74%
25	8.9	81%	7.5	67%

Although the peak strength values of assemblies made with and without CBA are comparable, Figures 5.7-5.9 show that after reaching to maximum weld strength; the strengths of assemblies made with CBA decrease by approximately 50% with further increase in power. Conversion of

CBA is likely causing this decrease in strength. Samples without CBA, on the other hand, stay at a constant level after reaching the maximum. Detailed explanation can be found by observing the weld width and the maximum load at yield curves presented in Figures 5.10-5.15.

Figure 5.10-5.12 shows the comparison of weld widths for samples with and without CBA. It can be observed in general that for the same scan speed, weld width increases with power which is logical. As found by previous researchers, (Chen, 2009; Maram, 2010) as the power is increased, a greater fraction of the beam width has the power flux able to initiate melting at the weld seam. Interestingly, it is found that the weld width of the samples with CBA is 15-28% higher than that of the samples without CBA. One possible explanation to this might be the presence of CBA. On the other hand the carrier polymer resin which was compounded with CBA to form masterbatch, which is unknown from the data sheet supplied by the manufacturer, might have a slightly lower melting point which could result in widening of the weld seam.

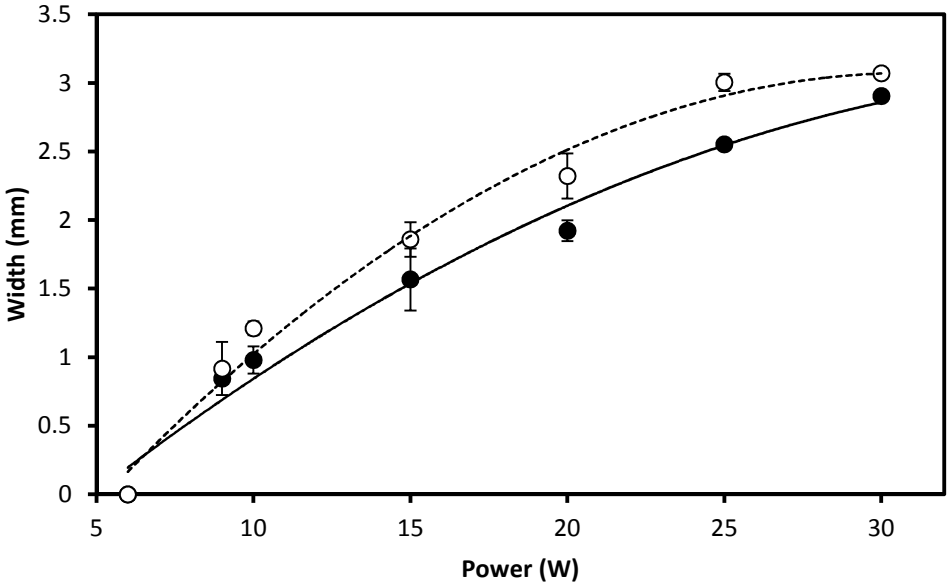

Figure 5. 10: Comparison of weld width at 5 mm/s scan speed for samples with & without CBA (Error bars represent maximum/minimum values)

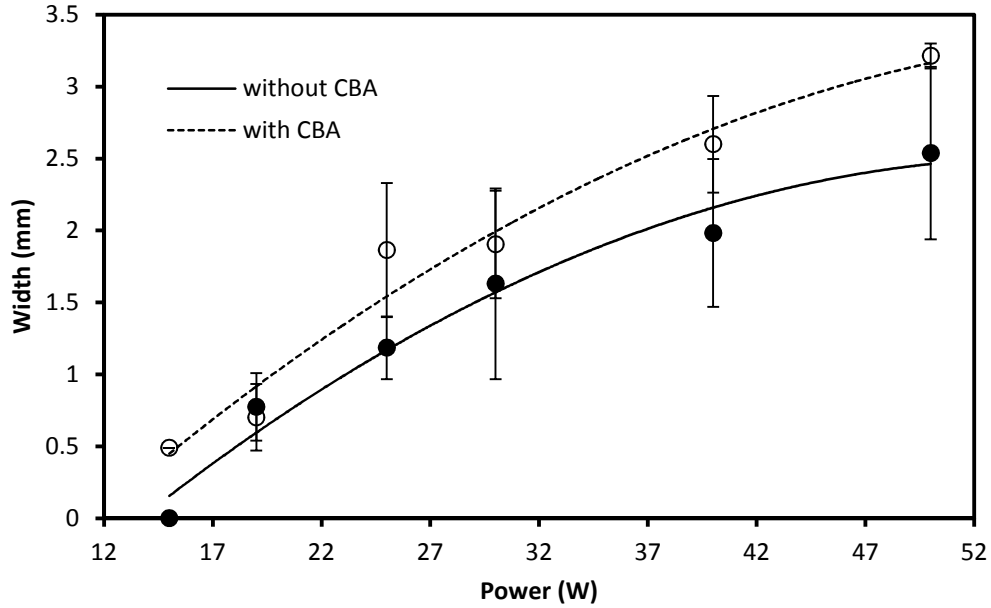

Figure 5. 11: Comparison of weld width at 15 mm/s scan speed for samples with & without CBA (Error bars represent maximum/minimum values)

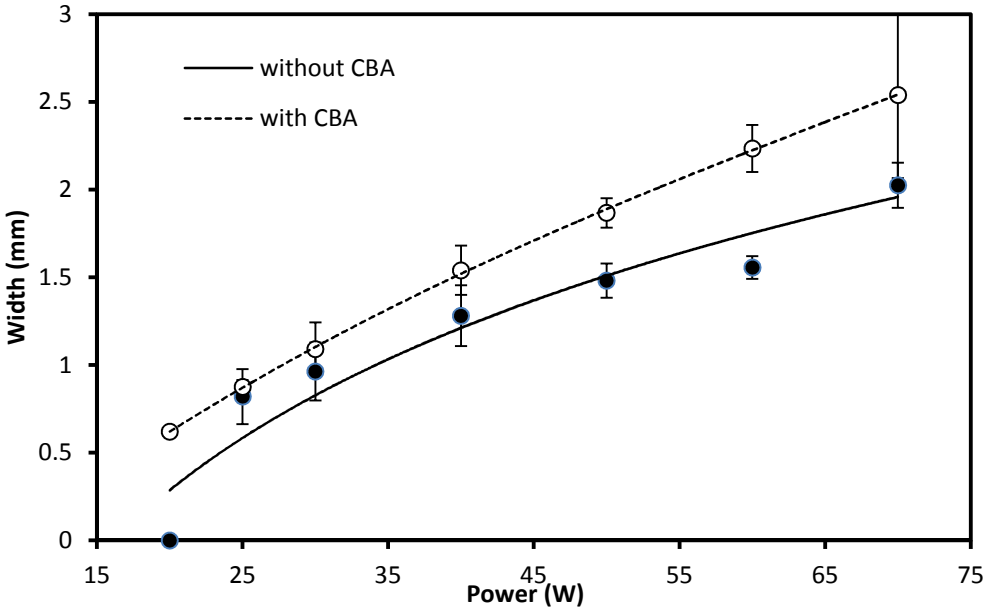

Figure 5. 12: Comparison of weld width at 25 mm/s scan speed for samples with & without CBA (Error bars represent maximum/minimum values)

Figures 5.13-5.15 show the maximum load to break the weld at pull-test as a function of power for three different scan speeds (5, 15 and 25 mm/s) with no gap. The curves for all samples show that load at yield increases with power. At low powers, the maximum load at yield is same for samples with and without CBA. For higher powers, the maximum load for samples with CBA is lower than that of the samples without CBA. The power at which the CBA maximum load falls below that of the non-CBA material is speed dependent: 9 W at 5 mm/s, 25 W at 15 mm/s and 40 W at 25 mm/s. This may be the caused by the conversion of some of the CBA at the higher temperatures associated with the higher powers. It would appear from the power and speed data that a line energy of approximately 1.6-1.9 J/mm is required to initiate the conversion. From Figures 5.10-5.15 it can be observed that the wider weld width and the lower maximum load are responsible for weaker apparent weld strengths of samples with CBA.

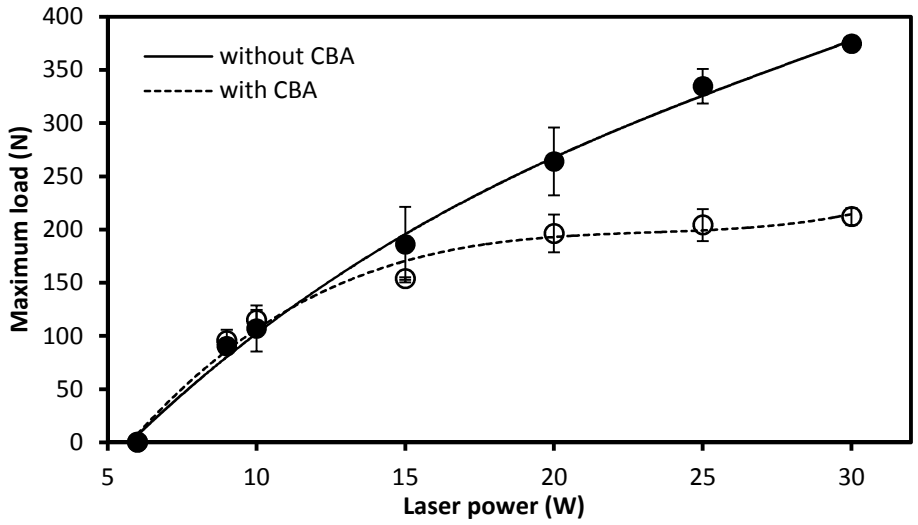

Figure 5. 13: The maximum load as a function of power for welding at 5 mm/s scan speed and no gap condition (Error bars represent maximum/minimum values)

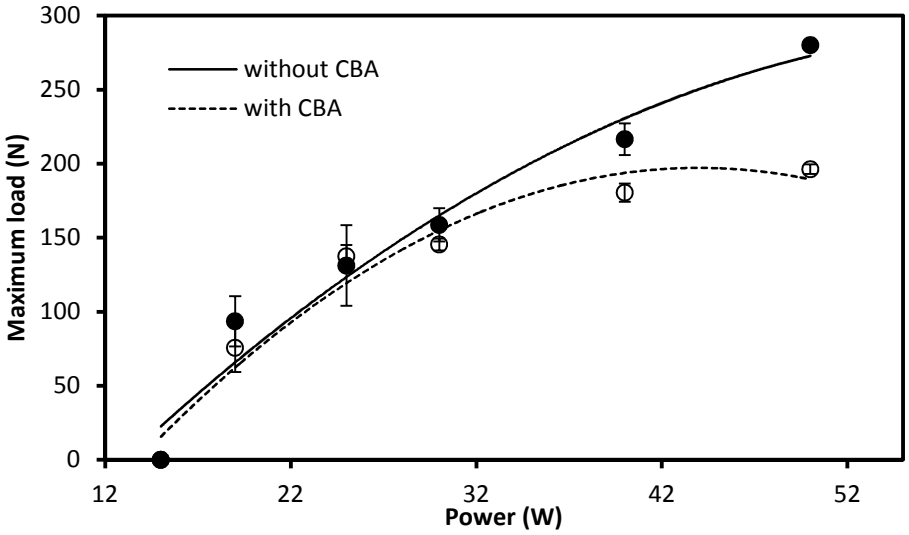

Figure 5. 14: The maximum load as a function of power for welding at 15 mm/s scan speed and no gap condition (Error bars represent maximum/minimum values)

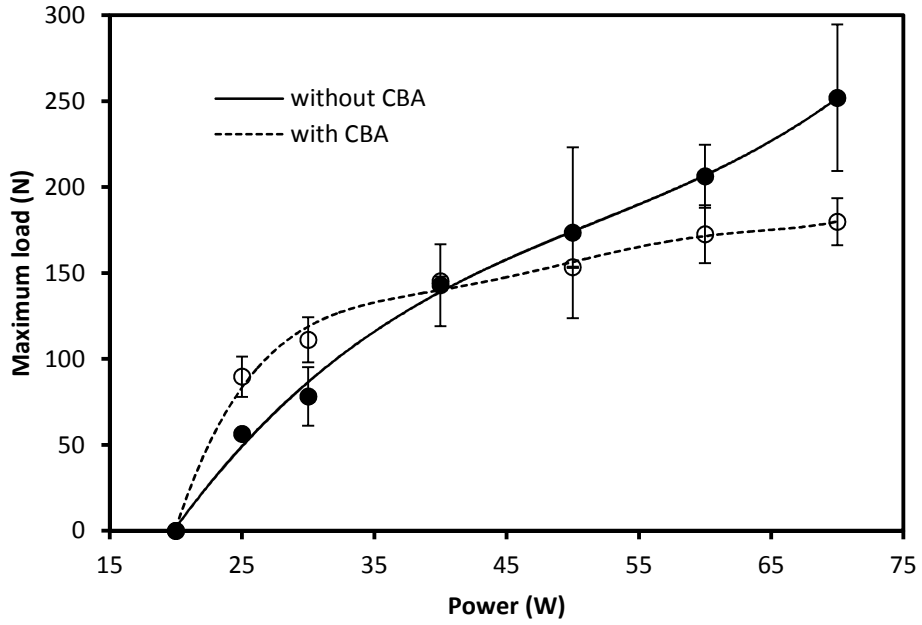

Figure 5. 15: The maximum load as a function of power for welding at 25 mm/s scan speed and no gap condition (Error bars represent maximum/minimum values)

5.2.2 Welding with gap at different powers and speeds

Figures 5.16-5.18 show the minimum power required to bridge a specific gap thickness for samples with and without CBA for three different scan speeds (5, 15 and 25 mm/s). To determine the minimum power required to bridge a gap, the power was increased gradually starting from no gap condition. Increased power increases the temperature and allows more thermal expansion of the molten material which in turn facilitates gap bridging. Once a weld was formed, the welding procedure was repeated twice with the same power for making two more welded samples as replicates of the pull-test.

It can be observed that, at a speed of 5 mm/s, the presence of CBA generally lowered the required power to bridge a particular gap. In other words, for the same laser power, samples with CBA show better gap bridging by releasing gas and creating localized thermoplastic foam. The samples without CBA did not produce gas to create thermoplastic foam. These samples bridge the gap only by thermal expansion. However, as the scan speed increases, the required power to bridge larger gaps (0.508-0.762 mm) becomes same for both CBA and non-CBA containing compounds (Figures 5.17 and 5.18). There could be several factors responsible for this. Formation of thermoplastic foam is a complex process which is dependent on a number of process parameters (temperature, mixing, viscosity, time etc.). With higher speed, the temperature of molten polymer at a certain location is raised only for a short period of time which might not be enough to create foam. On the other hand, higher speed might not allow the heat to penetrate as deep to create a bigger volume of foamed thermoplastic. A more detailed discussion on this will be presented on chapter 7 based on modelling of the CBA degradation.

For this material and experimental conditions, best gap bridging performance was observed at the lowest scan speed (5 mm/s). Lower scan speeds result in a longer heating time and may allow more time for the foaming conversion to occur.

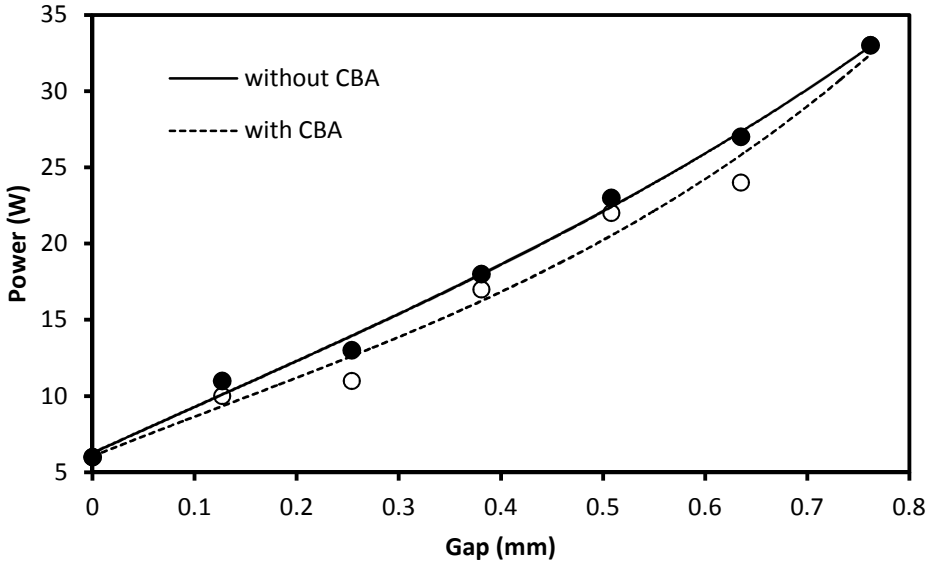

Figure 5. 16: Comparison of minimum power required to bridge gap between samples with and without CBA at 5 mm/s scan speed

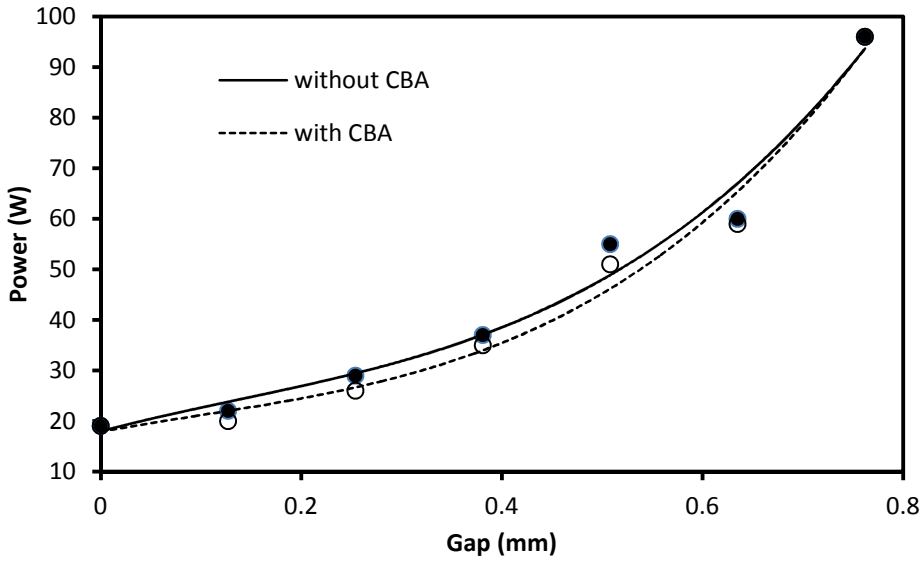

Figure 5. 17: Comparison of minimum power required to bridge gap between samples with and without CBA at 15 mm/s scan speed

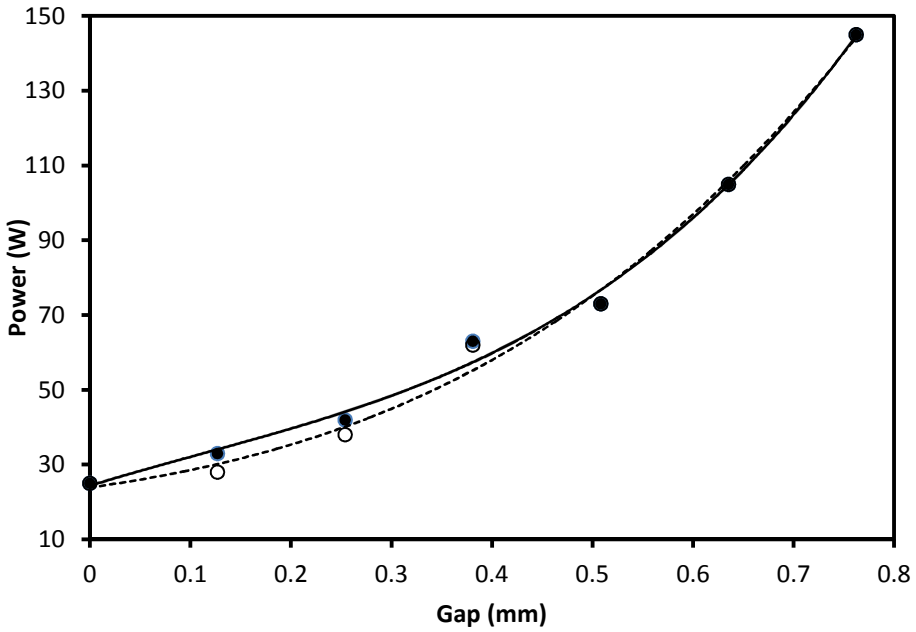

Figure 5. 18: Comparison of minimum power required to bridge gap between samples with and without CBA at 25 mm/s scan speed

Figures 5.19-5.21 show the weld strengths of samples made with and without CBA. In general it can be said that samples with gaps have lower strength than those without gaps. As the gap size increases, the strength decreases further. This phenomenon was also observed by Chen (2009) in his gap bridging work. The lower strength is caused by voids that are created after cooling and shrinkage in the gap regions.

It is also evident from Figures 5.19 -5.21 that the presence of CBA lowers the strength of the assembly. This is logical because the foamed thermoplastic would have bubbles which would lower the mechanical strength of the weld. In addition, for some high gap thicknesses, the welded samples broke before putting them in the universal tasting machine for pull-test. For these broken samples, 0 weld strength was counted while calculating the average and standard deviation was not determined. These samples are denoted as red dots without any error bar in this study.

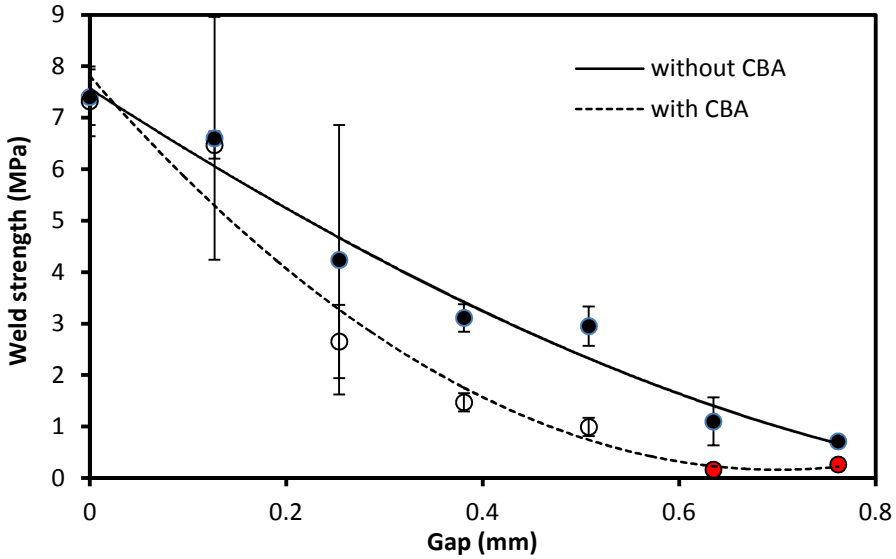

Figure 5. 19: Comparison of the apparent weld strengths with different gaps (and different powers) between samples with and without CBA at 5 mm/s scan speed (Error bars represent maximum/minimum values)

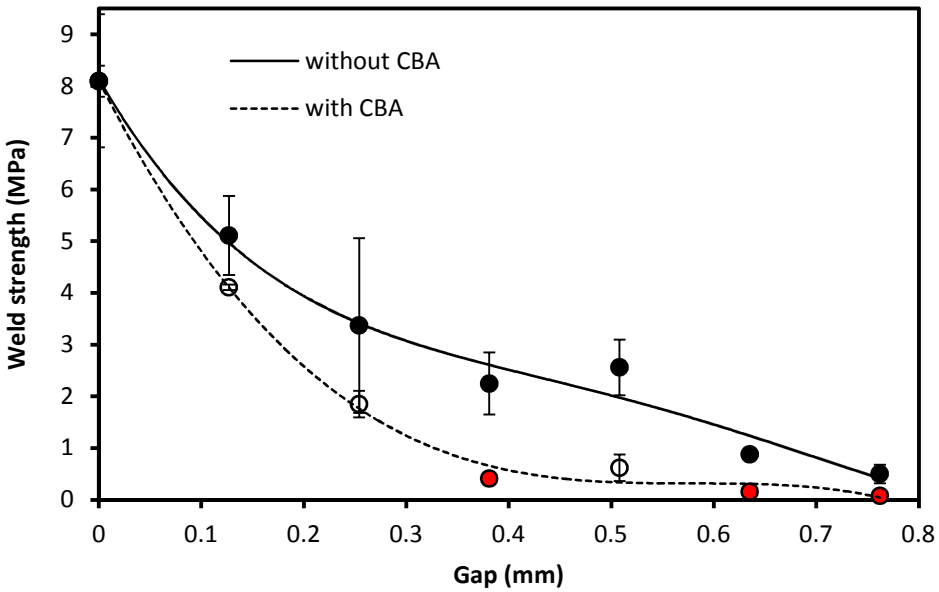

Figure 5. 20: Comparison of apparent weld strengths with different gaps (and different powers) between samples with and without CBA at 15 mm/s scan speed (Error bars represent maximum/minimum values)

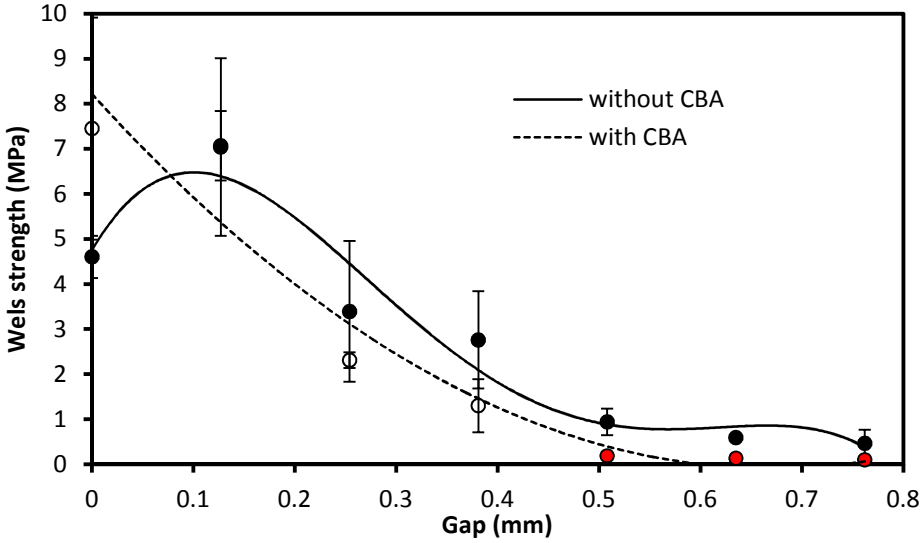

Figure 5. 21: Comparison of apparent weld strengths with different gaps (and different powers) between samples with and without CBA at 25 mm/s scan speed (Error bars represent maximum/minimum values)

Figures 5.22-5.24 show the comparison of the width for welding with gaps at three different scan speeds (5, 15 & 25 mm/s) and different powers. No significant difference is observed in weld widths of the samples with and without CBA. It should be noted that for contact condition, the width of the samples with CBA was found to be 15-28% higher than that of the samples without CBA. For non-contact tests, the samples without CBA require higher power than the samples with CBA to bridge the same gap. Higher *LE* causes widening of the weld seam which is responsible for minimizing the difference in weld width between both sets of sample.

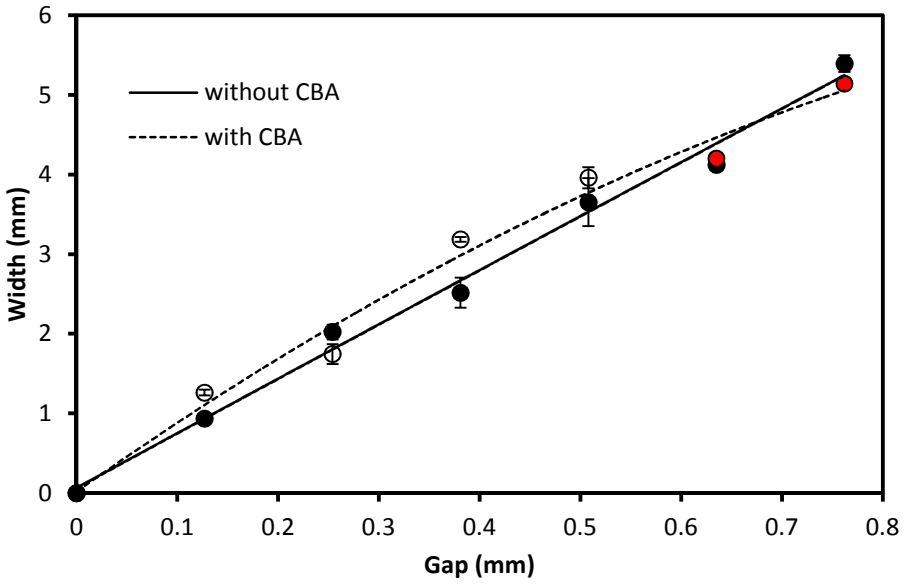

Figure 5. 22: Comparison of weld width for samples with & without CBA at 5 mm/s scan speed and different gaps (Error bars represent maximum/minimum values)

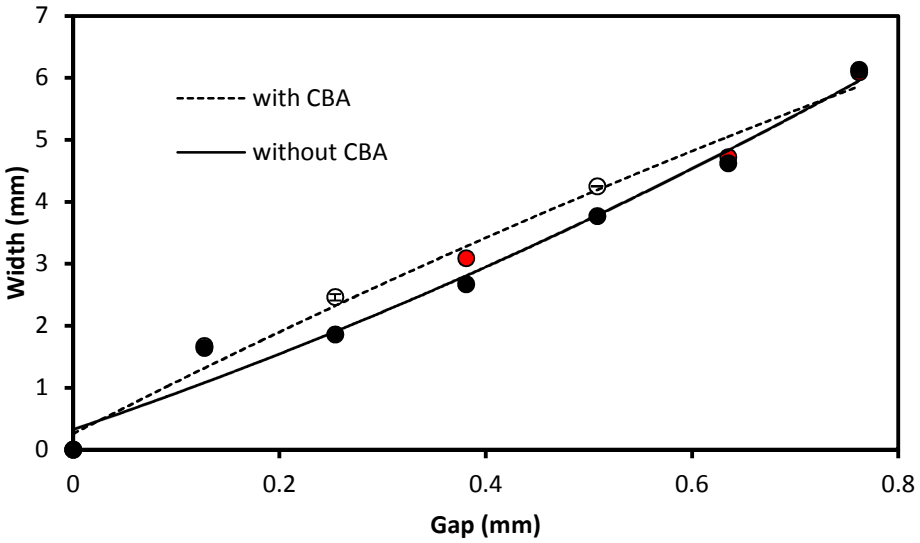

Figure 5. 23: Comparison of weld width for samples with & without CBA at 15 mm/s scan speed and different gaps (Error bars represent maximum/minimum values)

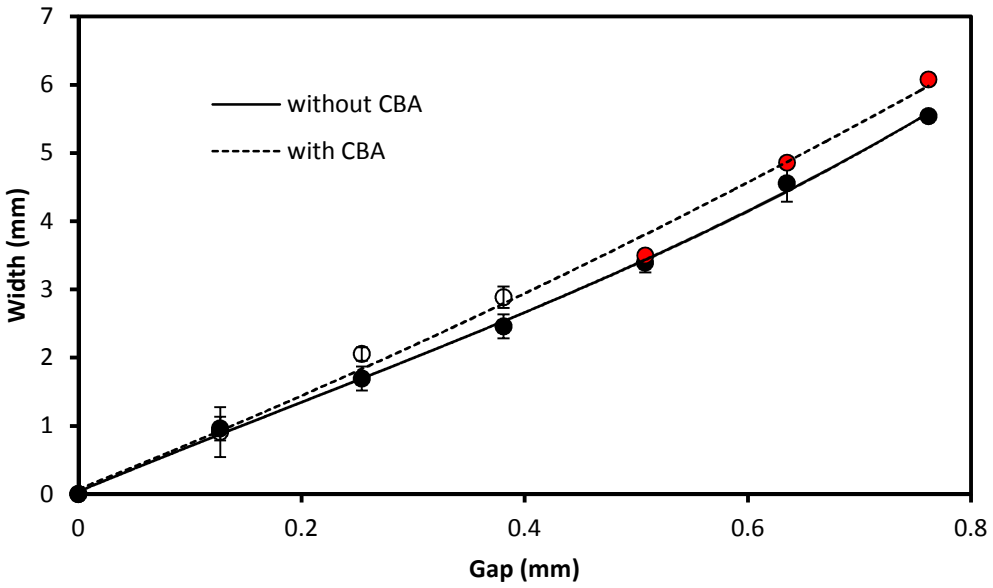

Figure 5. 24: Comparison of weld width for samples with & without CBA at 25 mm/s scan speed and different gaps (Error bars represent maximum/minimum values)

Figures 5.25-5.27 show maximum load required to break the weld during pull-test as a function of gap thickness for three different scan speeds (5, 15 & 25 mm/s). It can be seen that, for most of the data points, the maximum load at yield for samples without CBA is higher than the sample with CBA. This can be explained by the fact that the non CBA materials are bridging gap by thermal expansion while the CBA containing material thermally expands and creates foam. Foamed thermoplastic contains less plastic (more gas) between the mating parts which is likely responsible for weaker weld. It can be observed that the maximum load curve for samples without CBA has a general trend to go upward, achieve a maximum and then start to decrease. To bridge a higher gap, higher power is required which in turn increases thermal expansion. Increased thermal expansion increases the contact area between both of the mating parts which increases the maximum load at yield. After reaching to a maximum, the load starts to decrease. This might be caused by some degradation of the base material.

The maximum load curve for samples with CBA, on the other hand, shows a monotonic decrease. The volume of foamed thermoplastic increases with the increase in power. This foamed thermoplastic then takes part in bridging higher gaps. With the increase in gap, the contact area between the mating parts may have been reduced which might be responsible for this decrease in maximum load.

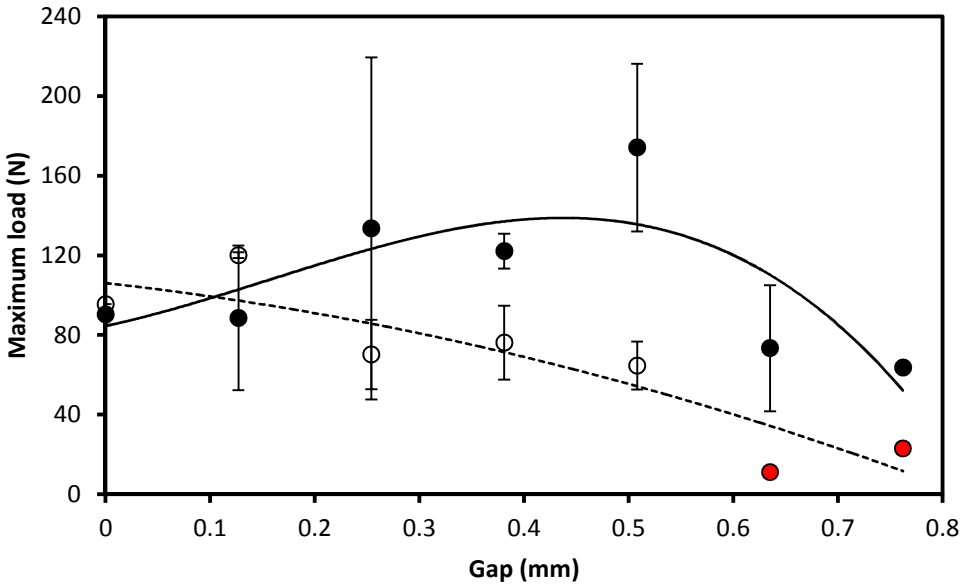

Figure 5. 25**: The maximum load as a function of gap thickness for welding at 5 mm/s scan speed (and different powers) (Error bars represent maximum/minimum values)**

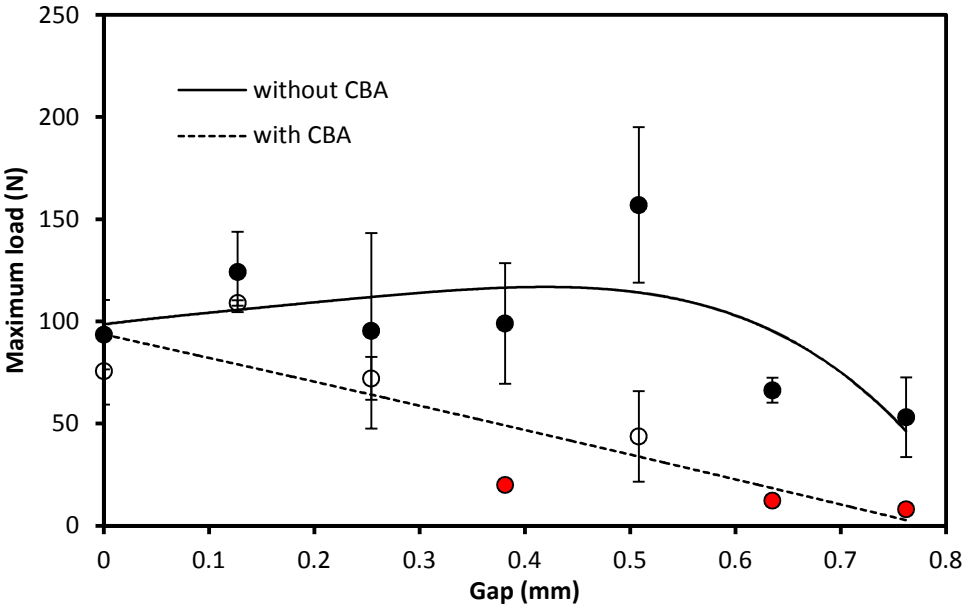

Figure 5. 26: The maximum load as a function of gap thickness for welding at 15 mm/s scan speed (and different powers) (Error bars represent maximum/minimum values)

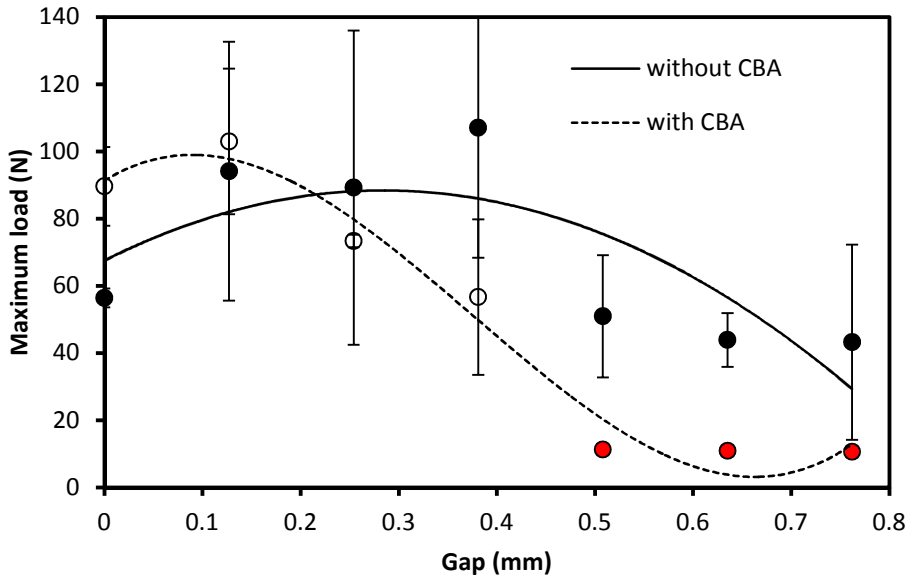

Figure 5. 27: The maximum load as a function of gap thickness for welding at 25 mm/s scan speed (and different powers) (Error bars represent maximum/minimum values)

5.2.3 Weld strength at constant gap (0.508mm) and different powers

Figures 5.28-5.30 represent the weld strengths of assemblies made with a 0.508 mm gap at different powers (20W-130W). It can be seen that samples without CBA have a general trend to increase weld strength with increasing power at low powers. Higher powers result in higher temperatures and increase the thermal expansion and gap-bridging ability of the material. After reaching to a highest level, the increase in weld strength levels off at strength of 2-3.5 MPa. However, samples with CBA have lower weld strengths of 0.5-1.5 MPa. The lower weld strengths are likely due to the lower mechanical properties of the foamed material in the weld interface. The change in strength with power is small. Higher powers result in higher temperatures leading to more thermal expansion (which as seen above is good for strength) but

it also leads to more CBA conversion and gas formation. These two effects appear to cancel each other out leading to a more constant strength as a function of power. The maximum strength decreases with laser scan speed regardless of having or not having CBA. Slower scan speeds are good for thermal conduction which allows the weld to get stronger.

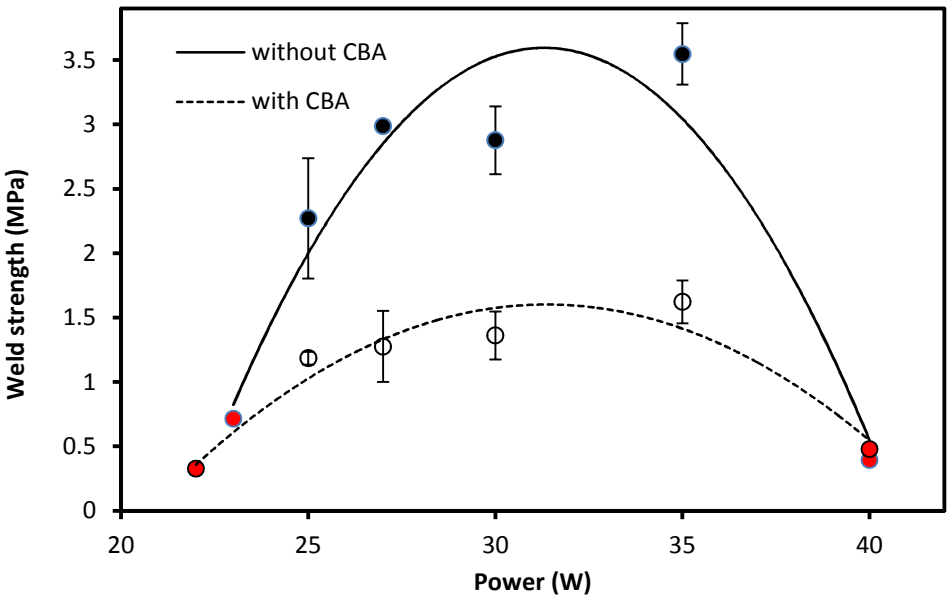

Figure 5. 28: Comparison of apparent weld strengths at 0.508 mm gap between samples with and without CBA at 5 mm/s scan speed (Error bars represent maximum/minimum values)

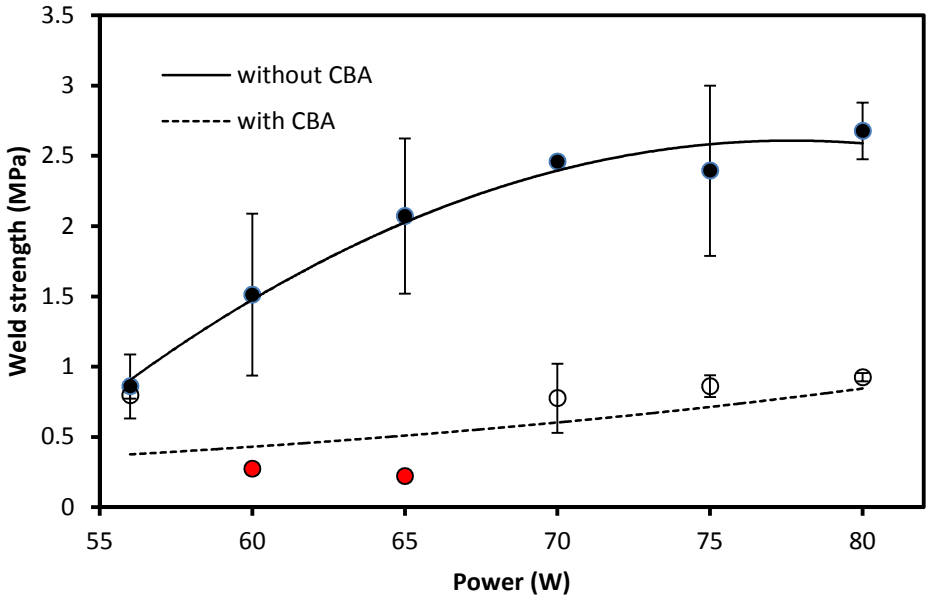

Figure 5. 29**: Comparison of apparent weld strengths at 0.508 mm gap between samples with and without CBA at 15 mm/s scan speed (Error bars represent maximum/minimum values)**

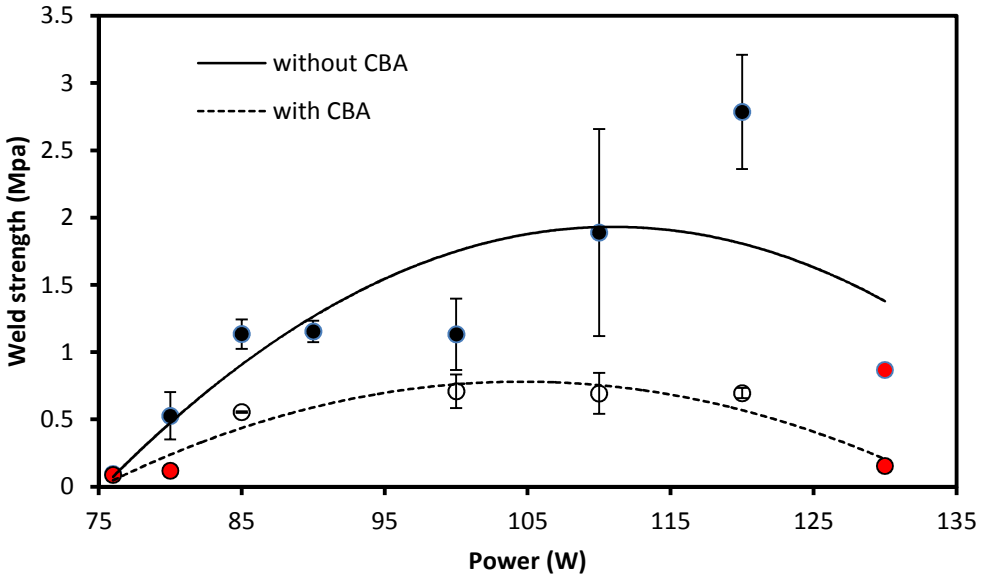

Figure 5. 30: Comparison of apparent weld strengths at 0.508 mm gap between samples with and without CBA at 25 mm/s scan speed (Error bars represent maximum/minimum values)

Figures 5.31-5.33 show the weld widths at 0.508 mm gap and three different scan speeds (5, 15 & 25 mm/s) for samples with and without CBA. Similar to results presented previously, it can be found that the weld width for samples with CBA is 8-10% higher than the samples without CBA.

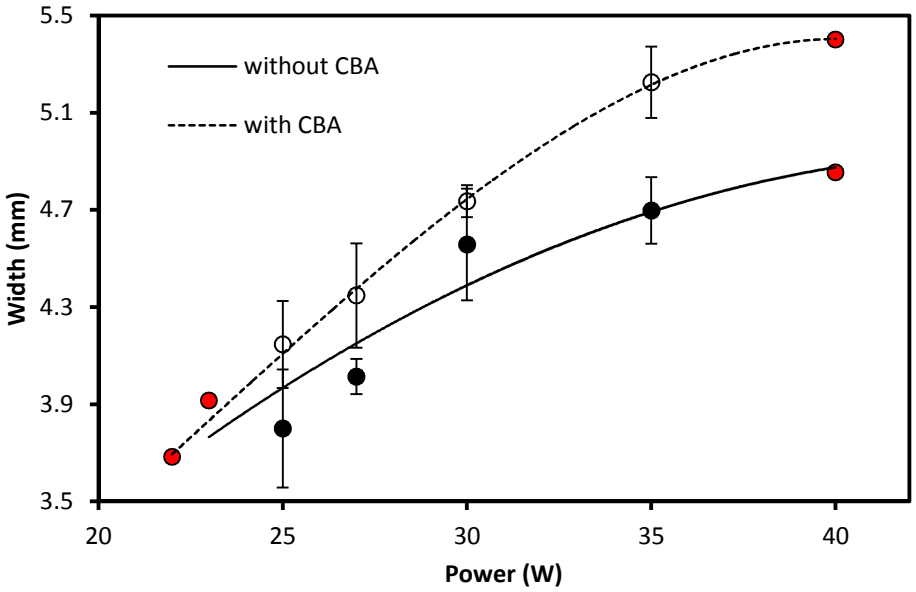

Figure 5. 31: Comparison of weld width for samples with and without CBA at scan speed 5 mm/s and 0.508 gap (Error bars represent maximum/minimum values)

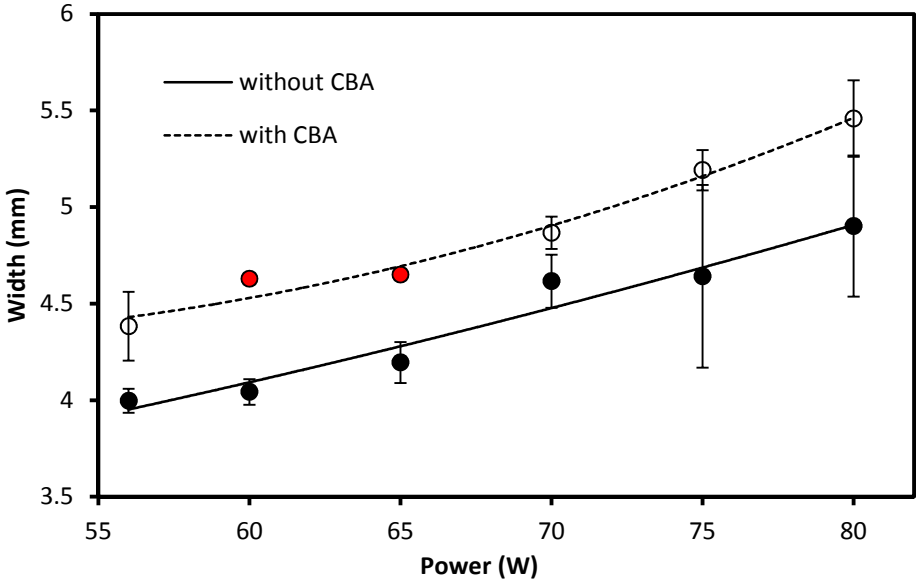

Figure 5. 32: Comparison of weld width for samples with and without CBA at scan speed 15 mm/s and 0.508 gap (Error bars represent maximum/minimum values)

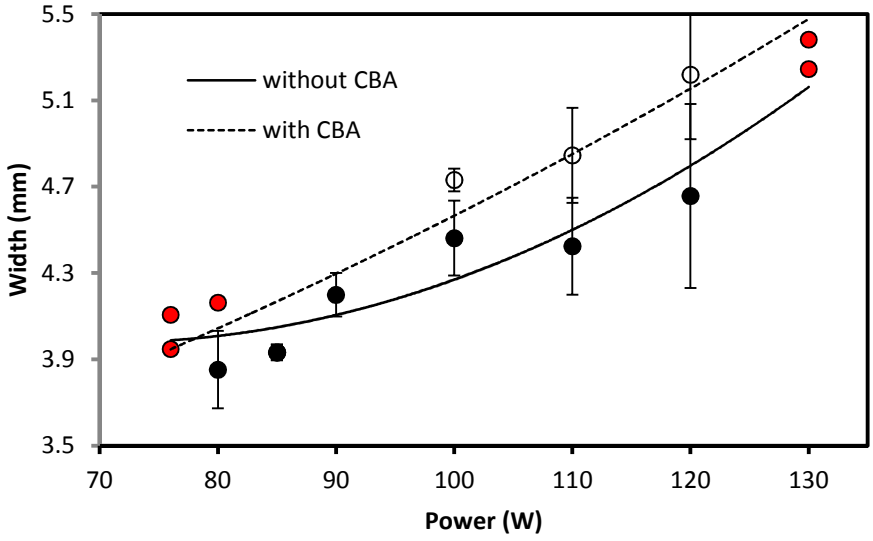

Figure 5. 33: Comparison of weld width for samples with and without CBA at scan speed 25 mm/s and 0.508 gap (Error bars represent maximum/minimum values)

Figures 5.34-5.36 show the maximum load required to break the weld at three different scan speeds (5, 15 & 25 mm/s) for samples with and without CBA. At low powers, it can be found that the maximum load curve has an upward trend for samples with and without CBA but the slope of the increase in load is not the same for each. The gap bridged by foam is expected to have lower strength than a gap bridged by thermal expansion.

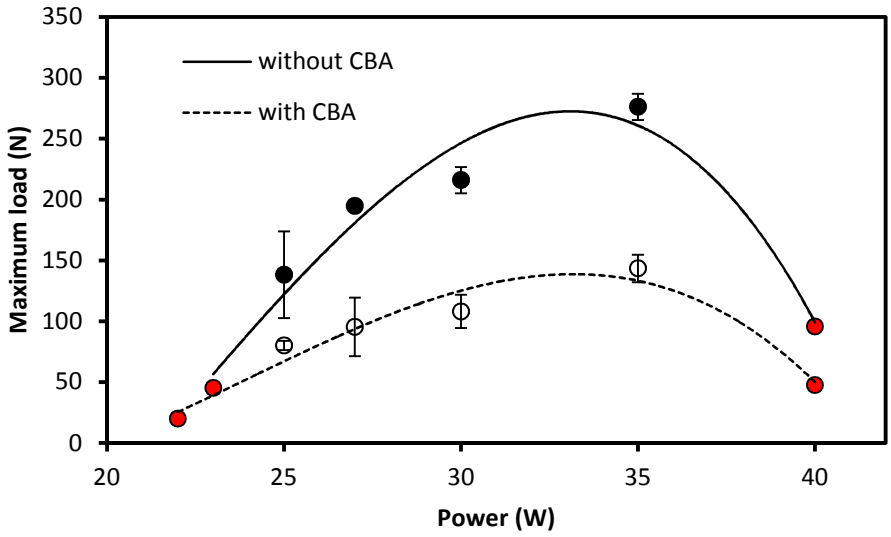

Figure 5. 34: Comparison of maximum load for samples with and without CBA at scan speed 5 mm/s and 0.508 gap (Error bars represent maximum/minimum values)

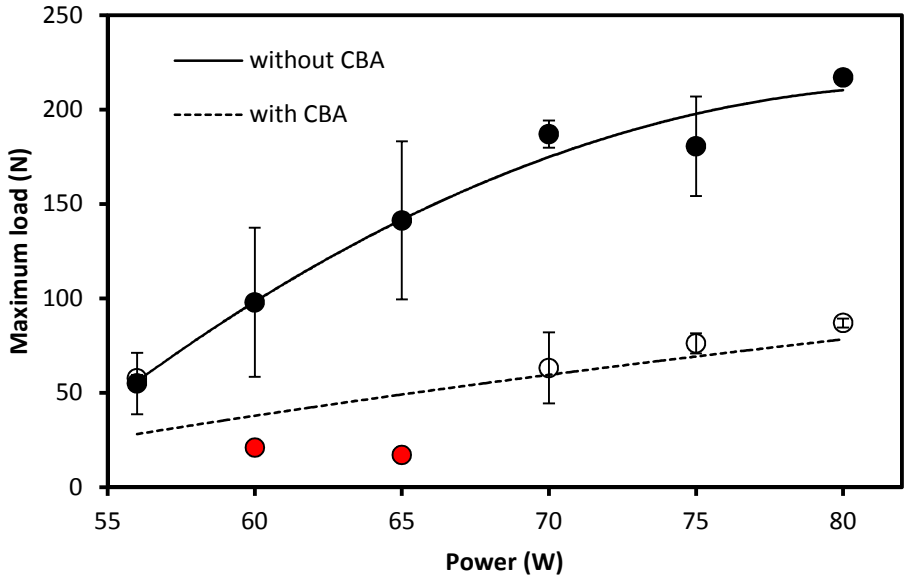

Figure 5. 35: Comparison of maximum load for samples with and without CBA at scan speed 15 mm/s and 0.508 gap (Error bars represent maximum/minimum values)

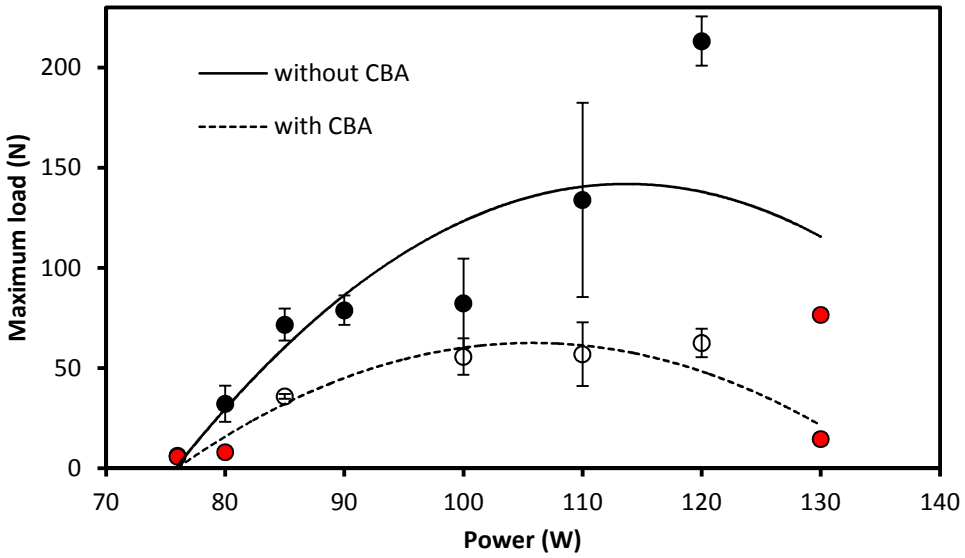

Figure 5. 36: Comparison of maximum load for samples with and without CBA at scan speed 25 mm/s and 0.508 gap (Error bars represent maximum/minimum values)

5.2.4 Weld Microstructure

Weld microstructural analysis is used to observe what happened to the welded region. In this work, the fractured surface of the weld after pull-test was observed using two methods: (i) the scanned image of the fracture surface of the absorbent part and (ii) sectioned view which allows the height of the raised foamed thermoplastic to be viewed using scanning electron microscopy.

Figure 5.37 shows the fractured surface of the absorbent part of the specimens welded at different powers and gap settings after the pull-test. These welding experiments were performed at 5 mm/s scan speed. These images were taken using a table top scanner. The samples with CBA have porous surface which reveals the formation of bubbles during LTW. As will be discussed later, this observation is consistent with the CBA conversion model described in section 7.7.2. The conversion of CBA starts from 10W and the percentage increased with power. The bubbles in Figure 5.37 (b) also become prominent with increases in power. Similar behaviour was observed for all other scan speeds. With increasing powers, the width of the weld line increases. From close observation it can be seen that the contact between the mating parts exists at the edges while the middle portion becomes depressed. This depression is visible even after performing pull-test. To further illustrate this pattern, a schematic diagram of the gap bridged sample is presented in Figure 5.38. When the absorbent part is irradiated by laser, thermal expansion allows the material to touch the transparent part to bridge the gap. When the laser beam moves forward, the heating stops and the expanded material starts to cool down. Thermal shrinkage then causes creation of voids in the center of the weld where the temperature was highest during welding. This type of phenomenon is also observed but not discussed by Chen (2009) on his gap bridging study. The cooler edges of the weld line thus stay in touch while the middle portion becomes depressed as a result of the voids.

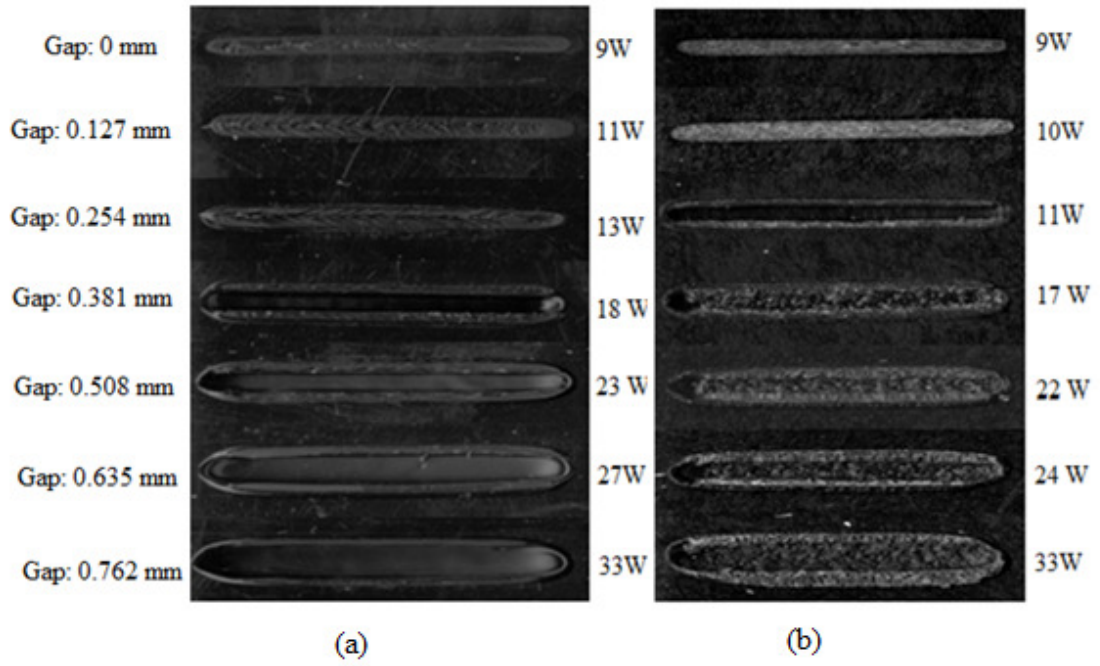

Figure 5. 37: Weld fracture images of samples welded at 5 mm/s scan speed (a) without and (b) with CBA after pull-test.

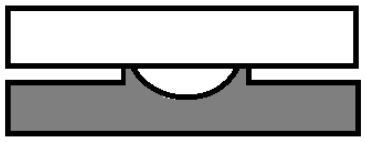

Figure 5. 38: Schematic diagram of the welded samples with gaps

To observe the welded zone better, cross sections of the welded samples were observed using scanning electron microscope (SEM). A small portion of the absorbent part (after fracturing during pull-test) was first cut using a band saw. Then one end of the part was cut using a microtome to obtain a smooth surface to observe under SEM. Figure 5.39 shows the heights of the raised edges at two different welding conditions. The white bits on the right hand side might

be the carrier material compounded with CBA to form masterbatch. Later in Figure 7.8 from the modelling section, it can be found that for the power and speed combination presented in Figure 5.39 (b), the depth of 80% CBA conversion is 0.3 mm. At same power and scan speed, the sample with CBA raises higher than the one without CBA. The localized foaming helps the sample to rise more. However it can be seen that the heights of the edges are actually lower than the gaps created using shims. The elasticity of the material is likely responsible for this type of behaviour.

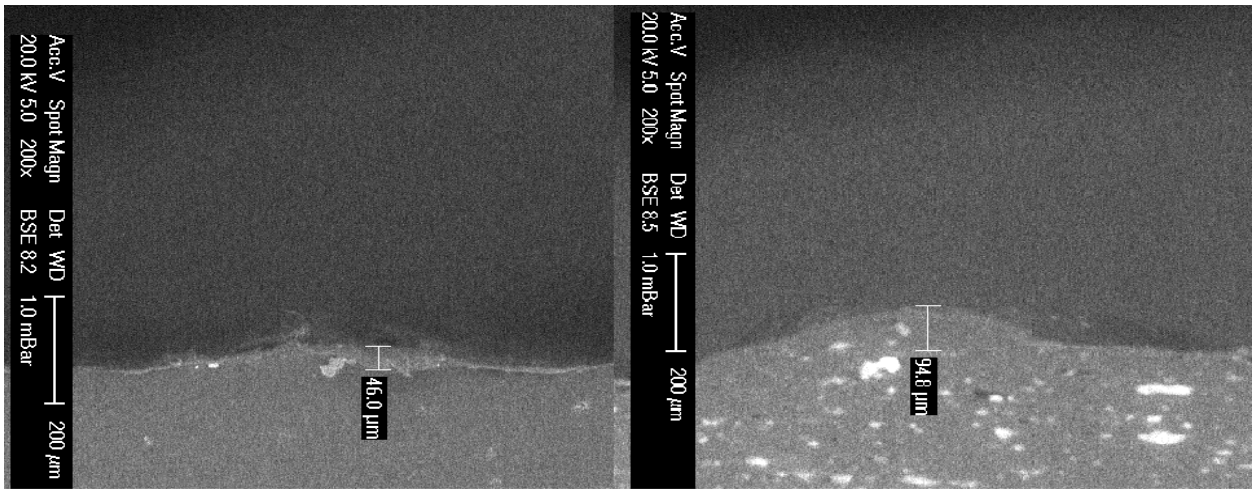

(a) (b)

Figure 5. 39: Absorbent part after fracture welded at 5 mm/s (a) 11W, 0.127 mm gap, without CBA (b) 11W gap, 0.254 mm gap, with CBA

Figure 5.40 shows the cross section of the fractured surfaces welded at 15 mm/s and 0.635 gap. With the existence of bubbles at the raised edges, the surface of sample with CBA looks different from that one without CBA. Presence of bubble creates a little circular hollow spot in the absorbent part. With very careful observation, bubbles can be identified as shown in Figure 5.40 (b). All of these findings reveal the conversion of CBA and formation of foam during LTW.

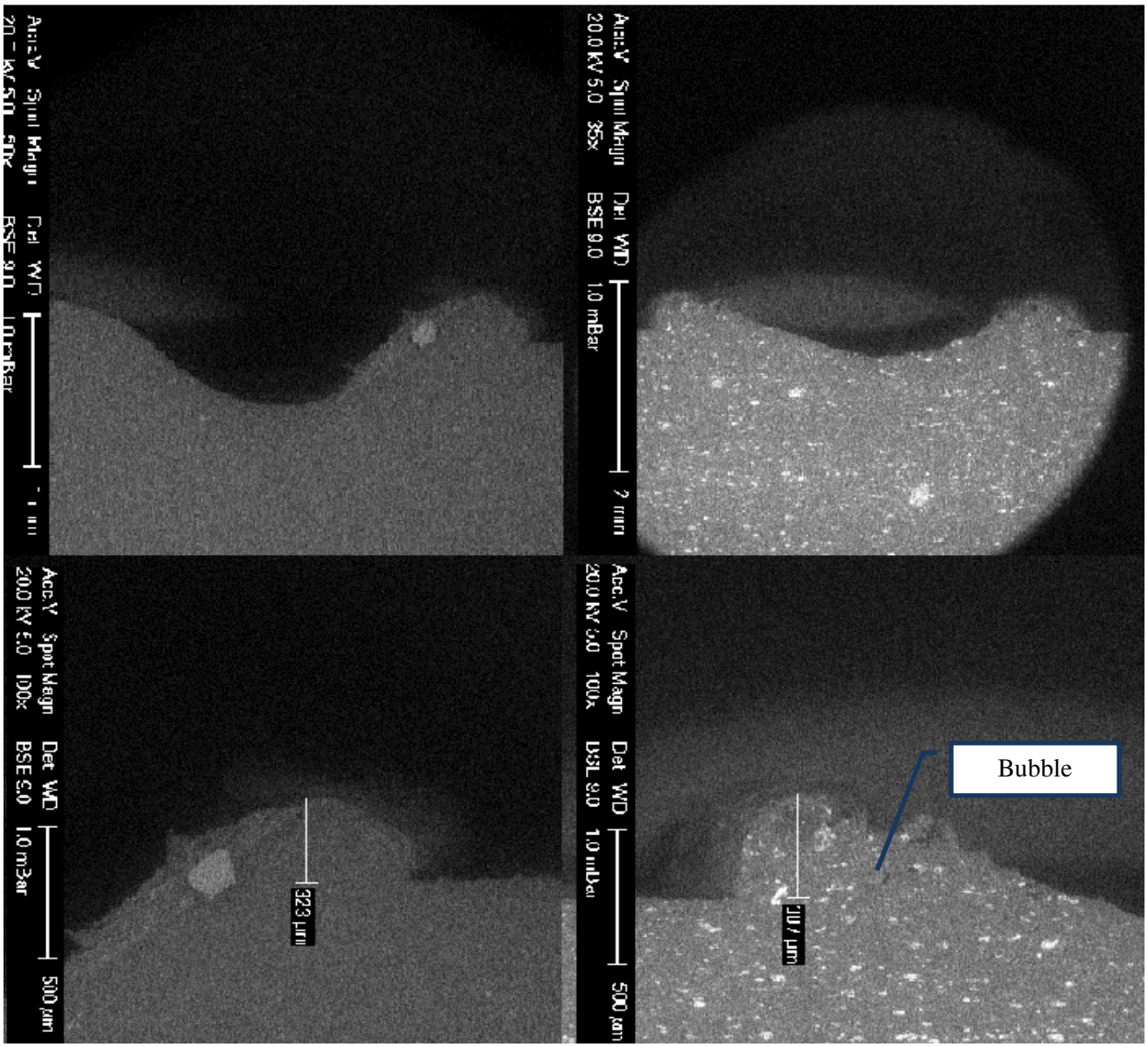

(a) (b)

Figure 5. 40: Absorbent part after fracture welded at 15 mm/s and 0.635 mm gap. Images at the top show the welded region with both edges. Bottom ones show height of the edges. (a) 60 W, without CBA (b) 59 W, with CBA

Chapter 6

Modelling

Modelling enables one to choose the optimum material and operating conditions to achieve the desired output for any kind of experimental work. This section discusses the modelling of foaming during contour LTW. The properties required for modelling is described in section 6.1. The Finite Element Method (FEM) thermal simulation is presented in section 6.2. It provides the temperature distribution at different locations as a function of time. In section 6.3, the conversion of CBA is modelled using these temperature-time profiles to help explain the experimental findings of this study and to suggest possible measures to achieve better results.

6.1 Properties for Modelling

6.1.1 Optical properties

6.1.1.1. Transmittance

Transmittance of LDPE was measured using a power meter. The injection moulded plaques were cut into 15mm × 15mm × 3.2 mm square specimens. The power meter was placed at a distance of 82.5 mm from the laser head. Input power was determined by exposing the power meter with laser for 5 seconds and then taking the reading. Output power was measured by placing the specimen over the incident surface of the power meter and taking the reading after laser irradiation. The experiment was conducted for both 5W and 10W and each of them was repeated for ten times. Transmittance was calculated by dividing the output power by the input power. Average value of transmittance was taken for modelling.

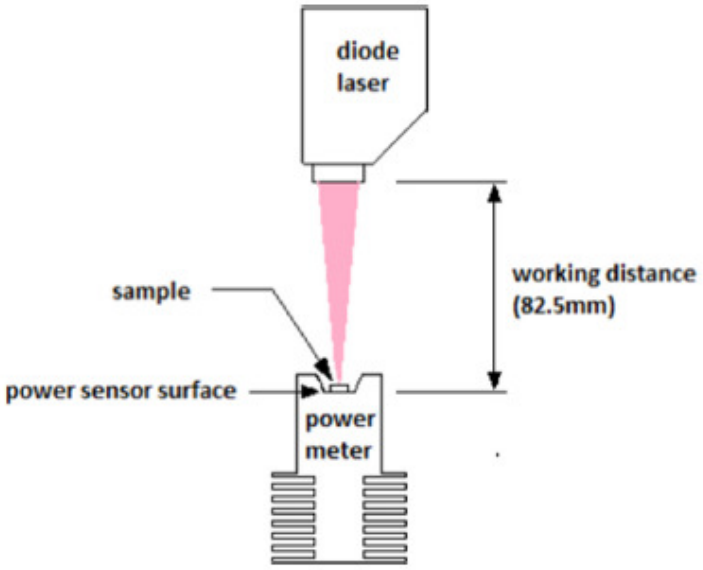

Figure 6. 1: Experimental set up for measuring transmittance of LDPE (Xu et al, 2015)

The average transmittance of LDPE was found to be 63%. No other data was found for the exact same material with given thickness in literature. For LLDPE, transmittance value was reported to be 55%. (Xu et al, 2015)

6.1.1.2. Surface Reflectance

The equation to measure surface reflectance of a polymer is described in section 2.1.3.1. The surface reflectance η was found to be 4.12% for LDPE. Maram (2010) reported the surface reflectance for a number of polymers which included both amorphous and semi-crystalline material. The values ranged between 3.7-8%, which indicates that the measured value for LDPE is reasonable.

6.1.1.3. Absorbance

For measuring absorbance of the laser absorbent part, the so-called direct scan method was used (Chen, 2009). In this method, the laser beam with uniform 1D distribution scans over the

absorbent part at a very high speed. For such a short irradiating period resulted by this, it can be assumed that no convective or conductive heat losses will occur. A series of scans are made increasing the power each time to obtain the minimum required power (P_{Lm}) to cause surface softening or melting. The following equation is used to calculate absorbance for semi-crystalline polymers.

$$A = \frac{Wv}{(1-R)P_{Lm}} [c\rho(T_m - T_i) + \Delta H] \quad \textbf{(6.1)}$$

Where W is the laser beam width, v is the scan speed, R is the total reflectance, c is the specific heat, ρ is the density, ΔH is the latent heat and T_m and T_i represents the melting and initial temperatures respectively.

The scan speed was 150 mm/s for this test. For such a high speed the irradiation time is so small that conduction effect can be neglected. The value of R was taken equal to the surface reflection parameter η (0.04) because for absorbent part, reflection only occurs at the surface and rest of the energy is absorbed by the carbon black. Heat capacity and latent heat data were taken from the DSC test. T_m and T_i was 110ºC and 20ºC respectively. The absorbance was found to be 4.7/mm.

6.1.1.4. Sigma-delta (TEDD method)

The power flux distribution after the laser beam passes through the transparent part can be obtained by the TEDD method proposed by Gene Zak (Zak et al, 2010). In this technique the transparent part is placed over an absorbent part and a series of scans are made increasing the power each time. Both of the parts are separated by two 0.3 mm shims and the absorbent part is examined to observe initiation of melting to severe degradation. The absorbent part could be made up of any material (with a high carbon black level, ~ 0.2 wt %) which can give a clear

view of melting. To measure the width of melted lines accurately, Image J software was used. The absorbent part was made of PP. This methods leads to the following equation:

$$\frac{P_o}{P_k}\psi^*(0) = \psi^*(\frac{w_k}{2}) \quad \textbf{(6.2)}$$

P_0 is the threshold power at which first visible melting is observed. W_k is the width of the weld line at any corresponding power P_k. $\psi^*(0)$ can be calculated from the area under the curve P_0/P_k versus $W_k/2$. $\Psi^*(\frac{W_k}{2})$, the T-NPFD of the beam at any position can be obtained from equation 6.2. Figure 6.2 shows the distribution of the power flux after passing through a LDPE plaque of 3.2 mm thickness compared to the un-scattered beam profile.

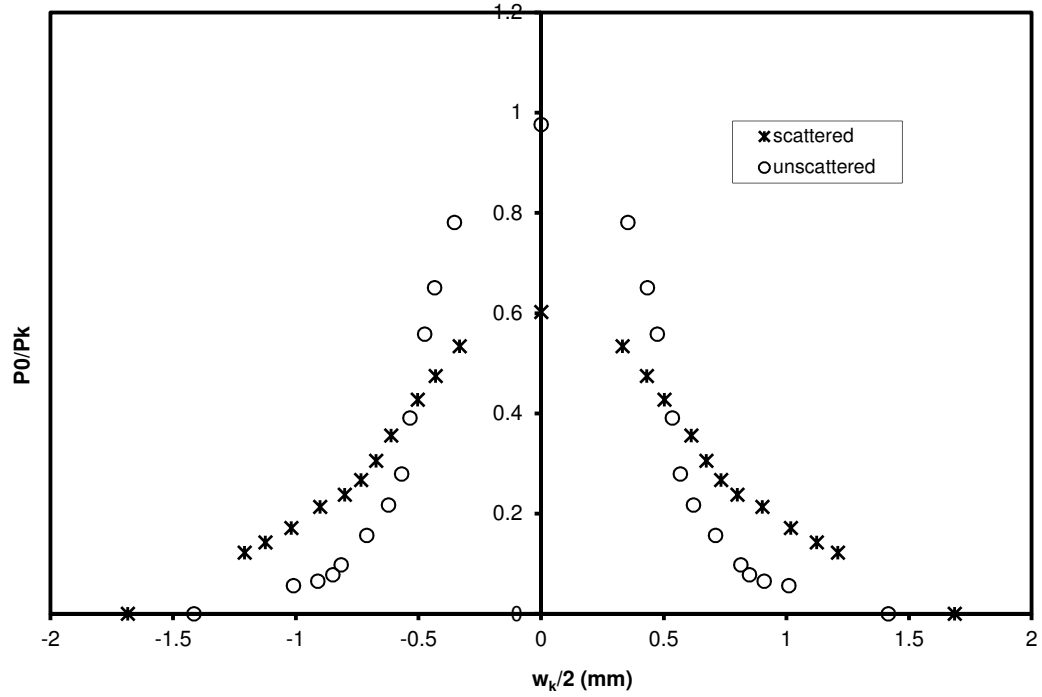

Figure 6. 2: T-NPFD of LDPE before and after scattering

Chen (2009) presented a model to describe the scattered beam profile in terms of NPFD (normalized power flux distribution) of the un-scattered beam and the properties of the transparent material. He defined two new parameters: σ and δ. δ is the scattered fraction of each

micro beam after it passes through the transparent part. The power flux distribution of the micro-beam after passing the transparent part can be described by a Gaussian distribution with a standard deviation σ. Combining this model with TEDD method (Maram, 2010), the following equation is obtained which is the basis for calculation of the scattered beam profile.

$$\frac{P_k}{P_0}\frac{1}{\psi^*(0)}\left[(1-\delta)\psi\left(\frac{w_k}{2}\right)+\sum\delta\psi(x_i)\,w_i P_0\left(\frac{w_k}{2}-x_i\right)\right]=1 \qquad \textbf{(6.3)}$$

P_0, P_k-w_k pairs and the T-NPFD of the un-scattered beam $\Psi(\frac{W_k}{2})$ were determined experimentally. Three fitting parameters (σ, δ *and* $\psi^*(0)$) of equation 6.3 was obtained using the MATLAB code given in appendix D. The value of σ and δ was found to be 0.9 and 0.64 respectively.

6.1.2. Thermal Properties

6.1.2.1. Heat capacity

Temperature dependent heat capacity of LDPE was calculated by the DSC Q100v9.6 Build 290 TA instrument located at Royal Military College of Canada. A heating rate of 10^0C/min was used. The measured heat capacity is presented at Figure 6.3. For 80ºC, the value of heat capacity was reported to be 2.35 J/gK for polyethylene in another study. (Gaur and Wunderlich, 1981)

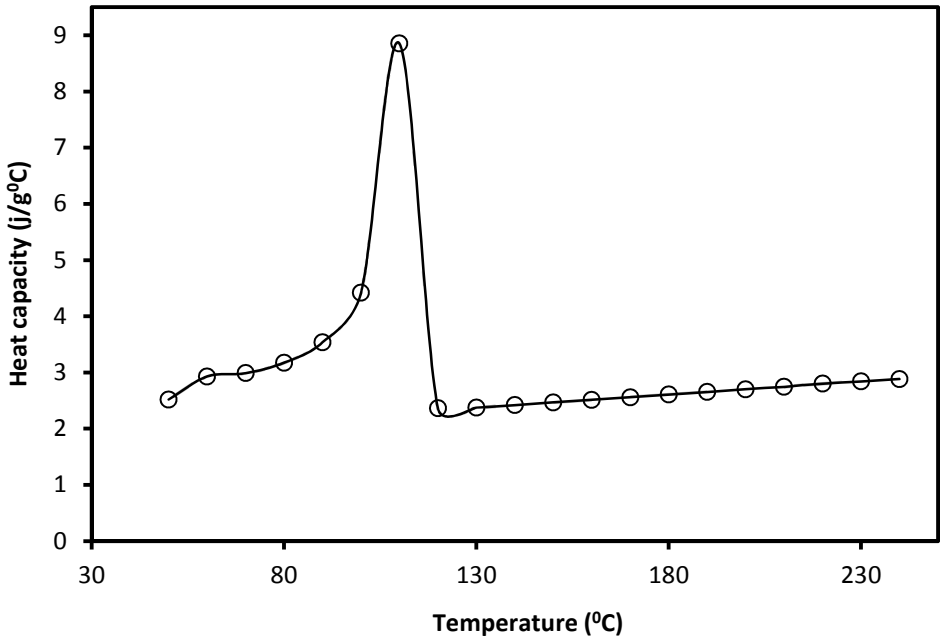

Figure 6. 3: Heat capacity versus temperature of LDPE

6.1.2.2. Density

Data from literature (Mark, 2006) was used to obtain the density. The literature reported the temperature dependent specific volume at different pressures. Density was calculated from the reciprocal of the specific volume and used in FE model. The temperature dependent density is presented in Figure 6.4.

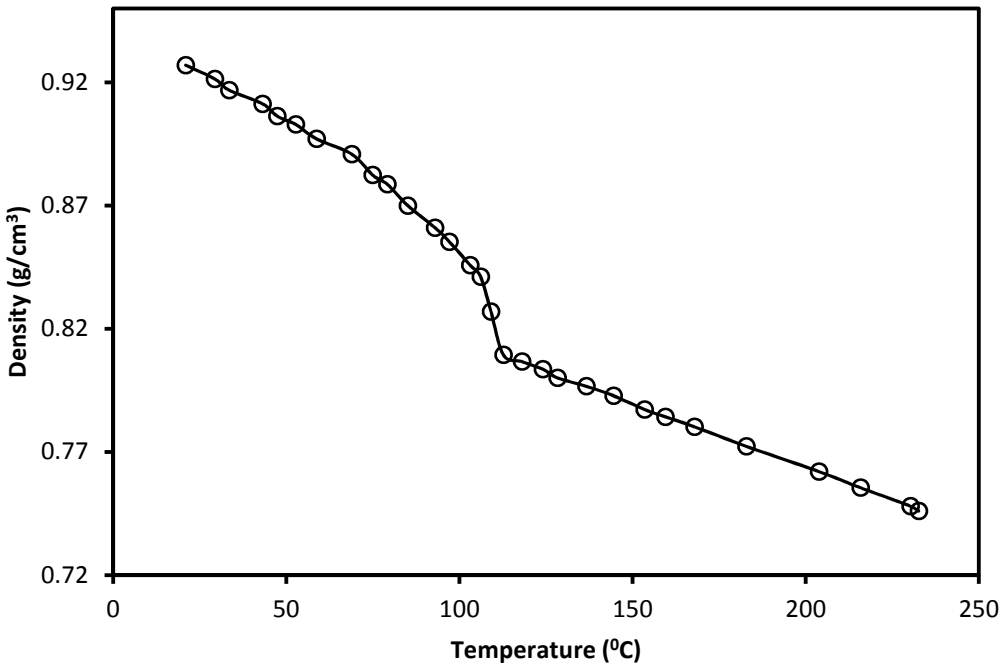

Figure 6. 4: Temperature dependent density of LDPE (Mark, 2006)

6.1.2.3. Thermal conductivity

Data from literature (Sombatsompop and Wood, 1997) was used to determine the thermal conductivity of LDPE. The temperature dependent thermal conductivity of LDPE is given in Figure 6.5. The solid lines represent the measured thermal conductivity by the authors mentioned above. The dashed lines were collected from literature. Values measured by the authors were used in this study.

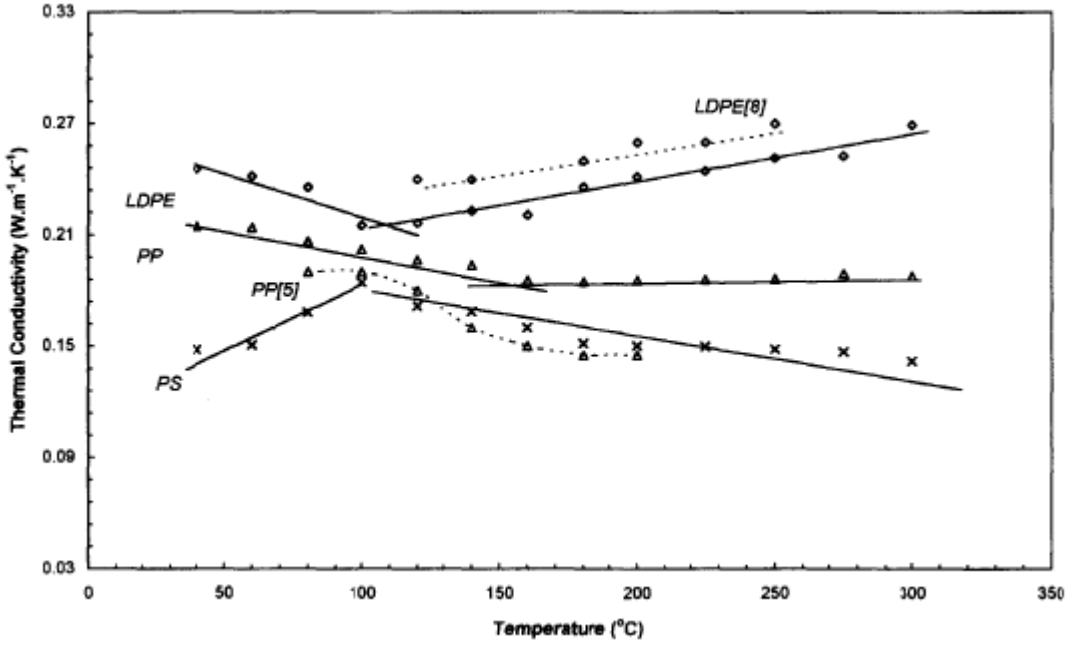

Figure 6. 5: Temperature dependent thermal conductivity of LDPE (Sombatsompop & Wood, 1997)

6.2. FEM

6.2.1. Background

This study uses a 2D, finite element model to simulate contour LTW. The original model was developed by Khosravi (2010). Contour LTW is basically a 3 dimensional, transient heat transfer problem which requires a large computing time and memory. Because of this problem, it was simplified to a 2D problem. The schematic view of the model is presented in Figure 6.6. The temperature of plane A is calculated by the model. The laser beam crosses the simulation plane A perpendicularly. For the sake of simplicity, heat generation in the transparent part was neglected. Transmittance is measured using the technique described in section 6.1. It was used

to calculate the energy reaching to the interface. Heat is conducted to the transparent part causing melting and welding. The heat transfer equation is:

$$c\rho\frac{\partial T}{\partial t} = k\nabla^2 T + Q \qquad \textbf{(6.4)}$$

where *c*, ρ and *k* are heat capacity, density and thermal conductivity of the material respectively. *Q* is the term for heat generation which can be calculated from the following equation. (Chen, 2009)

$$Q = \left|\frac{dP''(y)}{d(y)}\right| = (1-\eta)P''_L A_{1a} e^{(-A_{1t}D_t - A_{1a}y)} \qquad \text{for } 0<y<D_a \quad \textbf{(6.5)}$$

Where A_1 is apparent absorption coefficient, P''_L in the incident laser energy on top of the transparent part and *y* is the depth of the absorbent part. Using the equation 6.4 and 6.5, temperature at any depth *y* can be calculated.

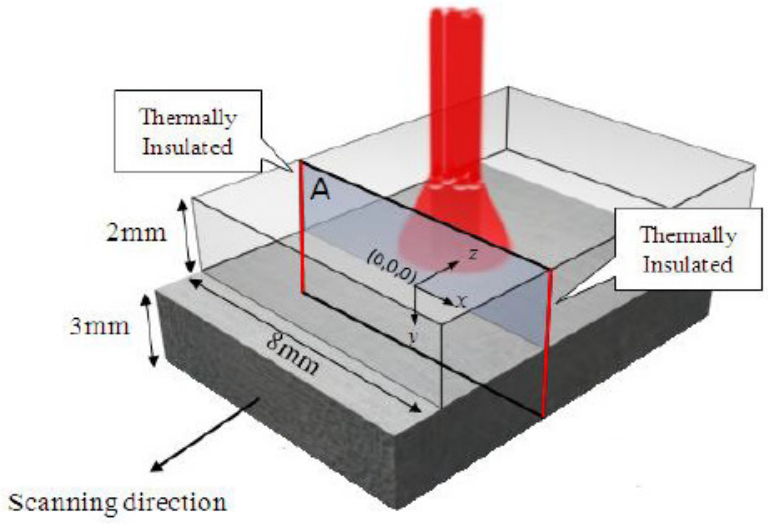

Figure 6. 6: Schematic view of the laser beam passing through plane A in the 2D model developed by Maram (2010)

This study includes both contact and non-contact conditions. In non-contact cases, the transparent and the absorbent parts are separated by a gap. There is no conductive heat transfer between the mating parts for non-contact welding. The input beam power profile at a focal

distance of 82.5 mm was obtained by the pinhole method (Mayboudi et al, 2006). The optical and thermal properties required for modelling can be found in Chapter 6. Some of these properties were determined by the author and some were taken from literature. Comsol® Multiphysics v4.2 software was used for simulation. The model consisted of 21758 elements with 43885 degrees of freedom. A Toshiba personal computer was used to run this model. The solution required approximately 4 minutes to converge.

6.2.2. Simulation results

Validation of the model is done by comparing the experimental welding results with those predicted by the model. The model can give the temperature as a function of time at any location. To determine the validity of the model and to apply the model outputs for modelling of CBA conversion, two measurable parameters were compared with model outputs: minimum power to melt and weld width. Sections 6.2.2.1. - 6.2.2.2 discuss these validation techniques. The temperature versus time at different locations is then discussed in 6.2.2.3.

6.2.2.1. Minimum power to melt

The comparison of minimum power required to start melting was carried out for welding without gaps. The simulation starts with both of the parts exposed to atmospheric temperature (20℃). The beam starts scanning from 16.5 mm behind the plane A to avoid any initial heating. As the beam passes through plane A, the temperature starts to rise very fast, reaches the maximum and the cools down slowly. The simulation work was carried out for 15 seconds. Figure 6.7 shows the time dependent temperature of a point situated 0.065 mm below the center point of the interface. The laser powers are 6, 15 and 20W for 5, 15 and 25 mm/s scan speeds respectively. These powers correspond to the onset of melting in the absorbent part during the

experimental LTW. It can be seen from Figure 6.7 that, as the scan speed increases, the maximum is achieved more quickly. The maximum temperatures are between 110℃-125℃ which is the melting temperature of LDPE according to the DSC test. This serves to partially validate the thermal model.

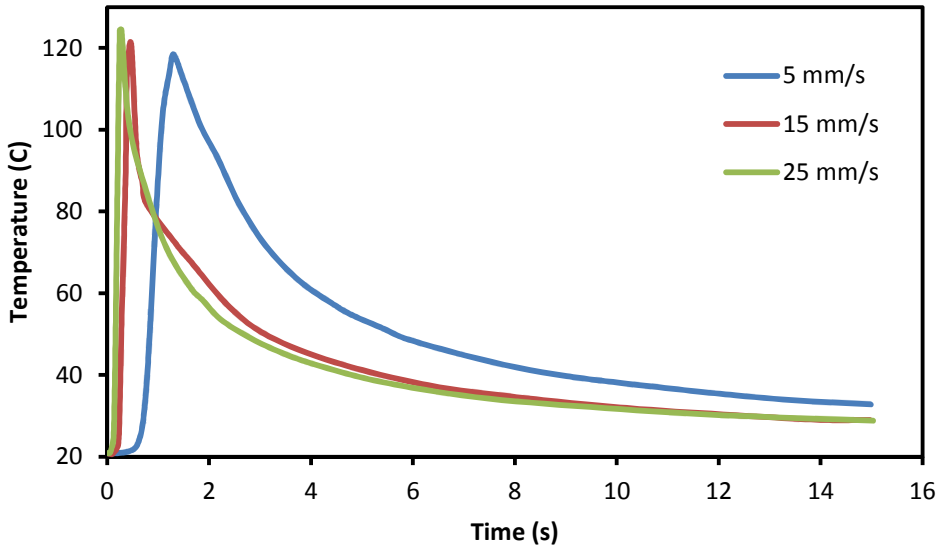

Figure 6. 7: FEM predicted temperature varying with time during contour LTW at various powers (6, 15 & 20W) and scan speeds (5, 15 & 25 mm/s respectively)

6.2.2.2. Weld width comparison

Weld width comparison was carried out for both contact and non-contact conditions. The width of the weld can be determined from the isotherms predicted by the model. Three different isotherms (90℃, 110 ℃ & 120 ℃) were considered for weld width measurement. These three temperatures correspond to the onset, peak and end of melting of LDPE for the DSC curve presented at section 6.1.2.1. The length (along x axis) at which these isotherms cross the interface is considered as weld width. Figure 6.8 represents the comparison of the experimental and model predicted weld width at a 5 mm/s scan speed without gap. Plots for two other scan

speeds without gap can be found in Appendix C. It can be seen that the samples with CBA have experimentally wider weld width compared to samples without CBA.

The model predicted widths are higher than the experimental ones. The 120℃ isotherm which gives the closest match to the experimental values is found to be 25% higher than the experimental width for samples with CBA. In case of samples without CBA the difference is 50%. One possible reason for this overestimation of interfacial temperature might be related to the higher estimation of the absorption coefficient than the actual one. Moreover, the absorption coefficient, which was considered constant in this model, may actually vary with the temperature (Geiger et al, 2009). The thermal conductivity which is collected from literature might be lower than the real value which would lower thermal conduction and thus predicting wider width.

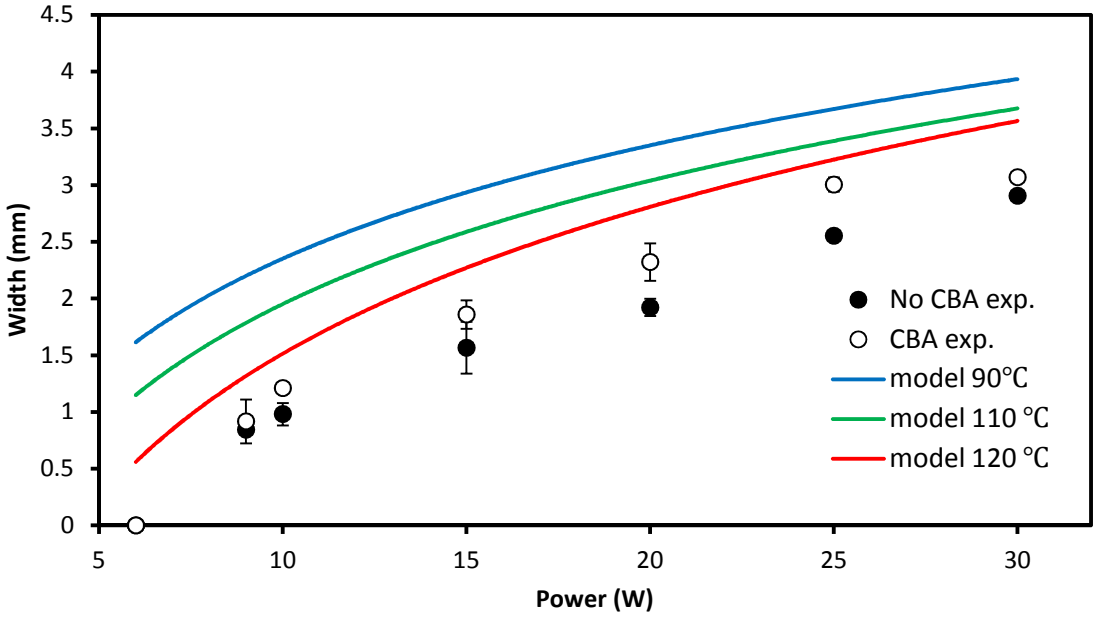

Figure 6. 8: Comparison of experimental and predicted weld width at 5 mm/s scan speed (without gap)

Figure 6.9 shows the comparison of experimental and model predicted weld widths at 5 mm/s scan speeds for welding with gaps. Figures for other speeds are given in Appendix C. It can be seen that for these non-contact tests, the model is again slightly over-estimating the width at low powers and under-estimating the width at high powers. In the middle of the power range, the model corresponds accurately with experiment. At high powers, polymer conversion takes place which might have widened the weld seam. FEM does not account for conversion; it only gives the temperature output. This might be the reason of under estimation of weld seam width at high powers.

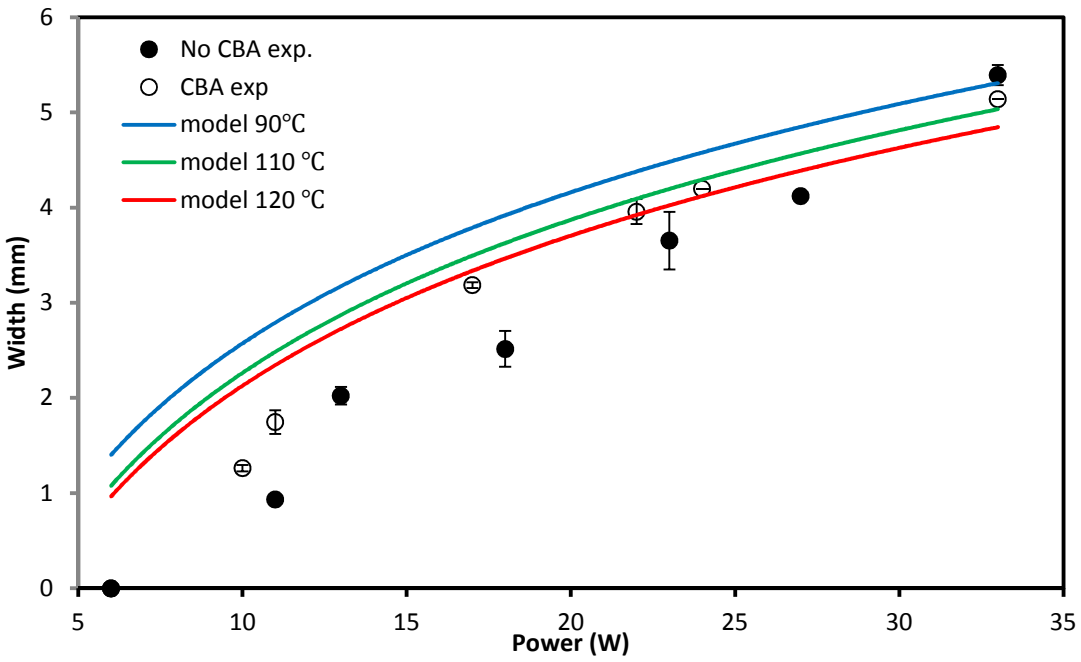

Figure 6. 9: Comparison of experimental and model predicted weld width at 5 mm/s scan speed and different gap settings

6.2.2.3. Temperature versus time at different locations

For a specific set of parameters, the FEM thermal simulation gives the temperature of any point within the geometry as a function of time. The temperature history of a point at any specific location thus can be extracted from simulation results. The extracted temperature-time profiles were used to calculate the conversion of CBA at different locations. Figure 6.10 shows a set of 16 points located within the right half of the absorbent part. Each of them were separated 0.8 mm along X axis and 0.4 mm along Y axis. The laser beam is centered at this (0,0). These 16 points served as a starting network for calculating CBA conversion. For each set of parameters (power, speed and gap), the values of conversion at those 16 points were calculated and plotted against location. Sigmaplot was used to create conversion plots. For some cases, 16 points were not enough to create smooth shaped plots. In those cases more points were taken within the given points to obtain conversion plots in smooth shape. Once conversion for this area is found, the other half of the symmetry plane can also easily be found.

The dimensions of the network shown in Figure 6.10 were chosen keeping the fact in mind that this area has to be big enough to fit the CBA conversion and molten volume inside for all of the LE used in this experiment. However while calculating the conversions, it was seen that for the largest LE, the conversion contour goes beyond the network of points. For that specific case extrapolation was used to obtain the full plot. All other conversion plots fit very well within the given network of Figure 6.10.

Figure 6.11 shows one typical temperature-time output plot. The four lines with different colors represent temperatures of 4 points situated at x=0.

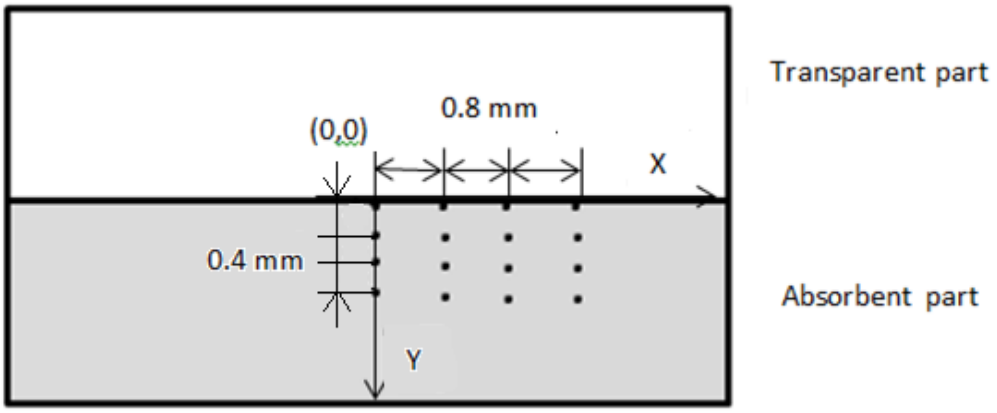

Figure 6. 10: Position of the points for determining temperature time profile at different locations.

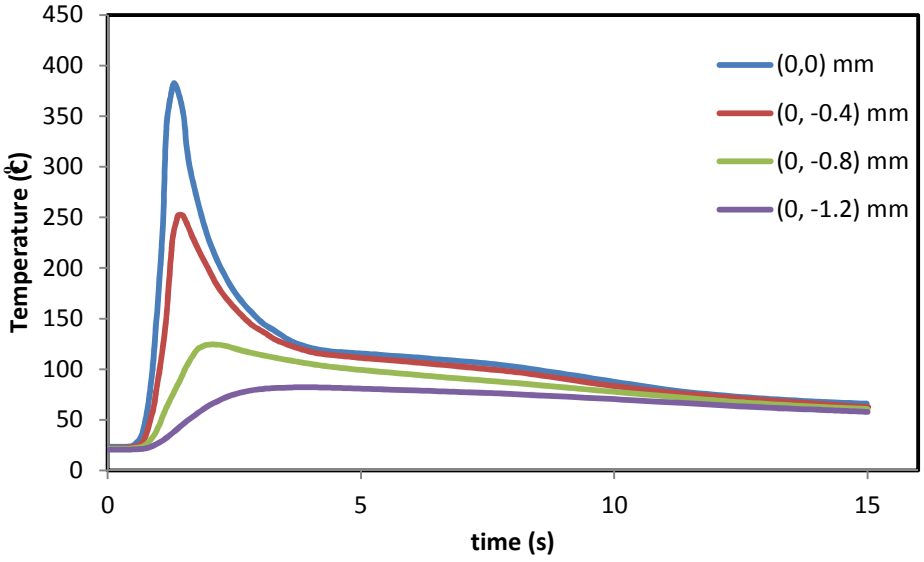

Figure 6. 11: Temperature versus time for four different points with x=0 and y=0, -0.4, -0.8 and -1.2 respectively.

6.3. Conversion of CBA

To study the gap bridging phenomenon during LTW, modelling of CBA conversion is the most crucial factor. Combining the temperature information from FEM with the kinetic parameters, conversion of CBA can be modelled. This conversion of CBA is the key factor to study foaming which makes the gap bridging possible.

6.3.1. Basics of the ODE

The details of kinetic analysis method can be found in Chapter 3. Thermal conversion of 5PT can be described by a nth order reaction order model. The equation for thermal decomposition of 5PT is given below:

$$\frac{d\alpha}{dt} = \boldsymbol{A}\, exp\left(-\frac{E}{\boldsymbol{RT}}\right)(1-\alpha)^n \qquad \textbf{(6.6)}$$

Where n = 1.6 and $\boldsymbol{A}$ = 2.4×10^{12} 1/s and E = 125 kJ/mol. At t=0, the initial conversion was taken as 0. The temperature T, which is a function of time, can be found from the FEM. However, the FEM output comes as discrete T-t pairs. The polynomial equations describing $T=f(t)$ were determined using Microsoft Excel. These polynomials can be found in appendix F.

6.3.2. Conversion of CBA at different locations

To determine the amount of conversion during LTW, a MATLAB code was developed by the author to solve eqn. 6.6 to obtain the CBA conversion at each specific point as a function of time. The code can be found in Appendix D. Initially there was no conversion of CBA. To obtain the conversion of each of the points shown in Figure 6.10, the code was run with the temperatures [$T=f(t)$] of that specific point for every single set of parameters (power, speed and

gap). To represent conversion at different locations graphically, Sigmaplot was used. The 3D contour plot option of Sigmaplot can show the percentage of conversion as different coloured region which is a convenient option to observe the conversion of CBA in the absorbent part.

The experimental part of this study includes both gap and without gap conditions. It is quite interesting to compare the extent of conversion for the hottest point at the same *LE* with & without gap. Figure 6.12 shows the comparative conversion of CBA of the hottest point. For the samples with gap (a), the hottest point is located at (0,0) while for samples without gap, the location is at (0, -0.065 mm). Laser power was 10W for this case with a scan speed of 5 mm/s. It can be observed that for the same power and speed, the extent of conversion reaches 100% for the sample with gap. On the other hand, the sample without the gap shows very little conversion. This type of behaviour is quite understandable and desired. With the same *LE*, the sample with the gap reaches a temperature that's almost double compared to the one without gap. This phenomenon is expected because where there is no contact, there is no chance for the heat to be conducted to the transparent part. This allows for higher temperatures in the absorbent part and permits the formation of localized gas generation at the places where gap is present. The lower temperature of the areas without gap should prevent the CBA from decomposing which is should ideally maintain weld strength equal to that of the sample without CBA.

From Figures 5.7 and 5.10, it can be seen that for this specific condition, the maximum load at break of the weld is same for samples with and without CBA under contact conditions. However, the weld width is higher for samples with CBA and this makes the weld strength of the CBA sample 17% lower than that of the sample without CBA. Thus, in spite of no theoretical CBA decomposition, the weld strength of CBA containing specimens is lower. This

might be caused by the blowing agent acting as a stress concentration or the addition of the carrier resin with CBA which might have lower properties than that of the base resin LDPE.

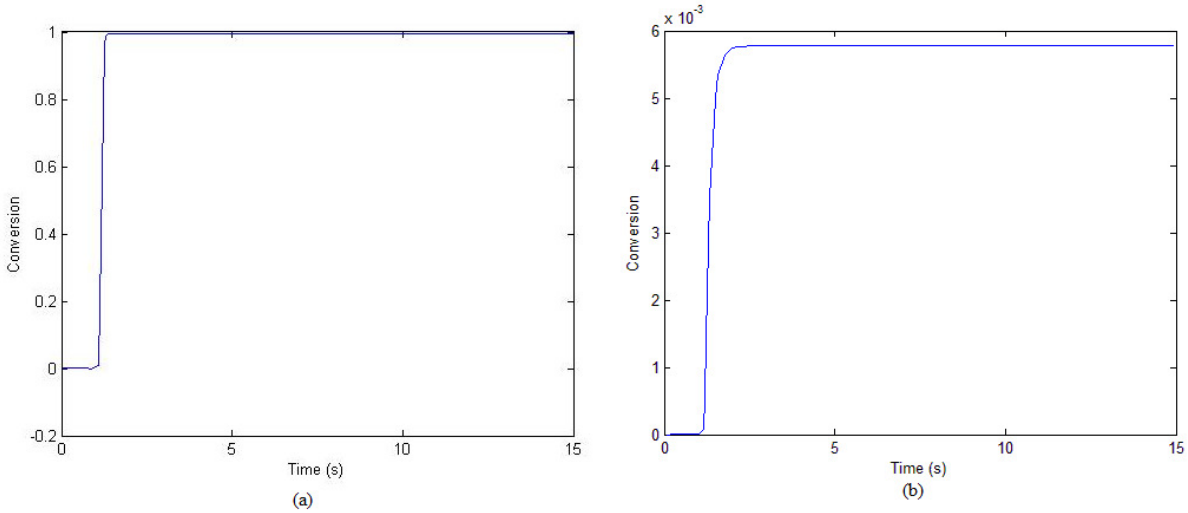

Figure 6. 12: Amount of conversion of CBA at the hottest spot with laser power: 10W and scan speed: 5 mm/s. (a) with 0.127 mm gap & (b) no gap.

Figure 6.13 shows the theoretical amount of degraded CBA for three different power and speed combinations. The laser power and scan speed for each of the plots are 11W/5 mm/s (LE: 2.2 J/mm); 26W/15 mm/s (1.73 J/mm) and 38 W/25 mm/s (1.52 J/mm) respectively from left to right. All of these samples bridged 0.254 mm gap. Figures of all other gaps can be found in Appendix E.

It can be seen from these conversion plots that, for 5 mm/s scan speed, the volume of material exhibiting a CBA conversion bigger than zero is larger compared to cases at higher speed. For the two other speeds, there is not much difference observed in the volume of foamed material. It is hypothesized that slower speed facilitates thermal conduction which in turn gives the material the chance to attain the temperature-time combination required to cause decomposition of CBA.

A larger volume of converted CBA would theoretically result in a larger foaming volume which would bridge gaps better. In reality there are a number of other factors which influences the actual foaming process such as viscosity of the resin, holding time etc. Despite of those facts, experimentally the best gap bridging was found at the slowest speed (5 mm/s) which is in accordance with the model.

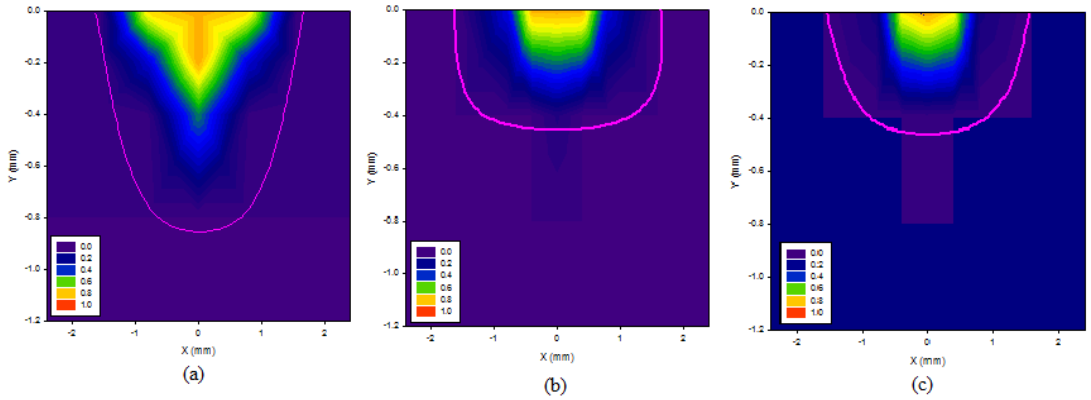

Figure 6. 13: Percentage of degraded CBA at different points for laser welding with 0.254 mm gap. (a) Laser power: 11W, scan speed: 5 mm/s (b) Laser power: 26W, scan speed: 15 mm/s (c) Laser power: 38 W, scan speed: 25 mm/s

It is also interesting to observe the amount of molten volume which is shown by the pink line in Figure 6.13. It is the region in which the material has reached a temperature of 120℃. It can be seen that the volume of foamed material, is smaller compared to the molten polymer volume (i.e. it is always situating inside the pink line). This shows that only a relatively small portion of the molten polymer actually foamed and took part in gap bridging. This helps explain the observation that the minimum power required to bridge a certain gap with samples having or not having CBA does not differ significantly. The large volume of molten polymer actually took part in gap bridging by thermal expansion as well. The selection of CBA has a big significance for such instances. The procedure described in this work can be used as an effective tool to find

a CBA with desired kinetic parameters which would allow bigger portion of molten polymer to be foamed.

It is interesting to examine the extent of conversion of CBA as a function of *LE* for different scan speeds. It gives a clearer indication of the effect of speed on gap bridging. Figure 6.14 shows the depth at which the CBA is 40% degraded as a function of *LE*. It can be seen that, at a speed of 5 mm/s speed, the depth continues to increase with *LE* whereas at higher speeds, the depth appears to level off. This plot suggests that, if all of the produced gas could be kept inside the polymer matrix, then the lowest speed would show significantly better gap bridging than the higher ones.

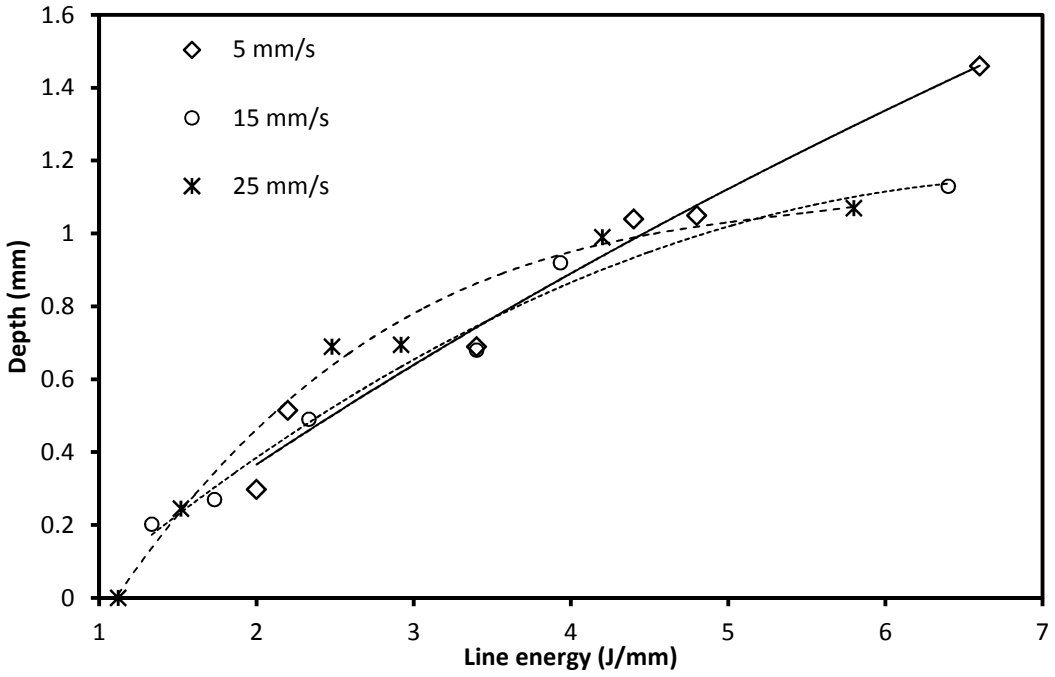

Figure 6. 14: Depth at which the material reaches to 40% conversion as a function of LE

Chapter 7

Summary

7.1. Conducted work

7.1.1. Experimental work

A brief survey was carried out on the thermal and kinetic properties of commercially available CBA materials. Four different CBA samples were collected and then TGA experiments were performed to choose the most suitable one for laser welding experiments. 5PT was found to be suitable mostly based on the decomposition temperature range and gas yield. A detailed thermal conversion analysis was then conducted to find the thermal degradation mechanism and reaction rate parameters of 5PT.

For the welding experiments, injection moulded samples were made using LDPE as base resin and CB as absorbing pigment. To observe the effect of adding CBA, two sets of samples were made with equal CB levels, one without CBA and the other one with CBA. A purpose built fixture was also constructed to create the desired gaps during welding.

Contour LTW was performed using a Rofin-Sinar DLx16 (940 nm wavelength) and UW200 workstation. Welding was performed with and without gaps for both set of samples. Weld strength was determined by pull-testing using an INSTRON 4206 Universal testing machine. The minimum power required to bridge a given gap, as well as weld strength were compared for samples with or without CBA. To better understand the observed results, weld microstructure

analyses were also performed using SEM. The experimental determination of the optical and thermal properties of the materials was performed to provide input for modelling.

7.1.2. Modelling work

The conversion of CBA during LTW was modelled using a 2D FEM using Comsol® Multiphysics software. This FEM can predict the temperature at different locations of the sample as a function of time. These temperature-time profiles were used later in combination with the kinetic parameters of thermal degradation of 5PT to calculate the percentage of conversion of CBA. A Matlab® code was written to solve the ODE of thermal degradation of 5PT. Sigmaplot software was used to plot level of conversion of CBA at different positions. The output from the modelling section gave a reasonable explanation of the findings from the experimental section.

7.2. Conclusions

From the conducted work presented above, the following conclusion can be made:

- This work is the first to conduct a comparative study to assess the effect of foaming to bridge gap during contour LTW. The comparison between two sets of material with identical CB level shows that addition of CBA creates thermoplastic foam which shows a limited improvement in gap bridging. Presence of CBA lowered the required power by 15% to bridge the same gap in case of best gap bridging experiment.
- The weld strength of the samples with CBA was found lower than ones without CBA which is logical because presence of thermoplastic foam is expected to decrease the contact area and hence weld strength.

- Thermal degradation analysis of 5PT was performed to find the kinetic triplet. There is no data available currently for this material regarding thermal degradation.
- A detailed method to model the CBA degradation during LTW was developed in this work. This model shows the conversion at different locations as a function of time. This model can be used to find the most effective CBA by calculating the amount of conversion each of the CBA would undergo for those particular operating conditions.
- This work is an exploration of the new concept of gap bridging by laser induced foaming. With the findings of the study, further work can be conducted with a good combination of base resin and CBA which would allow better foaming and gap bridging performance.

7.3. Recommendation

There is area for further research as a continuation of this work. Choosing a base resin with a higher viscosity might enable one to observe if it can "keep" all of the gas produced within the polymer matrix to give better foaming. A CBA with higher decomposition point might enable one to apply this technique to resins with higher melting temperature. Finding a better combination of the base resin and CBA which would foam a larger percentage of the molten polymer is necessary for a successful gap bridging work. More microstructural analysis work is needed to obtain a clear idea about what is happening in the HAZ of the absorbent part during laser heating.

Reference

1. Acherjee, B., Kuar, A. S., Mitra, S., Misra, D., *Effect of carbon black on temperature field and weld profile during laser transmission welding of polymers: A FEM study,* 2012, Elsevier, Optics & Laser Technology, vol. 44, pp514-521
2. Azhikannickal, E., Bates, P. J., Zak, G., *Thermal Imaging technique to characterize laser light reflection from thermoplastics,* 2012, Elsevier, Optics and laser technology, vol. 44, pp1456-1462
3. Bachmann, F. G., Russek, U. A., *Laser welding of polymers using high power diode lasers,* Proceedings of SPIE, vol. 5121, pp385-398
4. Bates, P. J., Druart, M-E., Chen, M., Zak, G., Billiet, J., *Influence of part thickness, glass fibre content and line energy on laser transmission welding of polyamide mXD6,* ANTEC 2007, pp2783-2787
5. Bates, P. J., Gak, G., Chen, M., *Contour laser transmission welding-how fast is fast enough,* ANTEC 2013, pp1652-1659
6. Baylis, B., Prabhakaran, R., Bates, P., Huang, Y. P., Xu, S. X., Watt, D., *Pyrometer measurements during laser welding of thermoplastic elastomers to polypropylene and of nylon to itself*, ANTEC 2003, pp1111-1115
7. Blais, L., *Introduction to laser welding,* 2006, CSTPQ.
8. Bryden, B., *High power diode laser transmission welding of plastics*, 2000, vol. 20, num. 2, pp136-139.
9. Bulow, J. F. V., Bager, K., Thirstrup, C., *Utilization of light scattering in transmission laser welding of medical devices,* 2009, Elsevier, Applied surface science, vol. 256, pp900-908

10. Cao, X., *Weld read-through defects in laser transmission welding,* 2010, MSc thesis, Queen's University, Kingston ON.
11. Chen, M., *Gap bridging in laser transmission welding of thermoplastics,* 2009, PhD thesis, Queen's University, Kingston ON.
12. Chen, M., Zak, G., Bates, P. J., Mcleod, M., Rouison, D., *Surface damage threshold in laser transmission welding of polycarbonate,* ANTEC 2007, pp1-5
13. Chen, M., Zak, G., Bates, P., Baylis, B., Mcleod, M., *Method of evaluating shear strengths in contour laser transmission welding,* 2007, SAE international.
14. Chrissafis, K., *Kinetics of thermal degradation of polymers. Complementary use of isoconversional and model-fitting methods,* 2009, Journal of thermal analysis and calorimetry, vol. 95, pp273-283
15. Coelho, J. P., Abreu, M. A., Pires, M. C., *High-speed laser welding of plastic films,* 2000, Elsevier, Optics and lasers in engineering, vol. 34, pp385-395
16. Eaves, D., *Handbook of polymer foams,* 2004, rapra technology.
17. Gaur, U., Wunderlich, B., *Heat capacity and other thermodynamic properties of linear macromolecules. II. Polyethylene,* 1981, Journal of physical chemistry, vol. 10, pp119-152
18. Geiger, M., Frick, T., Schmidt, M., *Optical properties of plastics and their role for the modelling of the laser transmission welding process,* 2009, Springer, Production engineering research and development, vol. 3, pp49-55
19. Grewell, D.A., *Applications with infrared welding of thermoplastics,* ANTEC 1999.
20. Grewell, D., Rooney, P., Kagan, V. A., *Relationship between optical properties and optimized processing parameters for through transmission laser welding of*

thermoplastics, 2004, Sage publications, Journal of reinforced plastics and composites, Vol. 23, pp229-247

21. Grewell, D., Benatar, A., *Experiments in micro-welding of polycarbonate with laser diodes,* ANTEC 2003, pp1039-1044
22. Grewell, D. A., Rooney, P., Kagan, V. A., *Relationship between optical properties and optimized processing parameters for through transmission laser welding of thermoplastics,* ANTEC 2002.
23. Haberstroh, E., Hoffmann, W-M., *Laser transmission welding of complex micro plastic parts,* 2008, SAGE publications, Proceedings of the Institution of Mechanical Engineers, vol. 222, pp47-54
24. Haberstroh, E., Schulz, J., Luetzeler, R., *Thermographic characterisation of polymers for the laser transmission welding,* ANTEC 2002, Institut für Kunststoffverarbeitung (IKV)
25. Hadriche, I., Ghorbel, E., Masmoudi, N., Casalino, G., *Investigation on the effects of laser power and scanning speed on polypropylene diode transmission welds*, 2010, Springer, International journal of advanced manufacturing technology, vol. 50, pp217-226
26. http://www.google.ca/url?sa=t&rct=j&q=&esrc=s&source=web&cd=4&ved=0CEcQFjAD&url=http%3A%2F%2Fwww.leister.com%2Fuploads%2Fpdf%2Fen%2Fleister_laser_eng.pdf&ei=zakeU_GJBYy2rgHsnoCYAw&usg=AFQjCNGBg7NrVHRa9Ec4_qnKXbNLe9j6aA&sig2=UlSJKZ1CVX5pyZePMaBfag&bvm=bv.62788935,d.aWM
27. https://www.google.ca/search?q=thermoplastic+foam&safe=active&source=lnms&tbm=isch&sa=X&ei=QSU7U5rAIdL82gXy0IGQDQ&ved=0CAYQ_AUoAQ&biw=1366&bih=631#facrc=_&imgdii=_&imgrc=S0VWy1jEPshJM%253A%3BNYYtqakvMwuDC

M%3Bhttp%253A%252F%252Fimg.directindustry.com%252Fimages_di%252Fphoto-g%252Ffire-resistant-thermoplastic-foam-panels-composites544992844113.jpg%3Bhttp%253A%252F%252Fwww.directindustry.com%252Fprod%252Fairex-ag%252Ffire-resistant-thermoplastic-foam-panels-composites-54499404668.html%3B1999%3B1500

28. http://www.twi-global.com/technical-knowledge/published-papers/industrial-lasers-and-applications-in-automotive-welding/
29. https://www.laserstar.net/medical-device/index.cfm
30. Huang, C., Gao, Y., Liu, H., Chen, H., Li, P., Wang, X., *Multi-factors interaction effects of process parameters on the joint strength of laser transmission joining between PC and PA66,* 2013, Key engineering materials vols. 579-580, pp91-96
31. Ilie, M., Cicala, E., Grevey, D., Mattei, S., Stoica, V., *Diode laser welding of ABS: Experiments and process modelling,* 2009.
32. Jimenez, P. E. S., Maqueda, L. A. P., Perejon, A., Criado, J. M., *Combined kinetic analysis of thermal degradation of polymeric materials under any thermal pathway,* 2009, Elsevier, Polymer degradation and stability, vol. 94, pp2079-2085
33. Jimenez, P. E. S., Maqueda, L. A. P., Perejon, A., Criado, J. M., *A new model for the kinetic analysis of thermal degradation of polymers driven by random scission,* 2010, Elsevier, Polymer degradation and stability, vol. 95, pp733-739
34. Kagan, V. A., Bray, R. G., Kuhn, W. P., *Laser transmission welding of semi-crystalline thermoplastics-Part I: Optical characterization of nylon based plastics,* 2002, Journal of reinforced plastics and composites, vol. 21, pp1101-1122
35. Kirkland, T. R., *Practical joint designs for laser welding of thermoplastics,* ANTEC 2004, pp1236-1240

36. Klein, R., Wissemborski, R., *Foam bridges joint gaps,* 2012, Kunststoffe international, pp57-59.

37. Kurosaki, Y., *Radiative heat transfer in plastic welding process,* 2005, Elsevier, Journal of quantitative spectroscopy & radiative transfer vol. 93, pp25-41

38. Lee, C., Ballou, R., *Laser energy transmission (LET) measurements of 30% glass reinforced nylon 6,* ANTEC 2007, pp1900-1904

39. Malek, J., *The kinetic analysis of non-isothermal data,* 1992, Thermochimica acta, vol. 200, pp257-269

40. Maram, S. K., *laser transmission welding of polybutylene terephthalate and polyethylene terephthalate blends,* 2010, MSc thesis, Queen's University, Kingston ON.

41. Mark, J. E., *Physical properties of polymers handbook,* 2006, Springer, 2nd ed.

42. Mayboudi, L. S., Birk, A. M., Zak, G., Bates, P. J., *A 3-D thermal model of laser transmission contour welding for a lap joint,* ANTEC 2007, pp2813-2817

43. Mayboudi, L. S., Chen, M., Zak, G., Birk, A. M., *Characterization of beam profile for high power diode lasers with application to laser welding of polymers,* ANTEC 2006, pp2274-2278.

44. Moskvitin, G. V., Polyakov, A. N., Birger, E. M., *Laser welding of plastics (review),* 2013, Taylor & Francis, Welding international, vol. 27, pp725-734

45. Okoro, T. B., *Thermal degradation of PC and PA6 during laser transmission welding,* 2013, MSc thesis, Queen's University, Kingston ON.

46. Park, J. W., Oh, S. C., Lee, H. P., Kim, H. T., Yoo, K. O., *A kinetic analysis of thermal degradation of polymers using a dynamic method,* 2000, Elsevier, Polymer degradation and stability, vol. 67, pp535-540

47. Potente, H., Korte, J., Becker, F., *Laser transmission welding of thermoplastics: analysis of the heating phase,* 1998, Society of plastics engineers.

48. Potente, H., Fiegler, G., Becker, F., Korte, J., *Comparative investigations on quasi-simultaneous welding on the basis of the materials PEEK and PC,* 2002, Institut für Kunststofftechnik.

49. Rhew, M., Mokhtarzadeh A., Benatar, A., *Diode laser characterization and measurement of optical properties of polycarbonate and high density polyethylene,* ANTEC 2003, pp1056-1060.

50. Russek, U. A., Palmen, A., Staub, H., Pohler, J., Wenzlau, C., Otto, G., Poggel, M., Koeppe, A., Kind, H., *Laser beam welding of thermoplastics,* 2003, Proceedings of SPIE, vol. 4977, pp458-472

51. Sombatsompop, N., Wood, A. K., *Measurement of thermal conductivity of polymers using an improved Lee's disc apparatus,* 1997, Elsevier, Polymer testing vol. 16, pp203-223

52. Speka, M., Mattei, S., Pilloz, M., Ilie, M., *The infrared thermography control of the laser welding of amorphous polymers,* 2008, Elsevier, NDT & E international, vol. 41, pp178-183

53. Steen, W. M., Mazumder, J., *Laser material processing,* 2010, Springer, fourth edition.

54. Vegte, E. V. D., Gurp, M. V., Hoekstra, H., Stroeks, A., *Engineering plastics for laser welding,* ANTEC 2007, pp1894-1899

55. Ven, J. D. V. D., Erdman, A. G., *Laser transmission welding of thermoplastics-Part II: Experimental model validation,* 2007, Journal of manufacturing science and engineering, vol. 129, pp859-867

56. Ven, J. D. V. D., Erdman, A. G., *Laser transmission welding of thermoplastics-Part II: Experimental model validation,* 2007, Journal of manufacturing science and engineering, vol. 129, pp859-867

57. Vyazovkin, S., Burnham, A. K., Criado, J. M., Maqueda, L. A. P., Popescu, C., Sbirrazzuoli, N., *ICTAC kinetics committee recommendations for performing kinetic computations on thermal analysis data,* 2011, Elsevier, Thermochimica acta vol. 520, pp1-19

58. Wang, C. Y., Bates, P. J., Zak, G., *Optical properties characterization of thermoplastics used in laser transmission welding: transmittance and reflectance,* ANTEC 2009, pp1278-1282

59. Wippo, V., Devrient, M., Kern, M., Jaeschke, P., Frick, T., Stute, U., Schmidt, M., Haferkamp, H., *Evaluation of a pyrometric-based temperature measuring process for the laser transmission welding,* 2012, Physics Procedia, vol. 39, pp128-136.

60. Woosman, N. M., Sallavanti, R. A., *Achievable weld strengths for various thermoplastics using the clearweld® process,* ANTEC 2003, pp2522-2526

61. Wu, C-Y., Cherdron, M., Douglass, D. M., *Laser welding of polypropylene to thermoplastic polyolefins,* ANTEC 2003, pp1147-1151

62. Wu, C-H., Chang, C-Y., Hor, J-L., Shih, S-M., Chen, L-W., Chang, F-W., *On the thermal treatment of plastic mixtures of msw: pyrolysis kinetics,* 1993, Waste Management, vol. 13, pp 221-235.

63. Xu, X. Q., Huang, Y. P., Watt, D., Baylis, B., *Diode laser welding of EPDM based elastomers,* ANTEC 2003, pp1105-1110

64. Xu, X. F., Bates, P. J., Zak, G., *Effect of glass fiber and crystallinity on light transmission during laser transmission welding of thermoplastics,* 2015, Elsevier, Optics and laser technology, vol. 69, pp133-139

65. Zak, G., Mayboudi, L., Chen, M., Bates, P. J., Birk, M., *Weld line transverse energy density distribution measurement in laser transmission welding of thermoplastics,* 2010, Elsevier, Journal of materials processing technology, vol. 210, pp24-31

66. Zweifel, H., Maier, R. D., Schiller, M., *Plastics additives handbook,* 2008, Hanser publication, 6th ed.

Appendix A

Laser beam profile of Rofin-Sinar DLx16 HP diode laser

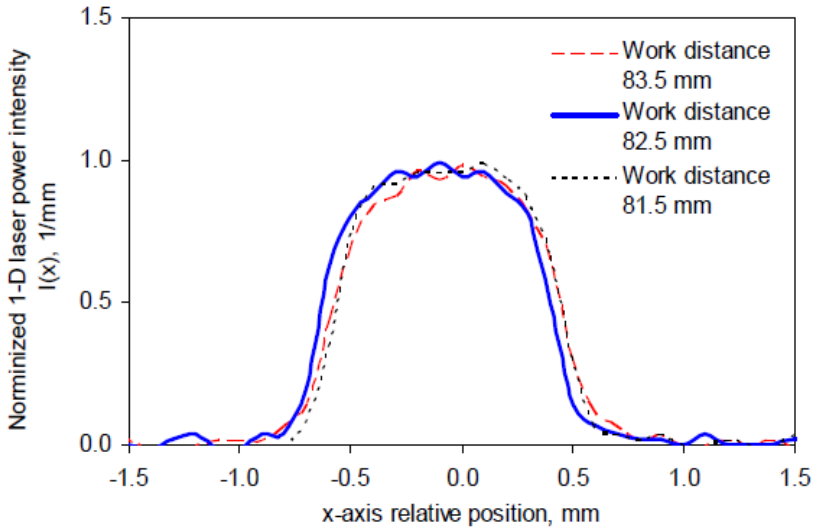

Figure A. 1: 1D laser beam profile along x axis at working distance 81.5-83.5 mm

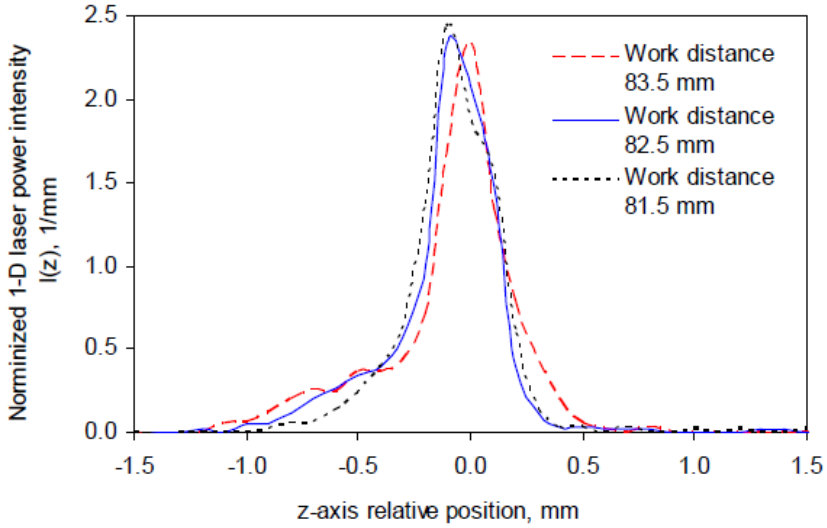

Figure A. 2: 1D laser beam profile along z axis at working distance 81.5-83.5 mm

Appendix B

Thermal degradation curves of CBA samples at different heating rates

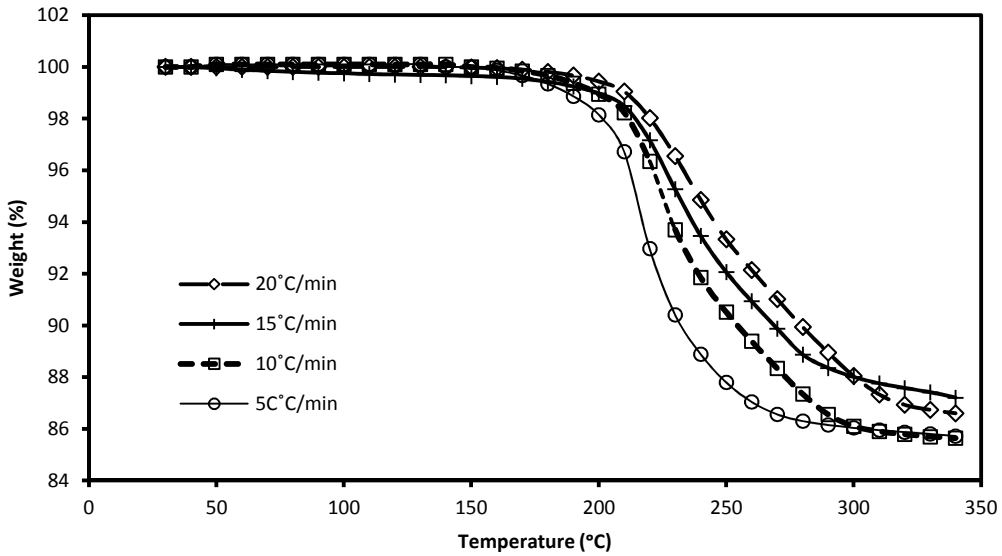

Figure B. 1: Thermal decomposition curves for TRACEL® IM 2240 ST (5PT)

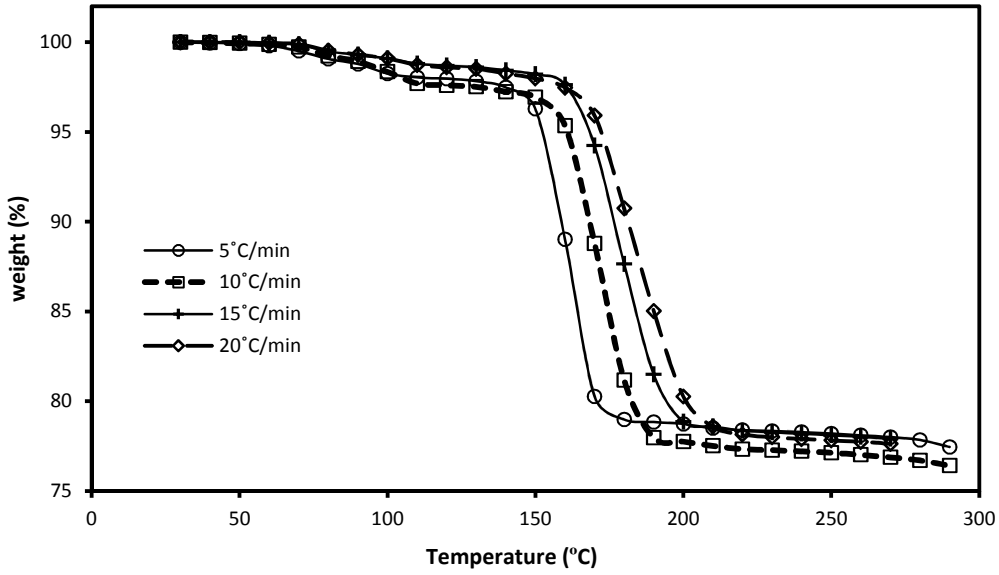

Figure B. 2: Thermal decomposition curves for TRACEL® NE 7200 ($NaHCO_3$+Citric acid)

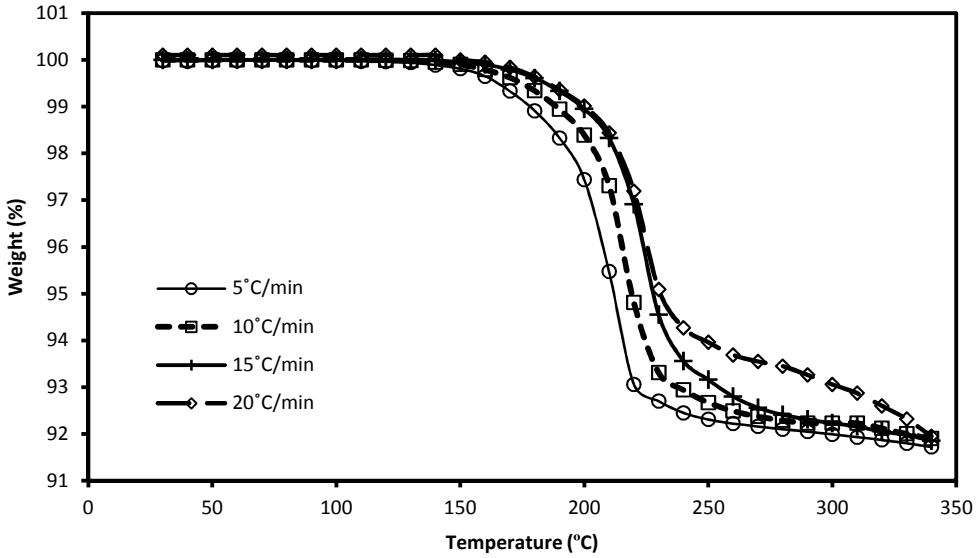

Figure B. 3: Thermal decomposition curves for BERGEN XO-331 (Modified Azodicarbonamide)

Appendix C

Comparison of experimental and model predicted weld widths

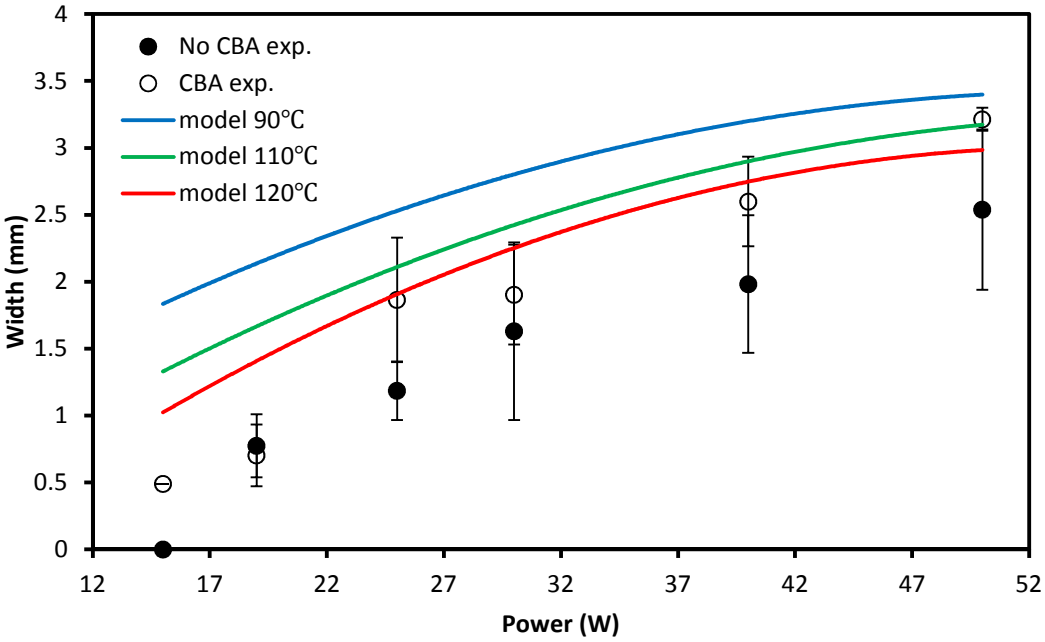

Figure C. 1: Comparison of experimental and model predicted weld width at 15 mm/s scan speed (without gap)

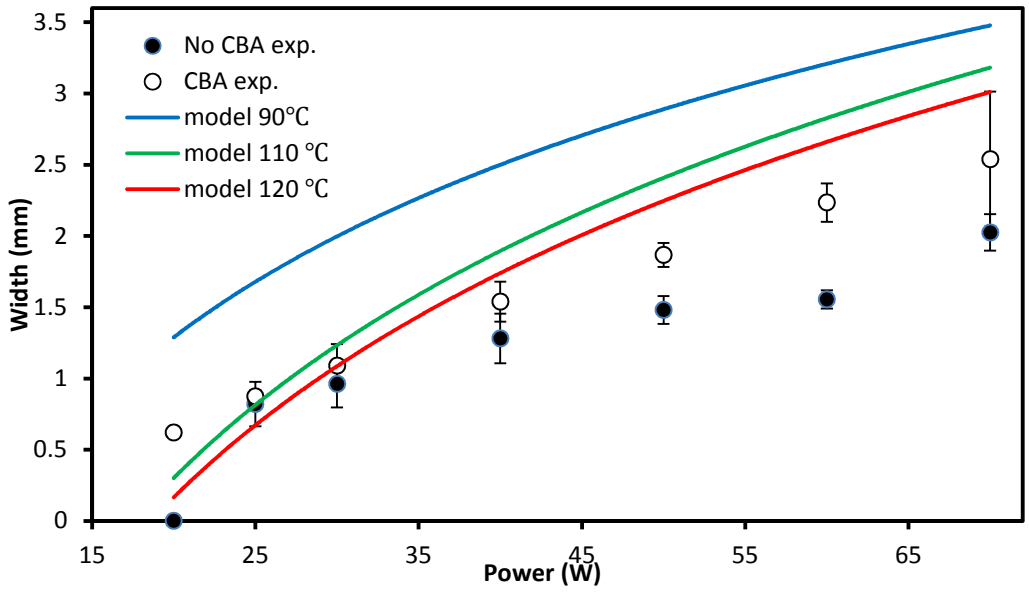

Figure C. 2: Comparison of experimental and model predicted weld width at 25 mm/s scan speed (without gap)

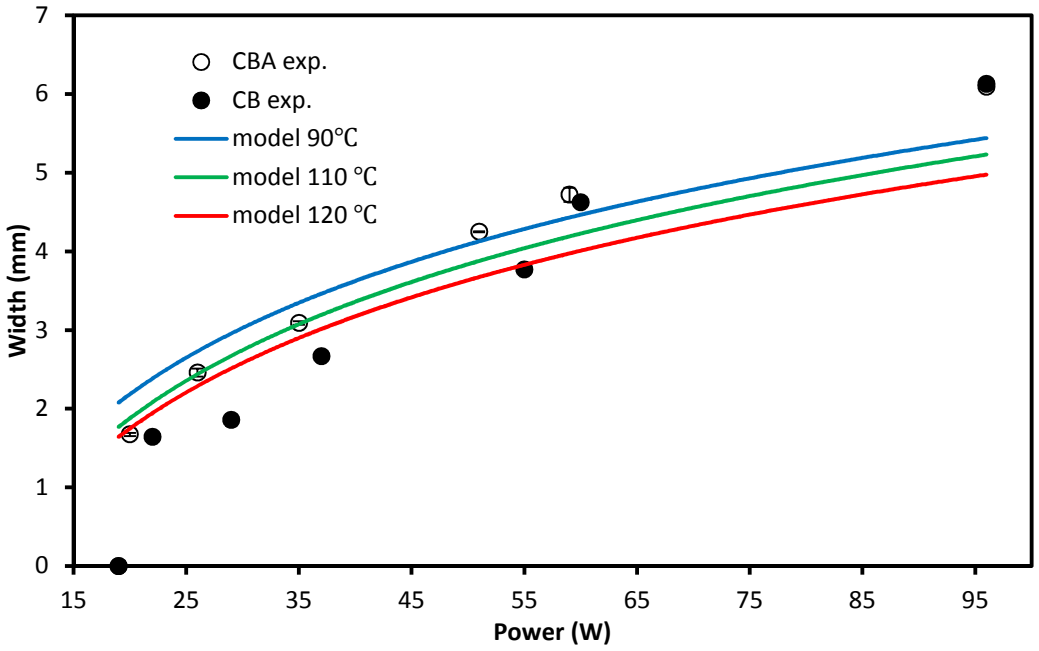

Figure C. 3: Comparison of weld width at 15 mm/s scan speed and different gap settings

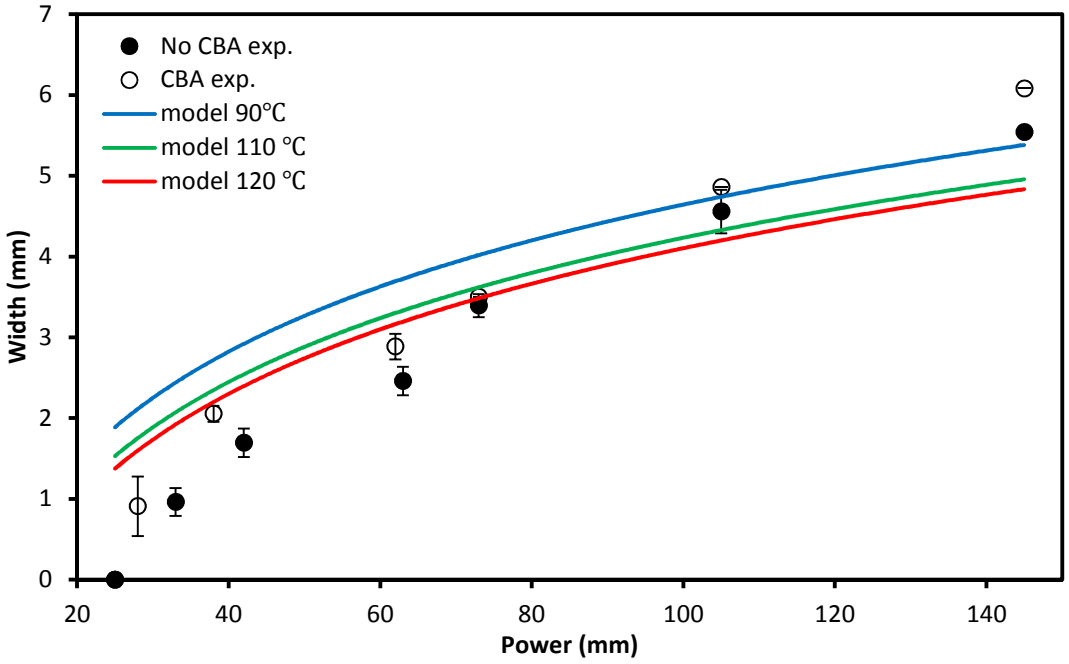

Figure C. 4: Comparison of weld width at 25 mm/s scan speed and different gap settings

Appendix D

Matlab code to calculate the amount of degradation as a function of time during laser heating

```
clc
clear all
time    = xlsread('10W5mms0mm.xlsx','Sheet1','C6:C33');
%SEPERATE DATA INTO HEATING AND COOLING
AFIRST = 1;
ASECOND = 9;
%Heating time
t_1 = time (AFIRST:ASECOND);
%cooling time
t_2 = time (ASECOND:end);
%Heating temperature in kelvin
T_1 = - 3004.4*t_1.^5 + 9272.4*t_1.^4 - 9637.1*t_1.^3 + 4166*t_1.^2 - 650.36*t_1 + 306.75;
%Cooling temperature in kelvin
T_2 = - 0.0215*t_2.^5 + 0.9885*t_2.^4 - 17.192*t_2.^3 + 139.8*t_2.^2  - 531.58*t_2 + 1146.6;
%PARAMETERS
k = 2.232*10^12;
E= 125;
n =1.6;
R =0.0083144621;
%Integrating the kinetic equation using ode 45
```

```
%heating phase

dy = @(t_1,y1)(k.*exp(-(E./(R*(- 3004.4*t_1.^5 + 9272.4*t_1.^4 - 9637.1*t_1.^3 +
4166*t_1.^2 - 650.36*t_1 + 306.75)))).*((1-y1).^n));
% initial value of conversion
y0
=0.000000000000000000000000000000000000000000000000000000000000000000000
000000000000000000000000000000000000000000001;
[t_1,y1]= ode45(dy,t_1,y0);
%cooling phase
dy = @(t_2,y2)(k.*exp(-E./(R*((- 0.0215*t_2.^5 + 0.9885*t_2.^4 - 17.192*t_2.^3 +
139.8*t_2.^2  - 531.58*t_2 + 1146.6))))).*((1-y2).^n);
%y1(end) is the value of conversion after heating which becomes the initial value of conversion
for cooling
y0 =y1(end);
[t_2,y2]= ode45(dy,t_2,y0);
y_1= [y1' y2'];
t = [t_1' t_2'];
figure (1)
plot (t,y_1)
ylabel('Conversion')
xlabel ('Time (s)')
```

Matlab code to calculate sigma and delta to get the scattered beam profile (Alexander perkinson 2013)

```
%This script will estimate the value of delta,sigma and psiStar. The

%arguments are your initial guesses

clear all

close all

disp('Welcome to the TEDD-Chen Variable Estimator!')

disp('Please hit enter to find your unscattered beam profile data (Psi(x)): ')

pause;

[filename, pathname] = uigetfile('*.txt','Find your Psi(x) Data input file: ');

Psi = dlmread([pathname filename]);

disp('File read. Please hit enter to find your Po/Pk data file - this is required: ');

pause;

[filename,pathname] = uigetfile('*.txt','Find your Po/Pk Data input file:');

PoPk = dlmread([pathname filename]);


A = transpose(Psi);

fileID = fopen('Psi1.txt','w');

fprintf(fileID,'%12.8f %12.8f\n',A);

fclose(fileID);

A = transpose(PoPk);

fileID = fopen('PoPk1.txt','w');

fprintf(fileID,'%12.8f %12.8f\n',A);
```

```
fclose(fileID);


% areaPsi = 0;
% for i=1:length(Psi)
%     areaPsi = areaPsi+Psi(i,1)*Psi(i,2);
% end
% areaPoPk = 0;
% for i=1:length(PoPk)
%     areaPoPk = areaPoPk+PoPk(i,1)*PoPk(i,2);
% end
% Psi = Psi/areaPsi;
% PoPk = PoPk/areaPoPk;


% disp('Next, we need some estimates from you. Please give as your initial estimate of' )
% x0(1) = input(' Delta: ');
% x0(2) = input(' Sigma: ');
% x0(3) = input(' PsiStar: ');
% disp('One more set of estimates needed! Enter them as requested: ')
% lb(1) = input(' Lower Bound, Delta: ');
% ub(1) = input(' Upper Bound, Delta: ');
% lb(2) = input(' Lower Bound, Sigma: ');
% ub(2) = input(' Upper Bound, Sigma: ');
% lb(3) = input(' Lower Bound, psiStar: ');
% ub(3) = input(' Upper Bound, psiStar: ');
```

```
% disp(' Thank you! Finally ready to get started. Hit enter to compute!')
% pause;
lb = [0.01 0.01 0.01];
ub = [1 6 1];
x0 = [0.2 0.2 0.2];

options = optimset('Display','iter','MaxIter',10000,'Algorithm','interior-
point','MaxFunEvals',10000);
[x,fval] = fmincon(@TEDDChenObjCreator,x0,[],[],[],[],lb,ub,[],options);

delta = x(1)
sigma = x(2)
psiStar = x(3)
tau = 1/psiStar
brute20130311(delta,sigma,psiStar,-3:0.1:3);
```

Appendix E

CBA conversion plots at different power, scan speed and gaps

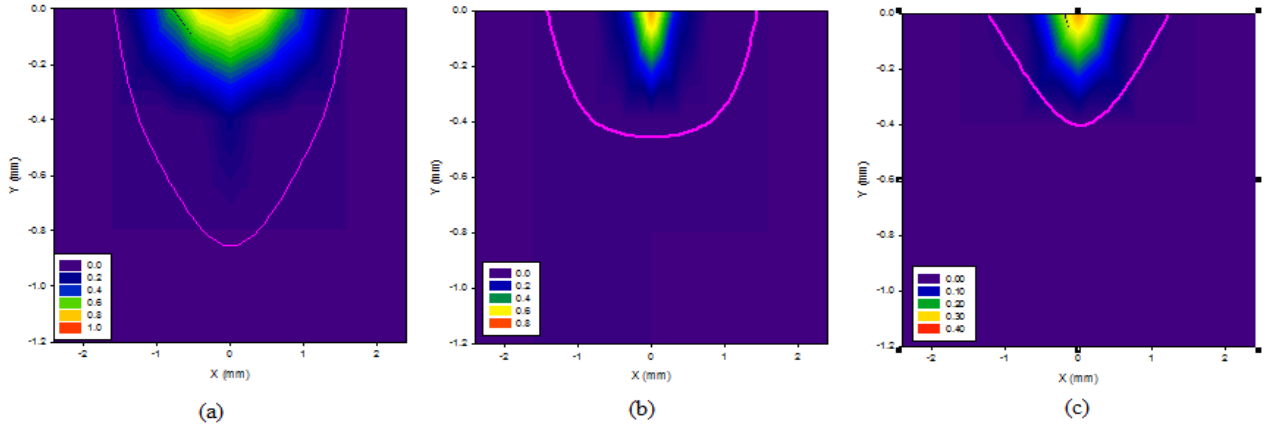

Figure E. 1: Percentage of degraded CBA at different points for LW with 0.127 mm gap. (a) Laser power: 10W, scan speed: 5 mm/s (b) Laser power: 20W, scan speed: 15 mm/s (c) Laser power: 28 W, scan speed: 25 mm/s

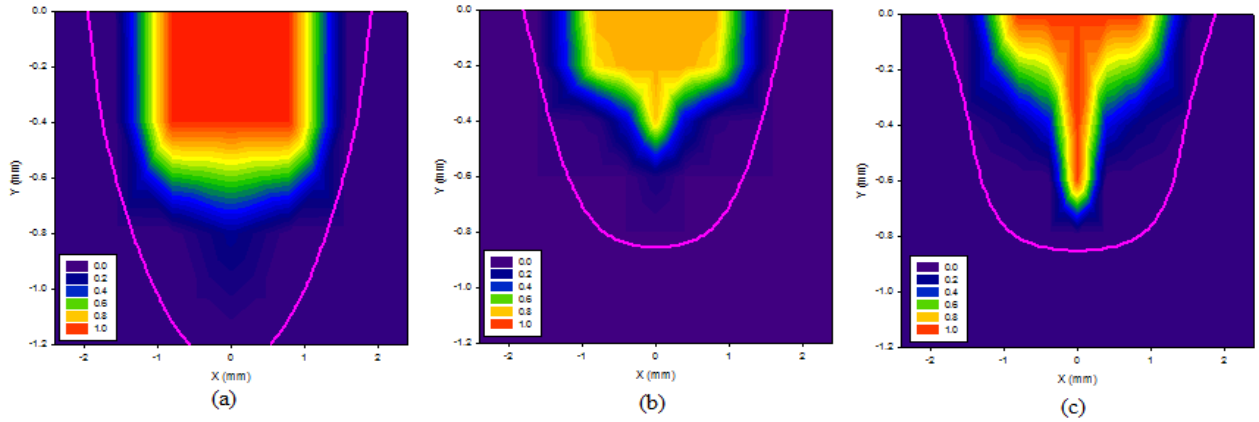

Figure E. 2: Percentage of degraded CBA at different points for LW with 0.381 mm gap. (a) Laser power: 17W, scan speed: 5 mm/s (b) Laser power: 35W, scan speed: 15 mm/s (c) Laser power: 62 W, scan speed: 25 mm/s

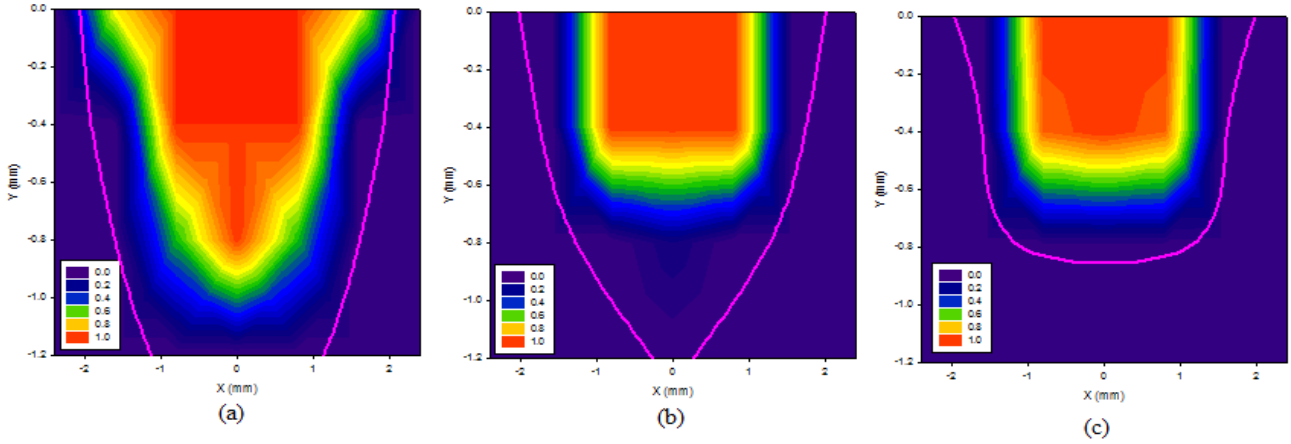

Figure E. 3: Percentage of degraded CBA at different points for LW with 0.508 mm gap. (a) Laser power: 22W, scan speed: 5 mm/s (b) Laser power: 51W, scan speed: 15 mm/s (c) Laser power: 73 W, scan speed: 25 mm/s

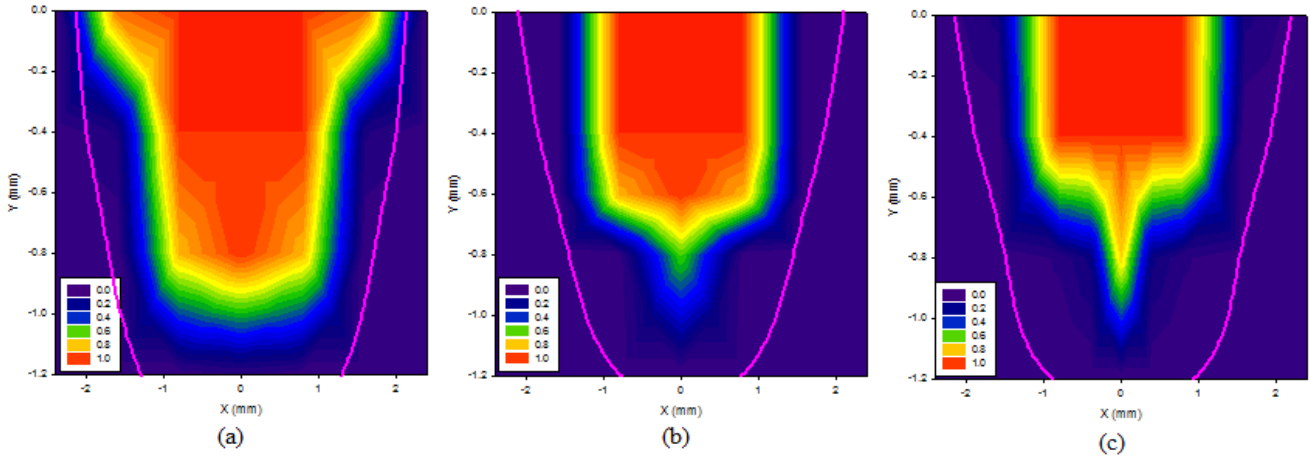

Figure E. 4: Percentage of degraded CBA at different points for LW with 0.635 mm gap. (a) Laser power: 24W, scan speed: 5 mm/s (b) Laser power: 59W, scan speed: 15 mm/s (c) Laser power: 105W, scan speed: 25 mm/s

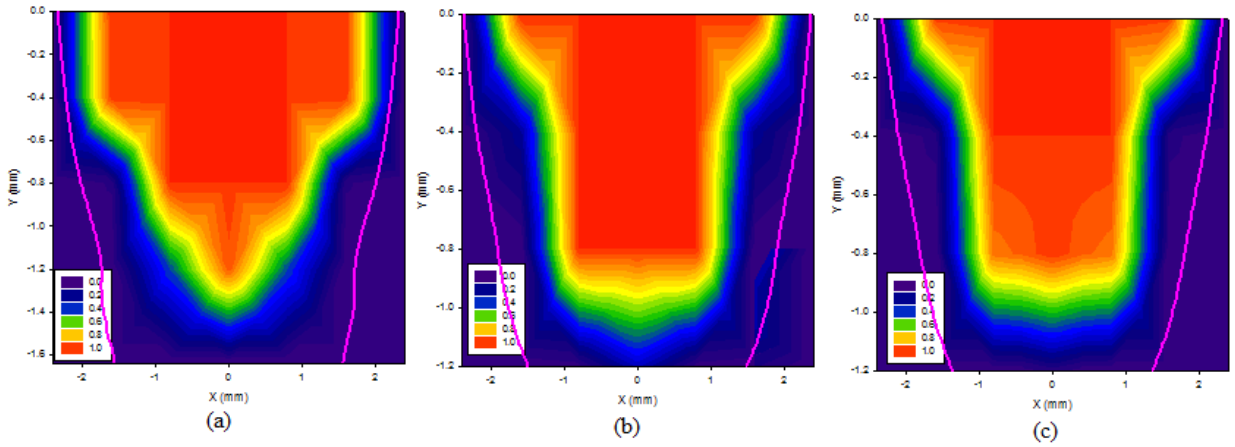

Figure E. 5: Percentage of degraded CBA at different points for LW with 0.762 mm gap. (a) Laser power: 33W, scan speed: 5 mm/s (b) Laser power: 96W, scan speed: 15 mm/s (c) Laser power: 145W, scan speed: 25 mm/s

Appendix F

Temperature polynomials to determine conversion of CBA at different locations

Table F. 1: Temperature polynomials at scan speed 5 mm/s

Power (W)	Position		f(t)=T	
	X (mm)	Y (mm)	Heating	Cooling
10	0	0	$T = -3004.4t^5 + 9272.4t^4 - 9637.1t^3 + 4166t^2 - 650.36t + 306.75$	$T = -0.0215t^5 + 0.9885t^4 - 17.192t^3 + 139.8t^2 - 531.58t + 1146.6$
	0	-0.4	$T = -360.49t^4 + 1155.8t^3 - 965.66t^2 + 256.13t + 283.08$	$T = 0.0676t^4 - 2.4716t^3 + 31.682t^2 - 171.68t + 709.09$
	0	-0.8	$T= -41.192t^4 + 131.04t^3 - 75.817t^2 + 7.7697t + 295.02$	$T= -0.0246t^3 + 0.8448t^2 - 12.981t + 420.39$
	0	-1.2	$T = 0.5081t^5 - 3.3889t^4 + 0.4817t^3 + 28.269t^2 - 18.976t + 295$	$T = -0.0535t^2 - 1.273t + 361.72$
	0.8	0	$T = -1886.4t^5 + 5820.2t^4 - 6023.4t^3 + 2613.6t^2 - 408.07t + 296.64$	$T = -0.0179t^5 + 0.809t^4 - 13.721t^3 + 108.3t^2 - 398.78t + 930.85$
	0.8	-0.4	$T = -323.45t^4 + 1003.6t^3 - 845.4t^2 + 227.94t + 288.14$	$T = 0.0423t^4 - 1.5455t^3 + 19.816t^2 - 108.97t + 586.74$
	0.8	-0.8	$T = 26.011t^5 - 160.46t^4 + 321.45t^3 - 209.86t^2 + 42.365t + 293.42$	$T = 0.1313t^2 - 5.9453t + 390.46$
	0.8	-1.2	$T = 1.2279t^4 - 12.929t^3 + 41.37t^2 - 24.372t + 295.16$	$T = 0.0135t^3 - 0.4294t^2 + 2.3588t + 344.06$
	1.6	0	$T = -347.8t^4 + 922.2t^3 - 655.32t^2 + 133.24t + 295.27$	$T = 0.0097t^4 - 0.3852t^3 + 5.6069t^2 - 37.348t + 436.04$
	1.6	-0.4	$T = -109.58t^4 + 314.38t^3 - 219.91t^2 + 40.616t + 295.79$	$T = -0.02t^3 + 0.7212t^2 - 9.9732t + 379.79$
	1.6	-0.8	$T = 4.0749t^4 - 31.737t^3 + 76.183t^2 - 38.612t + 296.15$	$T = 0.0056t^3 - 0.1184t^2 - 0.8117t + 343.16$
	1.6	-1.2	$T = 0.3175t^4 - 4.0116t^3 + 14.915t^2 - 7.5033t + 293.67$	$T = -0.0259t^2 - 0.1996t + 329.67$
	2.4	0	$T = -84.095t^5 + 219.9t^4 - 156.71t^3 + 34.582t^2 - 0.7599t + 295.64$	$T = -0.0008t^5 + 0.036t^4 - 0.5959t^3 + 4.5502t^2 - 15.808t + 338.65$
	2.4	-0.4	$T = 0.951t^5 - 6.6251t^4 + 6.6946t^3 + 20.563t^2 - 15.294t + 296.38$	$T = -0.0143t^2 + 0.1222t + 316.87$
	2.4	-0.8	$T = 0.0043t^6 - 0.1313t^5 + 1.5016t^4 - 7.9061t^3 + 17.951t^2 - 7.6393t + 294.34$	$T = 0.0152t^3 - 0.5652t^2 + 6.8083t + 287.88$
	2.4	-1.2	$T = 0.0002t^6 - 0.0076t^5 + 0.1381t^4 - 1.1506t^3 + 4.0637t^2 - 1.3583t + 293.6$	N/A

Power (W)	Position		f(t)=T	
	X (mm)	Y (mm)	Heating	Cooling
11	0	0	$T = 480.23t^2 - 420.34t + 331.45$	$T = -0.0256t^5 + 1.1748t^4 - 20.495t^3 + 168.15t^2 - 648.28t + 1316.2$
	0	-0.4	$T= 350.37t^2 - 409.55t + 384.81$	$T = -0.0091t^5 + 0.4466t^4 - 8.3545t^3 + 74.374t^2 - 318.37t + 898.53$
	0	-0.8	$T = -71.942t^4 + 270.7t^3 - 258.8t^2 + 83.356t + 267.34$	$T = 0.0114t^4 - 0.4436t^3 + 6.2847t^2 - 42.894t + 478.18$
	0	-1.2	$T = -2.0039t^6 + 25.062t^5 - 117.79t^4 + 248.93t^3 - 215.33t^2 + 73.612t + 267.04$	$T= -0.0555t^2 - 2.1118t + 371.45$
	0.8	0	$T = -1926.9t^6 + 6809.8t^5 - 8354.8t^4 + 4290.5t^3 - 730.77t^2 - 48.004t + 310.02$	$T = -0.0252t^5 + 1.1038t^4 - 18.189t^3 + 140.13t^2 - 507.59t + 1084.9$
	0.8	-0.4	$T = -670.76t^5 + 2594.9t^4 - 3486.8t^3 + 2074.2t^2 - 531.06t + 340.11$	$T = -0.0096t^5 + 0.4338t^4 - 7.4124t^3 + 59.909t^2 - 233.91t + 738.45$
	0.8	-0.8	$T = 39.028t^5 - 258.01t^4 + 587.39t^3 - 518.44t^2 + 180.11t + 276.17$	$T = 0.1773t^2 - 7.0788t + 401.38$
	0.8	-1.2	$T = 0.2725t^5 - 1.5t^4 - 4.3216t^3 + 34.115t^2 - 27.772t + 297.63$	$T = 0.0112t^3 - 0.3499t^2 + 1.4109t + 351.64$
	1.6	0	$T = -268.08t^4 + 857.94t^3 - 795.03t^2 + 258.45t + 272.59$	$T = -0.0019t^5 + 0.0907t^4 - 1.6442t^3 + 14.572t^2 - 66.865t + 478.35$
	1.6	-0.4	$T = -67.06t^4 + 209.28t^3 - 150.18t^2 + 27.555t + 295.05$	$T = -0.0233t^3 + 0.837t^2 - 11.491t + 390.01$
	1.6	-0.8	$T = -8.4172t^6 + 86.904t^5 - 339.75t^4 + 615.81t^3 - 503.96t^2 + 172.23t + 277$	$T = 0.0303t^2 - 2.1048t + 350.38$
	1.6	-1.2	$T = -0.0769t^5 + 1.5012t^4 - 10.657t^3 + 31.321t^2 - 23.239t + 297.23$	$T = -0.0068t^2 - 0.6617t + 334.97$
	2.4	0	$T = -118.3t^4 + 396.7t^3 - 414.65t^2 + 159.97t + 280.52$	$T = 0.0005t^6 - 0.023t^5 + 0.442t^4 - 4.2203t^3 + 20.963t^2 - 50.951t + 368.9$
	2.4	-0.4	$T = 0.2832t^3 - 4.4475t^2 + 21.173t + 288.53$	$T = 0.0483t^2 - 1.2699t + 326.12$
	2.4	-0.8	$T = -0.7526t^2 + 9.2063t + 290.51$	$T = -0.0282t^2 + 0.5707t + 313.6$
	2.4	-1.2	$T = -0.0031t^5 + 0.0926t^4 - 0.975t^3 + 3.922t^2 - 1.3625t + 293.41$	$T = 0.0791t + 313.29$

Power (W)	Position		f(t)=T	
	X (mm)	Y (mm)	Heating	Cooling
17	0	0	$T = -5549.9t^6 + 17097t^5 – 18258t^4 + 8593.1t^3 - 1715.8t^2 + 110.7t + 298.36$	$T = -0.0445t^5 + 1.9929t^4 - 33.737t^3 + 268.55t^2 - 1013.9t + 1894.6$
	0	-0.4	$T = -967.76t^4 + 2877t^3 - 2314.3t^2 + 595.27t + 266.07$	$T = 0.1129t^4 - 4.3119t^3 + 58.545t^2 - 337.63t + 1104$
	0	-0.8	$T = -198.25t^4 + 693.93t^3 - 644.07t^2 + 194.64t + 283.68$	$T = 0.0152t^4 - 0.7064t^3 + 12.031t^2 - 91.402t + 644.49$
	0	-1.2	$T = -6.3072t^4 + 18.432t^3 + 18.04t^2 - 19.432t + 296.12$	$T = -0.0142t^3 + 0.6069t^2 - 10.732t + 429.16$
	0.8	0	$T = -3637.4t^5 + 11137t^4 – 11292t^3 + 4657.5t^2 - 656.01t + 298.1$	$T = -0.0391t^5 + 1.688t^4 - 27.501t^3 + 210.97t^2 - 772.09t + 1510.7$
	0.8	-0.4	$T = -1567.6t^5 + 5270.2t^4 - 5889.8t^3 + 2696.1t^2 - 433.53t + 303.14$	$T = -0.0097t^5 + 0.4569t^4 - 8.3261t^3 + 73.409t^2 – 321t + 966.05$
	0.8	-0.8	$T = -99.853t^4 + 346.88t^3 - 292.67t^2 + 77.497t + 291.87$	$T = -0.1149t^3 + 3.7135t^2 - 41.216t + 526.73$
	0.8	-1.2	$T = -9.6798t^3 + 49.313t^2 - 30.798t + 296.49$	$T = 0.1025t^2 - 4.7306t + 399.27$
	1.6	0	$T = 104.04t^3 - 2.1146t^2 - 29.103t + 298.29$	$T = -0.0071t^5 + 0.3231t^4 - 5.5983t^3 + 45.792t^2 - 180.56t + 659.89$
	1.6	-0.4	$T = -169.82t^4 + 502.71t^3 - 368.73t^2 + 78.827t + 294.35$	$T = -0.0625t^3 + 2.1142t^2 - 24.923t + 455.44$
	1.6	-0.8	$T = -5.5247t^6 + 54.503t^5 - 198.11t^4 + 309.8t^3 - 170.94t^2 + 26.467t + 294.3$	$T = 0.0098t^3 - 0.168t^2 - 2.0787t + 377.65$
	1.6	-1.2	$T = -0.0625t^5 + 1.4939t^4 - 11.816t^3 + 35.909t^2 - 21.492t + 296.12$	$T = 0.0149t^3 - 0.4503t^2 + 3.1191t + 342.39$
	2.4	0	$T = -69.737t^5 + 120.66t^4 + 43.098t^3 - 98.766t^2 + 24.808t + 297.86$	$T = -0.0242x^3 + 0.6614x^2 - 5.6342x + 349.1$
	2.4	-0.4	$T = -2.4286t^2 + 22.849t + 290.77$	$T = 0.0486t^2 - 1.3755t + 339.7$
	2.4	-0.8	$T = 0.0581t^3 - 1.6737t^2 + 14.502t + 290.03$	N/A
	2.4	-1.2	$T = 0.0202t^3 - 0.7295t^2 + 8.6453t + 290.5$	N/A

Power (W)	Position		f(t)=T	
	X (mm)	Y (mm)	Heating	Cooling
22	0	0	$T = -6610.8t^5 + 19055t^4 - 17679t^3 + 6461.7t^2 - 806.86t + 320.56$	$T = 0.4063t^4 - 14.414t^3 + 178.08t^2 - 910.87t + 2074.8$
	0	-0.4	$T = -3253.5t^5 + 10414t^4 - 10810t^3 + 4383.3t^2 - 583.92t + 305.82$	$T = 0.1801t^4 - 6.6311t^3 + 86.821t^2 - 487.72t + 1428.8$
	0	-0.8	$T = -322.04t^4 + 1103.7t^3 - 999.42t^2 + 273.3t + 288.38$	$T = -0.2546t^3 + 8.5364t^2 - 94.813t + 739.59$
	0	-1.2	$T = -16.943t^4 + 65.745t^3 - 32.62t^2 - 1.685t + 295.18$	$T = -0.0479t^3 + 1.9374t^2 - 27.814t + 513.37$
	0.8	0	$T = -4071t^5 + 11789t^4 - 11163t^3 + 4493.7t^2 - 732.02t + 331.93$	$T = -0.058t^5 + 2.489t^4 - 40.12t^3 + 303.16t^2 - 1089.7t + 1967.7$
	0.8	-0.4	$T = -2565.6t^5 + 8376.7t^4 - 9017.6t^3 + 3891.3t^2 - 576.28t + 308.85$	$T = 0.1021t^4 - 3.9034t^3 + 53.516t^2 - 317.54t + 1108.6$
	0.8	-0.8	$T = -171.53t^4 + 593.91t^3 - 513.56t^2 + 140.57t + 288.33$	$T = -0.1755t^3 + 5.9122t^2 - 66.922t + 638.65$
	0.8	-1.2	$T = -5.1973t^4 + 14.301t^3 + 24.212t^2 - 21.044t + 296.37$	$T = -0.0213t^3 + 0.9369t^2 - 15.535t + 459.03$
	1.6	0	$T = -1896.4t^5 + 5769.5t^4 - 5823.1t^3 + 2423.8t^2 - 369.48t + 311.8$	$T = -0.0088t^5 + 0.4091t^4 - 7.2228t^3 + 60.793t^2 - 249.18t + 803.61$
	1.6	-0.4	$T = -257.86t^5 + 730.42t^4 - 521.66t^3 + 78.573t^2 + 20.698t + 296.5$	$T = -0.1388t^3 + 4.3206t^2 - 45.032t + 532.19$
	1.6	-0.8	$T = -6.8039t^4 + 11.268t^3 + 42.606t^2 - 28.894t + 297.65$	$T = 0.1864t^2 - 6.6628t + 413.85$
	1.6	-1.2	$T = 0.9663t^4 - 11.348t^3 + 40.241t^2 - 24.569t + 296.69$	$T = -0.012t^2 - 1.2987t + 371.24$
	2.4	0	$T = -234.23t^4 + 639.7t^3 - 490.58t^2 + 119.78t + 295.97$	$T = 0.0724t^2 - 1.9498t + 359.3$
	2.4	-0.4	$T = -0.0903t^3 - 3.255t^2 + 28.993t + 290.38$	$T = 0.0507t^2 - 1.4294t + 350.1$
	2.4	-0.8	$T = 0.0689t^3 - 2.0366t^2 + 18.143t + 291.26$	N/A
	2.4	-1.2	$T = 0.0003t^6 - 0.0144t^5 + 0.2637t^4 - 2.2385t^3 + 8.118t^2 - 2.8936t + 294.22$	N/A

Power (W)	Position		f(t)=T	
	X (mm)	Y (mm)	Heating	Cooling
24	0	0	$T = 1410.3t^3 - 1341.3t^2 + 323.34t + 294.35$	$T = -0.1071t^5 + 4.5004t^4 - 70.985t^3 + 524.27t^2 - 1832.8t + 2952.8$
	0	-0.4	$T = -6107.5t^5 + 20402t^4 – 23397t^3 + 11385t^2 - 2179.5t + 399.99$	$T = 0.1983t^4 - 7.3114t^3 + 95.828t^2 - 538.77t + 1546.3$
	0	-0.8	$T = -492.45t^4 + 1695.9t^3 - 1627.4t^2 + 500.2t + 268.92$	$T = -0.2728t^3 + 9.2588t^2 - 104.68t + 786.84$
	0	-1.2	$T = -36.434t^4 + 152.85t^3 - 143.08t^2 + 41.586t + 292.46$	$T = -0.0423t^3 + 1.9194t^2 - 30.019t + 536.65$
	0.8	0	$T = -5676.8t^5 + 16771t^4 – 16102t^3 + 6151t^2 - 829.23t + 325.72$	$T = -0.0643t^5 + 2.757t^4 - 44.371t^3 + 334.51t^2 - 1199.8t + 2137$
	0.8	-0.4	$T = -1908.1t^5 + 5887.2t^4 - 5752.6t^3 + 2232.3t^2 - 303.52t + 306.82$	$T = -0.0252t^5 + 1.1127t^4 - 18.72t^3 + 151.14t^2 - 604.84t + 1428.2$
	0.8	-0.8	$T = -253.74t^4 + 878.53t^3 - 796.79t^2 + 218.87t + 290.9$	$T = -0.1719t^3 + 5.99t^2 - 70.642t + 667.89$
	0.8	-1.2	$T = -10.384t^4 + 38.649t^3 - 4.8065t^2 - 10.959t + 295.76$	$T = -0.0299t^3 + 1.2874t^2 - 20.287t + 485.72$
	1.6	0	$T = -1838.7t^5 + 5669t^4 - 5784.6t^3 + 2434.3t^2 - 376.21t + 313.47$	$T = 2.7445t^2 - 58.949t + 642$
	1.6	-0.4	$T = -400.84t^4 + 1256.7t^3 - 1096.1t^2 + 315.38t + 280.67$	$T = -0.2035t^3 + 6.0344t^2 - 58.687t + 573.73$
	1.6	-0.8	$T = -11.288t^4 + 22.194t^3 + 46.537t^2 - 39.113t + 300.14$	$T = 0.2458t^2 - 8.2049t + 427.67$
	1.6	-1.2	$T = 1.0666t^4 - 12.6t^3 + 44.634t^2 - 26.669t + 296.07$	$T = 0.0181t^3 - 0.5199t^2 + 2.8159t + 367.47$
	2.4	0	$T = -235.68t^5 + 636.69t^4 - 504.54t^3 + 146.03t^2 - 13.907t + 303.52$	$T = 1.0912t^2 - 19.053t + 389.73$
	2.4	-0.4	$T = -20.984t^3 + 87.259t^2 - 51.663t + 302.32$	$T = -0.02t^2 + 0.0387t + 348.7$
	2.4	-0.8	$T = -0.0407t^5 + 0.9318t^4 - 7.2082t^3 + 20.396t^2 - 4.3084t + 295.49$	$T = -0.0557t^2 + 0.9595t + 337.46$
	2.4	-1.2	$T = 0.0205t^3 - 0.8521t^2 + 11.188t + 290.29$	N/A

Power (W)	Position		f(t)=T	
	X (mm)	Y (mm)	Heating	Cooling
33	0	0	$T = -14328t^5 + 42241t^4 - 41002t^3 + 16001t^2 - 2246.2t + 374.59$	$T = -0.1875t^5 + 7.8298t^4 - 122.27t^3 + 888.47t^2 - 3024.4t + 4478.7$
	0	-0.4	$T = 1353.4t^3 - 1570.5t^2 + 470.86t + 283.61$	$T = 0.3679t^4 - 13.351t^3 + 170.47t^2 - 921.02t + 2295.9$
	0	-0.8	$T = -1333t^5 + 4885.5t^4 - 5913.4t^3 + 2949.8t^2 - 549.49t + 320.79$	$T = -0.447t^3 + 14.709t^2 - 163.58t + 1037$
	0	-1.2	$T = -128.34t^4 + 547.36t^3 - 632.93t^2 + 238.92t + 282.18$	$T = 1.3196t^2 - 36.445t + 641.13$
	0.8	0	$T = 1156.5t^3 - 741.65t^2 + 37.697t + 315.6$	$T = -0.1059t^5 + 4.5297t^4 - 72.644t^3 + 543.99t^2 - 1925.9t + 3160.1$
	0.8	-0.4	$T = -4783.4t^5 + 16104t^4 - 18472t^3 + 8995.4t^2 - 1673.6t + 349.05$	$T = 0.2211t^4 - 8.2357t^3 + 108.87t^2 - 615.43t + 1743.4$
	0.8	-0.8	$T = -511.36t^4 + 1804.7t^3 - 1779.8t^2 + 578.98t + 262.9$	$T = -0.2701t^3 + 9.3296t^2 - 110.8t + 861.01$
	0.8	-1.2	$T = -43.099t^4 + 183.08t^3 - 171.48t^2 + 46.885t + 294.44$	$T = 0.9679t^2 - 27.33t + 579.39$
	1.6	0	$T = -2718.8t^5 + 8534.8t^4 - 8963.3t^3 + 3961.1t^2 - 659.3t + 320.34$	$T = -0.0182t^5 + 0.8164t^4 - 13.879t^3 + 111.81t^2 - 441.37t + 1158.2$
	1.6	-0.4	$T = 185.9t^3 - 110.09t^2 - 2.3242t + 304.3$	$T = -0.2341t^3 + 7.6491t^2 - 83.431t + 706.56$
	1.6	-0.8	$T = -87.125t^4 + 321.03t^3 - 292.5t^2 + 88.692t + 293.2$	$T = 0.6199t^2 - 17.733t + 508.25$
	1.6	-1.2	$T = -8.0753t^3 + 45.79t^2 - 29.188t + 298.47$	$T = 0.1277t^2 - 5.7715t + 428.98$
	2.4	0	$T = 53.136t^2 - 14.075t + 301.68$	$T = -1.2919t + 388.76$
	2.4	-0.4	$T = -11.269t^3 + 43.395t^2 - 2.4217t + 297.49$	$T = -0.8614t + 374.82$
	2.4	-0.8	$T = 0.4131t^4 - 5.3871t^3 + 19.358t^2 - 1.6594t + 296.53$	$T = 0.0426t^2 - 1.5648t + 370.25$
	2.4	-1.2	$T = 0.0007t^6 - 0.0303t^5 + 0.5327t^4 - 4.35t^3 + 15.452t^2 - 8.7109t + 297.11$	N/A

Table F. 2: Temperature polynomials at scan speed 15 mm/s

Power (W)	Position		f(t)=T	
	X (mm)	Y (mm)	Heating	Cooling
20	0	0	$T = -613478t^5 + 597234t^4 - 195363t^3 + 27687t^2 - 1656.4t + 326.9$	$T = 0.0097t^6 - 0.4376x^5 + 7.6059t^4 - 64.244t^3 + 273.31t^2 - 552.1t + 789.63$
	0	-0.4	$T = -2020.9t^3 + 2397.6t^2 - 455.66t + 314.05$	$T = -0.0106t^5 + 0.4074t^4 - 5.7095t^3 + 36.089t^2 - 109.25t + 496.42$
	0	-0.8	$T = 128.34t^4 - 436.39t^3 + 434.71t^2 - 59.968t + 294.13$	$T = 0.0175t^3 - 0.2806t^2 - 3.0868t + 367.92$
	0	-1.2	$T = 0.7987t^4 - 5.551t^3 + 6.22t^2 + 25.221t + 290.43$	$T = 0.0169t^3 - 0.4258t^2 + 0.9936t + 340.22$
	0.8	0	$T = 6816.5t^3 - 2182t^2 + 179.79t + 295.3$	$T = 0.01t^6 - 0.415t^5 + 6.5231t^4 - 49.42t^3 + 188.22t^2 - 346.06t + 612.51$
	0.8	-0.4	$T = -7122.2t^4 + 6265t^3 - 857.98t^2 - 57.409t + 300.23$	$T = -0.0425t^3 + 1.4655t^2 - 18.293t + 403.43$
	0.8	-0.8	$T = -93.583t^5 + 455.29t^4 - 784.89t^3 + 538.59t^2 - 68.897t + 295.01$	$T = -0.0028t^4 + 0.1007t^3 - 1.1216t^2 + 1.2533t + 349.2$
	0.8	-1.2	$T = -0.7821t^5 + 7.8942t^4 - 28.15t^3 + 37.52t^2 + 3.5143t + 292.59$	$T = -0.0019t^4 + 0.0817t^3 - 1.229t^2 + 5.8585t + 322.06$
	1.6	0	$T = 523.55t^2 - 78.27t + 296.61$	$T = 0.499t^2 - 10.492t + 357.64$
	1.6	-0.4	$T = -2637.1t^4 + 2554t^3 - 485.64t^2 + 16.187t + 294.82$	$T = -0.0108t^3 + 0.3723t^2 - 4.9151t + 336.97$
	1.6	-0.8	$T = 1.4752t^3 - 14.317t^2 + 37.69t + 289.69$	$T = 0.0053t^3 - 0.1373t^2 + 0.2545t + 319.29$
	1.6	-1.2	$T = -0.1536t^5 + 1.9102t^4 - 8.1969t^3 + 12.712t^2 + 2.7219t + 293.07$	$T = 0.0083t^3 - 0.2677t^2 + 2.227t + 308.19$
	2.4	0	$T = -0.2006t^2 + 3.5722t + 297.83$	N/A
	2.4	-0.4	$T = -0.0905t^2 + 1.8893t + 297.31$	N/A
	2.4	-0.8	$T = -0.003t^4 + 0.0999t^3 - 1.154t^2 + 5.6591t + 293.44$	N/A
	2.4	-1.2	$T = -0.0815t^2 + 1.9117t + 293.72$	N/A

Power (W)	Position		f(t)=T	
	X (mm)	Y (mm)	Heating	Cooling
26	0	0	$T = -236603t^5 + 71833t^4 + 81927t^3 - 36071t^2 + 4091.6t + 197.91$	$T = 0.0118t^6 - 0.5353t^5 + 9.3905t^4 - 80.521t^3 + 350.79t^2 - 732.35t + 965.52$
	0	-0.4	$T = -128703t^5 + 154084t^4 - 61292t^3 + 10501t^2 - 736.25t + 309.75$	$T = -0.0098t^5 + 0.4276t^4 - 6.8875t^3 + 50.643t^2 - 172.78t + 592.6$
	0	-0.8	$T = 249.53t^4 - 777.57t^3 + 729.31t^2 - 116.92t + 296.88$	$T = 0.1719t^2 - 7.0853t + 391.65$
	0	-1.2	$T = -2.0473t^5 + 18.985t^4 - 63.011t^3 + 80.367t^2 - 2.0059t + 292.69$	$T = 0.0234t^3 - 0.6629t^2 + 3.3244t + 343.56$
	0.8	0	$T = 2349.9t^2 - 388.28t + 305.02$	$T = 0.0945t^4 - 3.2442t^3 + 37.423t^2 - 169.27t + 610.16$
	0.8	-0.4	$T = -3031.6t^3 + 3206.9t^2 - 630.42t + 320.27$	$T = 0.0228t^4 - 0.806t^3 + 9.9847t^2 - 54.618t + 463.73$
	0.8	-0.8	$T = -98.696t^5 + 502.87t^4 - 914.82t^3 + 666.76t^2 - 94.569t + 295.84$	$T = 0.1239t^2 - 5.2443t + 372.45$
	0.8	-1.2	$T = -0.8185t^5 + 8.4003t^4 - 30.515t^3 + 40.777t^2 + 7.3903t + 292.2$	$T = -0.0017t^4 + 0.0778t^3 - 1.227t^2 + 6.0747t + 329.97$
	1.6	0	$T = -3645.6t^3 + 3409.6t^2 - 684.97t + 328.53$	$T = 0.4561t^2 - 10.37t + 371.68$
	1.6	-0.4	$T = -813.9t^3 + 902.8t^2 - 160.18t + 299.94$	$T = -0.0121t^3 + 0.4207t^2 - 5.7291t + 348.21$
	1.6	-0.8	$T = -16.598t^5 + 103.63t^4 - 224.62t^3 + 186.66t^2 - 20.975t + 293.83$	$T = 0.0122t^3 - 0.3067t^2 + 1.1907t + 325.06$
	1.6	-1.2	$T = 0.0521t^6 - 0.8541t^5 + 5.3923t^4 - 16.1t^3 + 20.455t^2 + 2.3669t + 293.17$	$T = 0.0085t^3 - 0.2721t^2 + 2.2282t + 313.51$
	2.4	0	$T = -0.1176t^2 + 2.3078t + 301.85$	N/A
	2.4	-0.4	$T = -0.1237t^2 + 2.5072t + 298.37$	N/A
	2.4	-0.8	$T = -0.0041t^4 + 0.1329t^3 - 1.4802t^2 + 7.104t + 293.6$	N/A
	2.4	-1.2	$T = 0.0085t^3 - 0.2887t^2 + 3.3613t + 293.28$	N/A

Power (W)	Position		f(t)=T	
	X (mm)	Y (mm)	Heating	Cooling
35	0	0	$T = 21921t^3 - 7911.1t^2 + 836.05t + 276.68$	$T = 0.2351t^4 - 7.862t^3 + 88.407t^2 - 389.5t + 936.08$
	0	-0.4	$T = -44516t^4 + 46045t^3 - 13056t^2 + 1264.2t + 265.26$	$T = 0.0869t^4 - 3.0445t^3 + 36.563t^2 - 179.73t + 682.53$
	0	-0.8	$T = 345.26t^4 - 1100.1t^3 + 1063.2t^2 - 191.63t + 300.97$	$T = 0.0105t^4 - 0.385t^3 + 5.058t^2 - 32.131t + 449.03$
	0	-1.2	$T = 6.4405t^4 - 38.397t^3 + 61.358t^2 + 13.557t + 291.68$	$T = 0.0095t^3 - 0.2754t^2 - 0.1914t + 364.69$
	0.8	0	$T = -10257t^3 + 10460t^2 - 1814.5t + 347.01$	$T = -0.0322t^5 + 1.3224t^4 - 19.924t^3 + 134.72t^2 - 404.4t + 814.54$
	0.8	-0.4	$T = -2485.2t^3 + 3267.7t^2 - 700.67t + 325.19$	$T = 0.0517t^4 - 1.7801t^3 + 21.047t^2 - 104.11t + 552.81$
	0.8	-0.8	$T = -398.19t^5 + 1575.1t^4 - 2303t^3 + 1440t^2 - 238.25t + 302.42$	$T = -0.0061t^3 + 0.3264t^2 - 7.8458t + 395.41$
	0.8	-1.2	$T = -8.1324t^2 + 44.846t + 288.89$	$T = 0.0139t^3 - 0.4011t^2 + 1.4793t + 349.45$
	1.6	0	$T = -36782t^4 + 35954t^3 - 10492t^2 + 1091.8t + 271.62$	$T = 0.0148t^4 - 0.5229t^3 + 6.4923t^2 - 35.041t + 409.94$
	1.6	-0.4	$T = -413.63t^3 + 488.69t^2 - 30.287t + 292.66$	$T = 0.2043t^2 - 5.7012t + 363.32$
	1.6	-0.8	$T = 11.239t^4 - 52.002t^3 + 58.662t^2 + 20.246t + 291.4$	$T = 0.0015t^3 - 0.0258t^2 - 1.1059t + 338.94$
	1.6	-1.2	$T = 0.1698t^4 - 1.4556t^3 + 1.4469t^2 + 14.693t + 291.95$	$T = 0.0057t^3 - 0.1946t^2 + 1.4737t + 322.34$
	2.4	0	$T = -0.1269t^2 + 2.5604t + 306.08$	N/A
	2.4	-0.4	$T = -0.1508t^2 + 3.1759t + 300.56$	N/A
	2.4	-0.8	$T = -0.1502t^2 + 3.209t + 296.65$	N/A
	2.4	-1.2	$T = -0.1183t^2 + 2.7957t + 294.82$	N/A

Power (W)	Position		f(t)=T	
	X (mm)	Y (mm)	Heating	Cooling
51	0	0	$T = 13210t^3 + 3345.4t^2 - 1608.5t + 379.67$	$T = 0.3967t^4 - 13.406t^3 + 151.69t^2 - 660.93t + 1323$
	0	-0.4	$T = -8150t^3 + 9408.2t^2 - 1806.9t + 355.66$	$T = 0.0034t^6 - 0.1741t^5 + 3.4892t^4 - 35.089t^3 + 187.24t^2 - 517.13t + 1011.4$
	0	-0.8	$T = -837.89t^3 + 1301.7t^2 - 268.16t + 305.65$	$T = 0.018t^4 - 0.7487t^3 + 11.179t^2 - 74.03t + 564.48$
	0	-1.2	$T = 19.382t^4 - 105.86t^3 + 168.01t^2 - 17.406t + 293.87$	$T = 0.1516t^2 - 6.1191t + 407.09$
	0.8	0	$T = 10798t^3 + 277.03t^2 - 621.99t + 339.12$	$T = -0.0472t^5 + 1.9523t^4 - 29.761t^3 + 205.59t^2 - 636.93t + 1108.8$
	0.8	-0.4	$T = -77704t^4 + 86169t^3 – 28933t^2 + 3557t + 183.21$	$T = 0.1191t^4 - 3.9197t^3 + 43.918t^2 - 203.46t + 727.63$
	0.8	-0.8	$T = 332.1t^4 – 1092t^3 + 1075.4t^2 - 176.72t + 301.6$	$T = -0.0853t^3 + 2.6085t^2 - 28.048t + 468.42$
	0.8	-1.2	$T = 8.4544t^4 - 49.399t^3 + 80.349t^2 + 8.9455t + 291.75$	$T = -0.0026t^4 + 0.0984t^3 - 1.2289t^2 + 3.1921t + 372.76$
	1.6	0	$T = 2243.4t^2 - 572.52t + 326.98$	$T = 0.9877t^2 - 21.95t + 448.64$
	1.6	-0.4	$T = 1501.5t^4 - 3470.2t^3 + 2480.1t^2 - 431.41t + 311.34$	$T = 0.2706t^2 - 7.7937t + 393.96$
	1.6	-0.8	$T = 7.0196t^3 - 45.518t^2 + 97.617t + 283.2$	$T = 0.0604t^2 - 2.7773t + 361.59$
	1.6	-1.2	$T = -3.1013t^2 + 24.678t + 290.62$	$T = -0.0201t^2 - 0.4529t + 341.05$
	2.4	0	$T = -0.2039t^2 + 4.0407t + 309.6$	N/A
	2.4	-0.4	$T = -0.2478t^2 + 4.8932t + 304.47$	N/A
	2.4	-0.8	$T = -0.2374t^2 + 4.9135t + 297.68$	N/A
	2.4	-1.2	$T = -0.1814t^2 + 4.203t + 294.55$	N/A

Power (W)	Position		f(t)=T	
	X (mm)	Y (mm)	Heating	Cooling
59	0	0	$T = -16459t^3 + 24018t^2 - 4743.5t + 424.13$	$T = 0.0651t^6 - 2.735t^5 + 43.494t^4 - 331.12t^3 + 1263.2t^2 - 2313.3t + 2102$
	0	-0.4	$T = -15258t^3 + 17033t^2 – 3679t + 444.04$	$T = -0.0342t^5 + 1.4316t^4 - 22.243t^3 + 159.58t^2 - 537.83t + 1118$
	0	-0.8	$T = -1762.7t^4 + 1637.3t^3 + 420.84t^2 - 170.94t + 302$	$T = -0.2145t^3 + 6.5773t^2 - 66.013t + 593.46$
	0	-1.2	$T = -49.966t^3 + 123.7t^2 + 6.4601t + 291.84$	$T = -0.0287t^3 + 1.0305t^2 - 14.538t + 439.46$
	0.8	0	$T = -42169t^3 + 36756t^2 - 6854.6t + 536.81$	$T = 0.2856t^4 - 9.9614t^3 + 117.03t^2 - 531.23t + 1155.2$
	0.8	-0.4	$T = -35321t^4 + 36162t^3 - 8946.6t^2 + 635.64t + 297.07$	$T = -0.0125t^5 + 0.5595t^4 - 9.4838t^3 + 75.612t^2 - 288.63t + 831.22$
	0.8	-0.8	$T = -461.41t^3 + 742.86t^2 - 94.29t + 293.65$	$T = -0.125t^3 + 3.7918t^2 - 39.21t + 508.68$
	0.8	-1.2	$T = 13.961t^4 - 79.025t^3 + 127.48t^2 - 4.578t + 293.33$	$T = -0.0008t^3 + 0.143t^2 - 5.3728t + 401.04$
	1.6	0	$T = -8410.6t^3 + 7725.5t^2 - 1470.2t + 341.59$	$T = -0.2561t^3 + 7.0992t^2 - 59.487t + 487.33$
	1.6	-0.4	$T = -10933t^4 + 11825t^3 – 3461t^2 + 389.95t + 285.27$	$T = -0.037t^3 + 1.2467t^2 - 15.358t + 416.47$
	1.6	-0.8	$T = 41.898t^4 - 160.85t^3 + 164.94t^2 + 14.661t + 292.66$	$T = -0.0043t^4 + 0.155t^3 - 1.8354t^2 + 5.9539t + 356.8$
	1.6	-1.2	$T = -0.5016t^5 + 5.4187t^4 - 20.767t^3 + 28.935t^2 + 10.809t + 292.19$	$T = 0.0186t^3 - 0.5506t^2 + 4.0361t + 335.29$
	2.4	0	$T = -0.2548t^2 + 4.9351t + 296.6$	N/A
	2.4	-0.4	$T = -0.2486t^2 + 4.8993t + 306.32$	N/A
	2.4	-0.8	$T = -0.2623t^2 + 5.4503t + 298.47$	N/A
	2.4	-1.2	$T = -0.1967t^2 + 4.6022t + 295.11$	N/A

Power (W)	Position		f(t)=T	
	X (mm)	Y (mm)	Heating	Cooling
96	0	0	$T = 137873t^3 - 53228t^2 + 5091.8t + 301.21$	$T = 0.6451t^4 - 21.757t^3 + 247.65t^2 - 1104.6t + 2045.3$
	0	-0.4	$T = 42847t^3 - 17532t^2 + 2176.7t + 222.71$	$T = 0.361t^4 - 12.611t^3 + 150.95t^2 - 723.29t + 1600.8$
	0	-0.8	$T = -11761t^4 + 13590t^3 - 3148.5t^2 + 207.56t + 293.5$	$T = -0.3602t^3 + 11.418t^2 - 118.42t + 798.84$
	0	-1.2	$T = 130.09t^4 - 630.14t^3 + 914.41t^2 - 262.3t + 312.19$	$T = -0.0676t^3 + 2.7396t^2 - 38.29t + 563.44$
	0.8	0	$T = 548.9t^3 + 14767t^2 - 3219.3t + 404.55$	$T = 10.152t^2 - 200.11t + 1173.9$
	0.8	-0.4	$T = -162862t^4 + 165820t^3 - 48086t^2 + 4750.1t + 185.63$	$T = 0.282t^4 - 9.3269t^3 + 105.03t^2 - 483.92t + 1219$
	0.8	-0.8	$T = -2505.2t^3 + 3453.7t^2 - 808.73t + 331.29$	$T = -0.2195t^3 + 7.1809t^2 - 78.155t + 672.45$
	0.8	-1.2	$T = -81.843t^3 + 210.13t^2 - 19.842t + 293.71$	$T = 0.6558t^2 - 17.35t + 487.69$
	1.6	0	$T = 3972.2t^2 - 860.53t + 332.45$	$T = 0.1002t^4 - 3.4781t^3 + 41.245t^2 - 197.47t + 718.2$
	1.6	-0.4	$T = -14479t^4 + 16501t^3 - 4894.8t^2 + 538.17t + 283.18$	$T = -0.1762t^3 + 5.1871t^2 - 49.369t + 535.62$
	1.6	-0.8	$T = 133.03t^4 - 490.56t^3 + 531.29t^2 - 71.743t + 296.97$	$T = 0.252t^2 - 8.083t + 423.66$
	1.6	-1.2	$T = 0.5863t^3 - 11.102t^2 + 57.245t + 284.55$	$T = 0.062t^2 - 3.0171t + 383.78$
	2.4	0	$T = -0.3545t^2 + 6.9977t + 324.69$	N/A
	2.4	-0.4	$T = -0.3429t^2 + 7.126t + 315.96$	N/A
	2.4	-0.8	$T = -0.4045t^2 + 8.1597t + 302.66$	N/A
	2.4	-1.2	$T = -0.3348t^2 + 7.4395t + 296.3$	N/A

Table F. 3: Temperature polynomials at scan speed 25 mm/s

Power (W)	Position		f(t)=T	
	X (mm)	Y (mm)	Heating	Cooling
28	0	0	$T = 6807t^2 - 941.64t + 318.24$	$T = 0.0502t^4 - 1.7126t^3 + 20.018t^2 - 96.548t + 498.49$
	0	-0.4	$T = -9467.4t^3 + 6101.1t^2 - 745.38t + 317.55$	$T = -0.0423t^3 + 1.4984t^2 - 18.897t + 399.05$
	0	-0.8	$T = -31.281t^2 + 84.979t + 290.36$	$T = -0.0042t^4 + 0.1426t^3 - 1.4497t^2 + 1.3179t + 347.47$
	0	-1.2	$T = -4.5074t^2 + 25.51t + 292.26$	$T = 0.007t^3 - 0.1253t^2 - 1.2969t + 333.93$
	0.8	0	$T = 3240t^2 - 386.73t + 305.07$	$T = 0.0282t^4 - 0.9899t^3 + 12.026t^2 - 61.404t + 439.64$
	0.8	-0.4	$T = -360.6t^3 + 7.1358t^2 + 281.86t + 278.42$	$T = 0.3858t^2 - 9.6202t + 369.68$
	0.8	-0.8	$T = -25.253t^2 + 67.444t + 291.82$	$T = -0.0019t^4 + 0.0656t^3 - 0.6475t^2 - 0.5992t + 338.2$
	0.8	-1.2	$T = -3.871t^2 + 21.42t + 291.97$	$T = 0.0099t^3 - 0.2463t^2 + 0.5555t + 322.21$
	1.6	0	$T = 1544.1t^2 - 220.03t + 301.08$	$T = 0.0146t^4 - 0.4889t^3 + 5.5001t^2 - 24.616t + 351.08$
	1.6	-0.4	$T = -279.08t^2 + 242.57t + 273.43$	$T = 0.0926t^2 - 2.6433t + 324.44$
	1.6	-0.8	$T = -5.7113t^2 + 22.012t + 293.72$	$T = 0.0099t^2 - 0.7671t + 314.86$
	1.6	-1.2	$T = -0.9993t^2 + 7.9558t + 293.53$	$T = -0.3746t + 310.59$
	2.4	0	$T = -0.0456t^2 + 0.9433t + 299.22$	N/A
	2.4	-0.4	$T = -0.0708t^2 + 1.3883t + 296.75$	N/A
	2.4	-0.8	$T = -0.0683t^2 + 1.4334t + 295.26$	N/A
	2.4	-1.2	$T = -0.0604t^2 + 1.3628t + 294.13$	N/A

Power (W)	Position		f(t)=T	
	X (mm)	Y (mm)	Heating	Cooling
38	0	0	$T = 11526t^2 - 1579.5t + 339.45$	$T = 0.0279t^6 - 1.1233t^5 + 17.013t^4 - 122.45t^3 + 434.86t^2 - 718.64t + 826.17$
	0	-0.4	$T = -21018t^3 + 14161t^2 - 2048.2t + 363.14$	$T = 0.0486t^4 - 1.6206t^3 + 18.342t^2 - 86.185t + 497.31$
	0	-0.8	$T = 17.59t^3 - 112.61t^2 + 182.63t + 280.28$	$T = 0.0146t^3 - 0.2081t^2 - 3.7372t + 373.58$
	0	-1.2	$T = -6.5164t^2 + 36.228t + 292.62$	$T = 0.0193t^3 - 0.5048t^2 + 1.7356t + 340.95$
	0.8	0	$T = 9777.6t^2 - 1789.4t + 360.87$	$T = 0.0083t^6 - 0.3705t^5 + 6.274t^4 - 50.611t^3 + 200.23t^2 - 367.81t + 621.09$
	0.8	-0.4	$T = -6772.1t^4 - 3656.9t^3 + 4225.8x^2 - 401.82t + 295.22$	$T = 0.0089t^4 - 0.3269t^3 + 4.4198t^2 - 29.419t + 418.84$
	0.8	-0.8	$T = 31.724t^3 - 121.91t^2 + 156.94t + 283.29$	$T = 0.0075t^3 - 0.0696t^2 - 3.4442t + 359.54$
	0.8	-1.2	$T = -5.2035t^2 + 29.562t + 291.74$	$T = 0.012t^3 - 0.3272t^2 + 1.0648t + 333.32$
	1.6	0	$T = 1425.8t^2 - 136.25t + 300.1$	$T = -0.0988t^3 + 2.6154t^2 - 20.745t + 369.98$
	1.6	-0.4	$T = -614.03t^3 + 390.19t^2 + 83.173t + 288.25$	$T = 0.1204t^2 - 3.5351t + 339.02$
	1.6	-0.8	$T = -1.4972t^4 + 12.771t^3 - 40.048t^2 + 56.473t + 290.51$	$T = 0.0039t^3 - 0.0949t^2 - 0.179t + 322.66$
	1.6	-1.2	$T = -1.5111t^2 + 11.66t + 293.57$	$T = 0.005t^3 - 0.1641t^2 + 1.1906t + 313.03$
	2.4	0	$T = -0.0582t^2 + 1.2943t + 303.08$	N/A
	2.4	-0.4	$T = -0.0769t^2 + 1.6554t + 299.59$	N/A
	2.4	-0.8	$T = -0.0034t^4 + 0.1093x^3 - 1.2193t^2 + 5.8192t + 294.27$	N/A
	2.4	-1.2	$T = 0.0071t^3 - 0.2416t^2 + 2.8114t + 293.66$	N/A

Power (W)	Position		f(t)=T	
	X (mm)	Y (mm)	Heating	Cooling
62	0	0	$T = 21723t^2 - 3231.2t + 391.31$	$T = 0.0158t^6 - 0.7398t^5 + 13.32t^4 - 116.39t^3 + 510.35t^2 - 1048.3t + 1198.5$
	0	-0.4	$T = -36204t^3 + 24730t^2 - 3591.3t + 417.09$	$T = 0.0998t^4 - 3.428t^3 + 40.133t^2 - 190.38t + 688.59$
	0	-0.8	$T = 925.13t^4 - 2099.6t^3 + 1406.3t^2 - 89.772t + 294.24$	$T = -0.0775t^3 + 2.2605t^2 - 24.102t + 447.92$
	0	-1.2	$T = -16.337t^2 + 71.824t + 288.01$	$T = -0.0171t^2 - 2.3528t + 372.74$
	0.8	0	$T = 20218t^2 - 3964.1t + 445.55$	$T = 0.0163t^6 - 0.7292t^5 + 12.413t^4 - 101.19t^3 + 407.38t^2 - 760.1t + 925.93$
	0.8	-0.4	$T = -17505t^3 + 11588t^2 - 1355.1t + 328.73$	$T = 0.0554t^4 - 1.9128t^3 + 22.561t^2 - 109.69t + 558.49$
	0.8	-0.8	$T = -421.45t^5 + 1380.3t^4 - 1614.4t^3 + 702.41t^2 + 56.62t + 287.98$	$T = 0.2073t^2 - 7.4779t + 398.84$
	0.8	-1.2	$T = -9.4952t^2 + 49.506t + 290.71$	$T = -0.0064t^2 - 1.9073x + 360.43$
	1.6	0	$T = 2631.6t^2 - 284.44t + 307.13$	$T = 0.6285t^2 - 14.101t + 401.03$
	1.6	-0.4	$T = -419.97t^2 + 399.23t + 271.54$	$T = 0.1875t^2 - 5.4556t + 365.74$
	1.6	-0.8	$T = -13.791t^2 + 50.965t + 295.1$	$T = 0.0081t^3 - 0.1828t^2 - 0.2089t + 339.87$
	1.6	-1.2	$T = -2.3666t^2 + 18.313t + 293.55$	$T = -0.0285t^2 - 0.043t + 328.21$
	2.4	0	$T = -0.1016x^2 + 1.977t + 310.97$	N/A
	2.4	-0.4	$T = -0.1123t^2 + 2.4158t + 304.25$	N/A
	2.4	-0.8	$T = -0.1612t^2 + 3.3937t + 297.5$	N/A
	2.4	-1.2	$T = -0.1281t^2 + 2.9996t + 295.12$	N/A

Power (W)	Position		f(t)=T	
	X (mm)	Y (mm)	Heating	Cooling
73	0	0	$T = 36713t^2 - 7268.4t + 575.62$	$T = 0.3698t^4 - 12.116t^3 + 131.89t^2 - 549.96t + 1118.7$
	0	-0.4	$T = -112936t^3 + 73630t^2 - 12103t + 806.55$	$T = -0.0185t^5 + 0.7869t^4 - 12.495t^3 + 91.934t^2 - 316.45t + 810.7$
	0	-0.8	$T = -723.89t^3 + 790.38t^2 + 48.97t + 286.45$	$T = 0.0149t^4 - 0.5901t^3 + 8.3288t^2 - 52.945t + 503.22$
	0	-1.2	$T = -21.154t^2 + 89.337t + 285.74$	$T = 0.0545t^2 - 3.9223t + 387.89$
	0.8	0	$T = -215702t^3 + 126807t^2 - 19011t + 1063.7$	$T = -0.0607t^5 + 2.407t^4 - 34.565t^3 + 218.29t^2 - 591.92t + 954.51$
	0.8	-0.4	$T = -75720t^3 + 46348x^2 - 6769.4t + 524.27$	$T = 0.0736t^4 - 2.5211t^3 + 29.545t^2 - 142.7t + 621.68$
	0.8	-0.8	$T = 511.47t^4 - 1255.1t^3 + 866.53t^2 - 5.595t + 290.73$	$T = 0.3578t^2 - 10.686t + 421.37$
	0.8	-1.2	$T = -13.768t^2 + 64.428t + 288.69$	$T = 0.0075t^3 - 0.1931t^2 - 0.8401t + 367.17$
	1.6	0	$T = 2731.7t^2 - 263.14t + 307.44$	$T = 0.7961t^2 - 17.619t + 423.86$
	1.6	-0.4	$T = -259.64t^2 + 324.52t + 280.05$	$T = 0.2317t^2 - 6.6285t + 378.56$
	1.6	-0.8	$T = -16.809t^2 + 60.273t + 294.73$	$T = -0.0018t^4 + 0.0699t^3 - 0.8942t^2 + 2.7869t + 343.07$
	1.6	-1.2	$T = -2.6266t^2 + 20.553t + 293.96$	$T = -0.0147t^2 - 0.3955t + 334.88$
	2.4	0	$T = -0.1891t^2 + 3.5582t + 313.84$	N/A
	2.4	-0.4	$T = -0.1672t^2 + 3.3591t + 305.27$	N/A
	2.4	-0.8	$T = -0.1782t^2 + 3.7107t + 299.11$	N/A
	2.4	-1.2	$T= -0.1479t^2 + 3.4648t + 295.38$	N/A

Power (W)	Position		f(t)=T	
	X (mm)	Y (mm)	Heating	Cooling
105	0	0	$T = 414809t^3 - 94560t^2 + 5535.5t + 229.16$	$T = 0.5706t^4 - 18.914t^3 + 209.07t^2 - 881.91t + 1558.5$
	0	-0.4	$T = -131682t^3 + 86930t^2 - 13922t + 876.99$	$T = 0.2775t^4 - 8.8966t^3 + 95.858t^2 - 416.78t + 1044.7$
	0	-0.8	$T = -2410.8t^3 + 2495.5t^2 - 189.5t + 292.95$	$T = -0.2344t^3 + 7.097t^2 - 69.781t + 603.6$
	0	-1.2	$T = -36.376t^3 + 62.293t^2 + 80.597t + 286.73$	$T = -0.0445t^3 + 1.4966t^2 - 18.808t + 453.8$
	0.8	0	$T = 28043t^2 - 3781t + 379.69$	$T = 9.0007t^2 - 171.79t + 949.25$
	0.8	-0.4	$T = 3796.3t^2 + 378.75t + 249.69$	$T = 0.0968t^4 - 3.4904t^3 + 43.513t^2 - 222.35t + 795.12$
	0.8	-0.8	$T = 1915.2t^4 - 4169.9t^3 + 2729.9t^2 - 273.3t + 300.88$	$T = -0.1393t^3 + 4.1939t^2 - 42.551t + 519.07$
	0.8	-1.2	$T = 12.142t^4 - 61.877t^3 + 77.357t^2 + 46.32t + 290.69$	$T = 0.1508t^2 - 5.8494t + 406.24$
	1.6	0	$T = 6553.7t^2 - 1089t + 335.54$	$T = 0.1095t^4 - 3.5085t^3 + 36.654t^2 - 143.23t + 556.26$
	1.6	-0.4	$T = -12130t^3 + 8476.1t^2 - 1229.6t + 341.48$	$T = 0.4682t^2 - 11.953t + 421.68$
	1.6	-0.8	$T = 11.822t^3 - 66.904t^2 + 124.03t + 289.81$	$T = 0.0867t^2 - 3.6035t + 375.19$
	1.6	-1.2	$T = -4.7898t^2 + 31.836t + 293.82$	$T = 0.0188t^3 - 0.5444t^2 + 3.7602t + 339.32$
	2.4	0	$T = -0.1106t^2 + 2.682t + 321.98$	N/A
	2.4	-0.4	$T = -0.1849t^2 + 3.9044t + 312.05$	N/A
	2.4	-0.8	$T = -0.227t^2 + 4.845t + 301.81$	N/A
	2.4	-1.2	$T = -0.211t^2 + 4.7828t + 296.75$	N/A

Power (W)	Position		f(t)=T	
	X (mm)	Y (mm)	Heating	Cooling
145	0	0	$T = 64785t^2 - 11659t + 749.47$	$T = 0.713t^4 - 23.872t^3 + 267.5t^2 - 1147.7t + 1953.6$
	0	-0.4	$T = 36170t^2 - 6955.8t + 547.55$	$T = 0.4002t^4 - 13.215t^3 + 146.99t^2 - 647.03t + 1385$
	0	-0.8	$T = -10702t^3 + 10271t^2 - 1843.4t + 375.66$	$T = -0.3058t^3 + 9.6273t^2 - 98.63t + 722.23$
	0	-1.2	$T = -129.41t^3 + 215.32t^2 + 88.292t + 286.51$	$T = 0.8826t^2 - 22.024t + 509.18$
	0.8	0	$T = 74942t^2 - 12204t + 613.66$	$T = 10.518t^2 - 204.3t + 1157.1$
	0.8	-0.4	$T = -160891t^3 + 86444t^2 - 9825.4t + 537.12$	$T = 0.2824t^4 - 8.9268t^3 + 94.811t^2 - 411.28t + 1062.9$
	0.8	-0.8	$T = 8460.7t^4 - 16005t^3 + 9527.9t^2 - 1416.1t + 346.52$	$T = -0.2029t^3 + 6.4361t^2 - 67.304t + 620.11$
	0.8	-1.2	$T = -33.122t^3 + 51.724t^2 + 98.922t + 286.62$	$T = -0.0384t^3 + 1.4559t^2 - 20.229t + 472.08$
	1.6	0	$T = 8021.2t^2 - 1066.8t + 335.8$	$T = 0.0869t^4 - 3.0351t^3 + 35.946t^2 - 169.2t + 662.11$
	1.6	-0.4	$T = -9408.6t^3 + 7282.6t^2 - 999.41t + 334.2$	$T = -0.1404t^3 + 4.1158t^2 - 39.535t + 501.6$
	1.6	-0.8	$T = -55.24t^2 + 151.95t + 293.55$	$T = 0.1373t^2 - 5.5067t + 405.62$
	1.6	-1.2	$T = -7.897t^2 + 47.843t + 292.32$	$T = 0.0157t^3 - 0.4333x^2 + 2.0514t + 361.81$
	2.4	0	$T = -0.312t^2 + 5.7309t + 332.67$	N/A
	2.4	-0.4	$T = -0.3765t^2 + 7.0865t + 315.65$	N/A
	2.4	-0.8	$T = -0.3481t^2 + 6.9762t + 304.8$	N/A
	2.4	-1.2	$T = -0.2988t^2 + 6.532t + 297.48$	N/A